77-16,954

EROL, Orhan, 1947-
  CLAY STRUCTURE AND CREEP BEHAVIOR OF
  CLAYS AS A RATE PROCESS.

  Iowa State University, Ph.D., 1977
  Engineering, civil

Clay structure and creep behavior of

clays as a rate process

by

Orhan Erol

A Dissertation Submitted to the

Graduate Faculty in Partial Fulfillment of

The Requirements for thd Degree of

DOCTOR OF PHILOSOPHY

Major: Civil Engineering

Approved:

Signature was redacted for privacy.

In Charge of Major Work

Signature was redacted for privacy.

For the Major Department

Signature was redacted for privacy.

For the Graduate College

Iowa State University
Ames, Iowa

1977

TABLE OF CONTENTS

INTRODUCTION

The shear strength of clays can be expressed as a function of the intergranular normal stress, and the slope and intercept of the shearing resistance-effective stress relationships. Although of considerable practical utility, these terms do not indicate the mechanism of shearing resistance in clay soils. In reality, shearing resistance of soils depends on many factors including material composition, stress history, temperature, strain, strain rate and structure. The strength parameters defined by classical failure theories, i.e., Mohr Coulomb, do not reveal the effect of these factors controlling the stress deformation behavior of soils. Thus a number of phenomenon related to shearing resistance of clays including creep behavior are poorly understood. Time dependency of stress strain behavior of soils commonly referred to as creep is especially important in geotechnical problems where long term behavior is of concern.

Extensive studies on creep phenomenon have shown that the rate process theory can provide theoretical basis for analysis of stress-strain-time behavior of materials including soils. The theory is helpful in providing both an insight into the fundamental nature of soil strength and means for mathematical formulation of soil behavior in terms of certain factors such as temperature, material properties and soil structure. However application of theory to soil behavior presents difficulties arising from inadequate knowledge of soil structure. Since soil is a particulate material its behavior depends essentially on its structure. The characterization of the structure of clayey soils and its analytical

evaluation, however, are difficult due to complex nature of clay structure and its continuous variation with progressive deformations. Number of different approaches has been followed to determine soil structure-soil behavior relationships. These include creep studies, rheological model studies and study of soil fabric with electron microscopy. However both the definition of soil structure and its effect on soil behavior are still highly qualitative and need further clarifications.

The scope of the present investigation was to study the creep behavior of soft clays emphasizing the effect of structural variations on time-deformation behavior of soils. For this purpose the rate process theory and electron microscopy techniques were employed, and a soil structure concept, which treats the fundamental soil parameters defined in the rate process theory as variables, was proposed. The proposed structure model was found to apply to real soil behavior and to clarify the meaning and quantification of soil structure.

THEORY AND BACKGROUND

Rate Process Equation

Deformation of soil involves time dependent structural rearrangement of the material due to its particulate nature. Basic laws describing the behavior of ideal continuum do not account for the structural rearrangement of the material and thus presents difficulties when applied to soils. There is a need for a fundamental theory which describes the mechanistic behavior of particulate materials and accounts for structural changes. The rate process theory provides parameters which relate material characteristics including structure of the material to its mechanistic behavior. The theory has been widely used in studying mechanistic behavior of soils in particular soil creep (1,4,12,49,52,53,56,59). Detailed theoretical development of the theory can be found in Glasstone et al. (31).

In the present study the following creep equation developed by Dorn (22) for metals and adopted to soil creep by Noble and Demirel (59) was employed to study time deformation behavior of clay soils:

$$\dot{\gamma} = A \ e^{-\frac{\Delta H^*}{kT}} \ e^{\beta \tau} \qquad \text{(Eq. 1)}$$

where

$\dot{\gamma}$ = shear strain rate

A = proportionality constant

ΔH^* = activation enthalpy

β = stress factor

τ = shear stress

k = Boltzman's constant

T = absolute temperature

In the derivation of the equation the following assumptions have been made (58): 1. Clay particles are bound to each other by chemical bonds (including van der Waals bonds). 2. The shear resistance of clay soils is due to existence of an energy barrier (activation energy) between the bonding units. 3. Displacement of a bonding unit occurs when it surmounts the activation energy. 4. The magnitude of the activation energy is equal to the energy of the chemical bond minus the mechanical energy absorbed by the bonding unit during deformation. 5. The energy necessary to surmount the barrier is supplied by the thermal motion of the bonding units. 6. The resultant strain rate, $\dot{\gamma}$, is proportional to the number of bonding units which have thermal energies equal to or greater than the activation energy. 7. The number of bonding units having energies equal to or greater than activation energy is given by Maxwell-Boltzman distribution law.

The preexponential term, A, in Equation 1 includes the proportionality factor (frequency factor) relating number of activated bonds to strain rate and the activation entropy which can be related to the relative degree of orderness of the bonding units undergoing the flow. The stress factor, β, is equal to $\frac{\beta'}{kT}$ in which β' is identified as the flow volume. The product $\beta'\tau$ corresponds to the mechanical energy acquired by each bonding unit when the rupture of a bond is followed by a displacement. The term β' is a product of average bond area times the average distance moved by a bonding unit when displaced, and therefore has the dimension of volume. This parameter gives quantitative description of flow mechanism.

The term ΔH^* is related to the bond energies involved in deformation process and reflects the strength and nature of bonding in clay soils.

When the parameters, A, ΔH^* and β, in Equation 1 are considered to be material constants the relationship expressed by Equation 1 indicates that the shear rate is independent of strain and time since neither of these quantities appear on the right side of the equation. Actually shear rate is time or strain dependent in soil creep. The experimental creep curves at low shear stresses show only a primary creep region which follows an initial deformation; then deformations terminate with time. At relatively high stresses (exceeding some limiting value) the curves are divided into three portions: primary, secondary and tertiary regions where shear rate decreases, remains constant and increases with time, respectively. In many instances secondary creep does not occur (17,58). In the present work the terms "tertiary creep" and "terminal creep" will be used to indicate type a and type b creep curves shown in Figure 1, respectively.

To account for the time dependence of shear rate a structure function is sometimes included in Equation 1 so that:

$$\dot{\gamma} = A\, e^{\frac{\Delta H^*}{kT}}\, e^{\beta\tau}\, s(\gamma,t) \qquad\qquad \text{(Eq. 2)}$$

where γ and t are strain and time respectively and $s(\gamma,t)$ is an unknown function representing the time or strain dependent changes in the structure of the material (22,43). The application of Equation 2 to shear deformations is not possible without the determination of the structure function or elimination of the effect of structure function on shear rate. To eliminate the structure effect, shear rates must be compared at
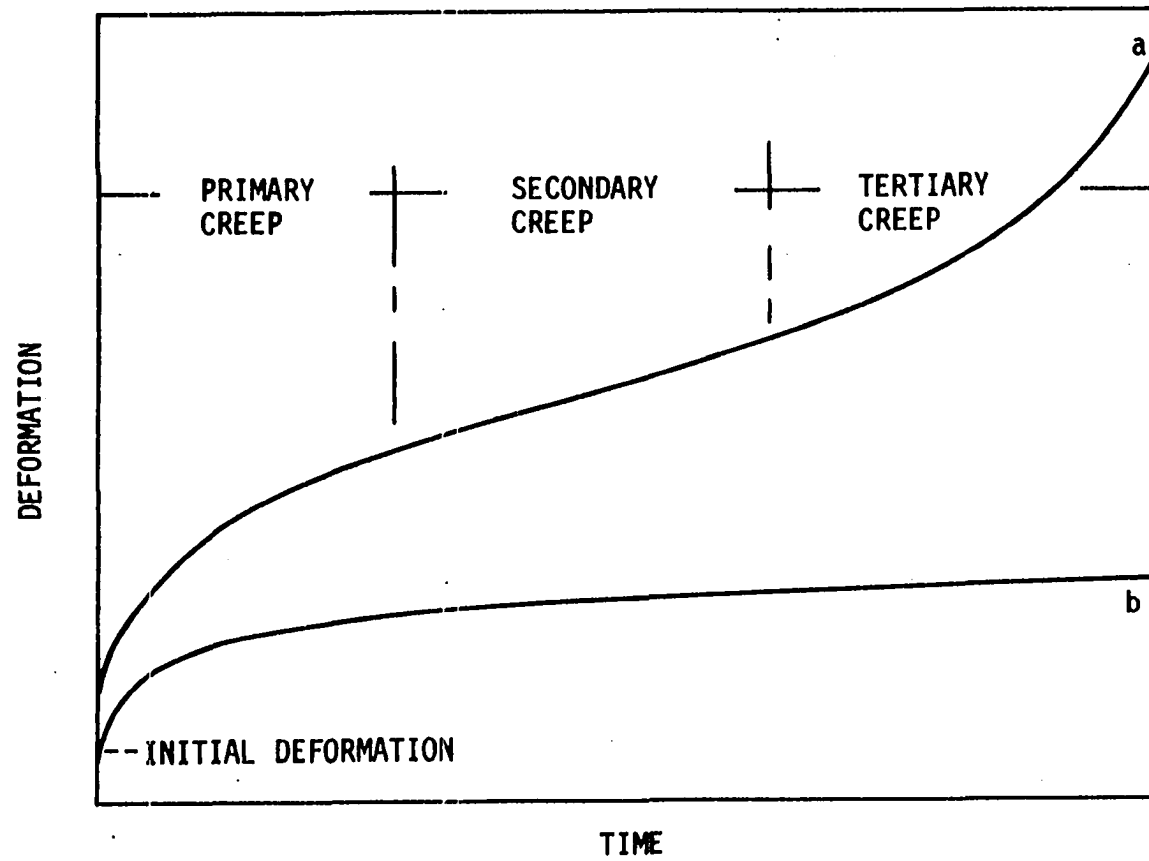
Figure 1. Time deformation curves for soil creep

identical structures on experimental creep curves. There are different

opinions in establishing a criteria for the occurrence of identical soil

structures. Noble and Demirel (59) and Schmid (70) proposed that the

soil structure is equivalent at inflection points of tertiary creep

curves. According to Mitchell et al. (49,52) identical structure is

attained at equivalent time of shear. Andersland et al. (4) suggested

step loading creep tests, and comparison of shear rates at the instant

when stress intensity is changed. In these investigations, emphasis was

placed for the experimental verification of the theory and determination

of soil parameters, and structural changes were not considered.

Soil Structure and Structural Changes

The following quote well describes the concept of soil structure

(94, p. 71):

> We define soil structure as that property of soil which provides
> the integrity of the system and which is responsible for response
> to externally applied and internally induced sets of forces and
> fluxes. Soil structure as a property includes gradation and
> arrangements of soil particles, porosity and pore size distribu-
> tion, bonding agents and specific interactions developed between
> particles through associated electrical forces.

As suggested by the definition of these authors, soil structure consists

of two major components. In clay soils these components are fabric which

characterize the geometrical arrangement of mineral particles and void

spaces, and particle interactions which describe the bonding mechanism and

nature of shear resistance. Both components are interrelated and struc-

tural changes associated with creep deformations are the result of

changes in both components.

Variety of methods, both direct and indirect, has been used to study the soil fabric and fabric-soil behavior relationships (50). Direct methods include optical and electron microscopy, X-ray diffraction and pore size distribution. These techniques provide direct data on specific fabric features unless the original fabric is not disturbed during sample preparation, as will be discussed in the following section. Indirect methods for fabric characterization include acoustical, dielectric, thermal and magnetic measurements on clay water systems. These measurements can be made directly on samples in their undisturbed, wet state. Since the measurements are made on physical properties of the system other than directly on fabric, the interpretation of data in terms of fabric characterization is seldom straightforward (50).

Among the available techniques the electron microscope is the only one that can reveal particle arrangements directly.

Fabric Studies with Electron Microscopy

Recent developments in electron microscopy techniques have made the observation of clay fabric and its alteration under the action of shear deformations possible. Due to the relative ease in sample preparation and the advantage of greater depth of field, scanning electron microscopy (SEM) has been found superior to transmission electron microscopy (TEM) and more frequently employed in clay fabric studies. However there are number of difficulties with this technique arising from fabric disturbances which occur during specimen preparations. In SEM studies observations are made in evacuated chambers. Therefore either removal or replacement of pore fluid from wet clay specimens is required. Both the

removal and replacement of pore fluid may cause fabric disruptions unless proper techniques are employed (25,88,89). In SEM, the observations are entirely dependent on the surface layers of the specimens which are most subject to disturbances during sampling and subsequent specimen preparation. Grinding and cutting may result in particle rearrangements on the surface (76). There may be loose particles on fracture surfaces obscuring the original fabric features (76,88). Therefore in some cases observed fabric of a specimen may reflect some features of preparation method, and this limitation should be taken into account in fabric studies.

Fabric studies of clay minerals by Smalley and Cabrera (81), O'Brien (60), Tovey (87), Sankaran et al. (69), and Barklay et al. (11) have shown that single isolated particle associations suggested by previous investigators (36,84) do not exist. Particle assemblages such as aggregates or pockets and pore spaces associated with them are common fabric elements and they occur in a variety of forms with complex geometries. The fabric of swelling type clay minerals consists of wrinkled continuous sheets or films and do not show a particulate nature (15,87,25). In nonswelling type clay minerals, the fabric is usually characterized by particle assemblages which consist of oriented, densely spaced clay particles. O'Brien (60) investigated the fabric of kaolinite and illite and noted that the fabrics of both clays are dominated by three dimensional network of twisted chains of face to face oriented platelets, and used the term "stair stepped cardhouse" to describe the fabric. The terms "domain" (2), "pockets or books" (80) were used by investigators to describe aggregates of parallel oriented clay platelets. The terms "bookhouse" "turbostratic fabric" were suggested to describe different arrangements

of aggregates in gross fabric. A summary of reported fabric features of monomineralic clays can be found in Mitchell (50) and Collins et al. (20). These studies have shown an apparent tendency for face to face attraction of clay platelets in forming the aggregates. However the nature of this attraction has not been stated by these investigators.

Studies of shear induced fabric revealed that failure of clay specimens tested in triaxial or direct shear results from formation of slip zones with thicknesses ranging from 40 µm to 100 µm (9,45,28,55). These shear zones are enclosed between two slip planes where perfect particle alignments occur in slip plane direction. The particle preferred orientations within these zones are less intense as compared to slip planes and they are inclined to slip planes (9). Morgenstern et al. (55) and Foster et al. (28) noted zones of minor discontinuities inclined to slip zones and detected high degrees of particle alignments in these minor discontinuities. In these investigations no information is given about the fabric changes prior to the formation of clearly defined failure planes.

There are only limited number of electron microscopy studies in literature describing the fabric alterations taking place at successive shear deformations. Vyalov et al. (91) investigated the changes in clay fabric at various stages of creep deformation under pure shear. The following quote summarizes the observations reported by the investigators (91):

> In case of creep having a damping character, changes in the structure were observed to be identical for the damping process of deformation and for the unsteady flow stage of the general non-damping creep process. These changes consist in the reduction of

the number and size of cavities and pores here and there to be compressed and elongated in the direction of shear, which indicates that there were local displacements of the particles and microaggregates and they were packed more compactly. The longer the duration of deformation process, the more were the cavities reduced in size and number. But the basic reduction took place in the initial period corresponding to the most intensive development of the deformation.

The reorientation of clay particles tending to locate the basal planes along shear direction took place during the steady flow stage. Simultaneously, it was observed that on one hand a clearly expressed flattening and elongation of cavities in the direction of reorientation of particles took place leading to the reduction of their size, while on the other, very fine wedge shaped fissures originating from the cavities or extending from one cavity to another, i.e., in the areas of least resistance developed.

During the stages of progressive flow (tertiary creep) an intensive development of macropores and microfissures was observed, and fused together and formed a network of micro and macro fissures. Often the fissures extended through the whole microsection, as if dividing the soil into separate parts. The prevailing orientation of the large fissures corresponded to the direction of shear.

The analysis of the structure revealed that independently of the size of the load and deformation duration, the failure started when the development of the fissures reached a certain magnitude which represents a constant for the given soil.

Foster et al. (28) studied the fabric of soft kaoline under direct shear. These authors suggested the following fabric alterations prior to the formation of slip zones considering their fabric observations with transmission electron microscopy and volume change behavior of specimens: "Initially random fabric collapsed under shear loading before peak shear stress. The particles slided and turned through angles between 0° and 90° and on average through an angle in excess of 45°, and consequently became highly oriented parallel to the direction of shear loading." These authors observed no sign of degradation of particles after shear loading and concluded that the rotational movement of particles took place without

mutual fracturing. According to the authors this well-oriented fabric would then be susceptible to formation of discontinuities and slip zones at peak stress intensity.

Implicit in a single and independent structure function concept as formulated by Equation 2 is the fact that the parameters, A, ΔH^* and β as stated earlier (p. 5), are structure independent material constants, and the structural variations are only accounted for through the structure function. Evaluation of the structure function may possibly be done by measuring the fabric variations observed by scanning electron microscopy and correlating them with the creep behavior. This approach is the primary objective in Vyalov et al. (91) and Zretskii and Vyalov's (95) investigations. The complex nature and heterogeneous geometry of clay fabric and lack of simple measurement techniques with SEM, however, make such an approach difficult. This difficulty on the one hand and the difficulty in describing for the material a reference state at which parameters A, ΔH^* and β would have their characteristic values on the other hand led the author of the present study to a different approach for evaluation of the clay structure and the structural changes occurring during deformation. In this approach the parameter A, ΔH^* and β are treated as structure dependent material properties and as such they describe total deformational (mechanistic) behavior of clay without a need for an additional structure function. A reference state, however, was still needed for the complete description of these parameters. The state of the clay material at the inflection point of creep curve was selected as the reference state. The value of A, ΔH^* and β in all of the other

states attained in the deformational history of the clay were evaluated in reference to those in the reference state. It is interesting and pleasing to note that the aforementioned SEM work by Vyalov et al. (91) is in complete support of the approach formulated in the present study. It seems appropriate to briefly discuss in reference to the parameters A, ΔH^* and β, the supporting evidence found in the work of Vyalov et al. (91) at this point and refer to it later when needed: 1) During the primary creep the structural defects are reduced causing more order in orientation, that would decrease A and causing closer particle association that would increase ΔH^* and β' through formation of stronger bonds and larger structural units, respectively. 2) At the secondary (steady state) creep highest order of orientation and closest particle orientation would cause A to attain its minimum value and ΔH^* and β attain their maximum values. The point of inflection represents the climax of secondary creep. 3) During the tertiary creep disintegration of microaggregates, growth of fissures and formation of new fissures destroy the orderliness of orientation cuasing an increase in A and loosen particle association which cause ΔH^* and β to decrease due to weakened bonds and reduced size of structural units, respectively.

A detailed SEM investigation aimed at studying the structural changes which occur in the shear zone during the various stages of deformation was initiated during the course of the present study. It was found that sample preparation techniques were of at most importance for obtaining meaningful results. The results of the investigation of sample preparation techniques can be found in Erol et al. (25). Due to complexity and

time consuming nature of SEM studies a full time research effort was
needed for the SEM work to obtain satisfactory results. Since the work
of Vyalov et al. (91) has provided convincing evidence, it was decided to
concentrate on mechanistic aspects of the study.

Particle Interactions and Bonding in Clay Soils

There are various interaction energies contributing to bonding forces
among clay particles. In clay water systems interaction between charged
clay surfaces and polar water molecules results in an increased structural
organization of water molecules close to particle surfaces (41,21,39).
The exact nature of this interaction is not known. Hydrogen bonding,
charged surface-dipole attractions, hydration of exchangeable cations
close to particle surfaces and other van der Waals attractions are the
possible mechanisms for clay-water interactions (39). Few molecular
layers of water, which is called adsorbed water, are strongly held on clay
surfaces due to these interactions and considered as an integral part of
clay particles. The properties of the adsorbed water including density,
viscosity, freezing point, bond strengths and thermodynamical properties
are known to be different than ordinary water (39,40,5,38,44). The ad-
sorbed water may partly account for bonding in clay soils (86), and asso-
ciated bond energies are expected to decrease with distance from clay
surfaces due to a decrease in surface force fields. The hydration of
charge compensating cations in the presence of water give rise to the
formation of diffuse double layers adjacent to clay surfaces (90). When
two particle faces are brought into close proximity, electrical forces

develop due to interference of double layers. These forces include double layer repulsions and London van der Waals attractions. The magnitude of the net interaction energy is dependent on distance between clay surfaces. Double layer interactions may contribute to bonding forces and partly account for bonding in clay soils. In addition, Coulombic attractions between positively charged edges and negatively charged surfaces of clay may give rise to bonding forces among clay particles (36,84). Thus bond energies in clay soils reflect the combined effect of various interactions.

The bond energies arising from clay-water, double layer, and surface interactions are dependent on particle arrangement and interparticle distances, therefore it is reasonable to expect that changes in soil structure due to changes in particle orientations and interparticle distances may cause variations in bond energies, and subsequently shear resistance of clay soils may vary with deformations.

One group of investigators (51,53,16) believe that the actual area of contacts between clay particles (asperity contacts) is so small that even at apparent stress levels much lower than yield stress of clay minerals, extremely high contact stresses develop at these asperities. Subsequent plastic yield at the contacts initiates primary type bonding in clay soils. Existence of adsorbed water layers, and high desorption energies required to remove these layers from clay surfaces (68) precludes possibility of direct mineral to mineral contacts in clays. In addition born repulsion forces become effective as mineral phases come in contact and resist interpenetration of crystal latices (90). Born repulsion may be

another reason which prevents primary type bonding in clays. In summary bonds in clay-water system are of a composite nature and probably van der Waals bonds in a broad sense that implies all electrical interactions (except ionic and covalent) and the hydrogen bond best describe the bonding in a clay water system. And as such the bond energy in a clay water system is an average interaction energy representing a weighted average of all states of electrical interactions which exist in the system. This does not violate any of the requirements of the rate process theory.

<center>Primitive Model</center>

A primitive model will be described here to define a reference state for stress-strain-time behavior of a real clay water system analogus to description of ideal gases or real solutions as opposed to real gases or real solutions.

In an experimental creep curve as shown by the solid line in Figure 2 (real creep behavior), the shear rate decreases over primary stage up to the inflection point I, then starts to increase in the tertiary stage. The theoretical expression given by Equation 1 implicitly states the following: If the structure had remained constant, creep curve would have been a straight line after an initial strain that is obtained immediately upon stressing. Then any deviation from the linear time deformation behavior can be attributed to the structural differences.

Following this line of reasoning the structure of the soil at inflection point was selected as a reference structure, and tangents to the creep curves at inflection points were drawn to represent a flow condition
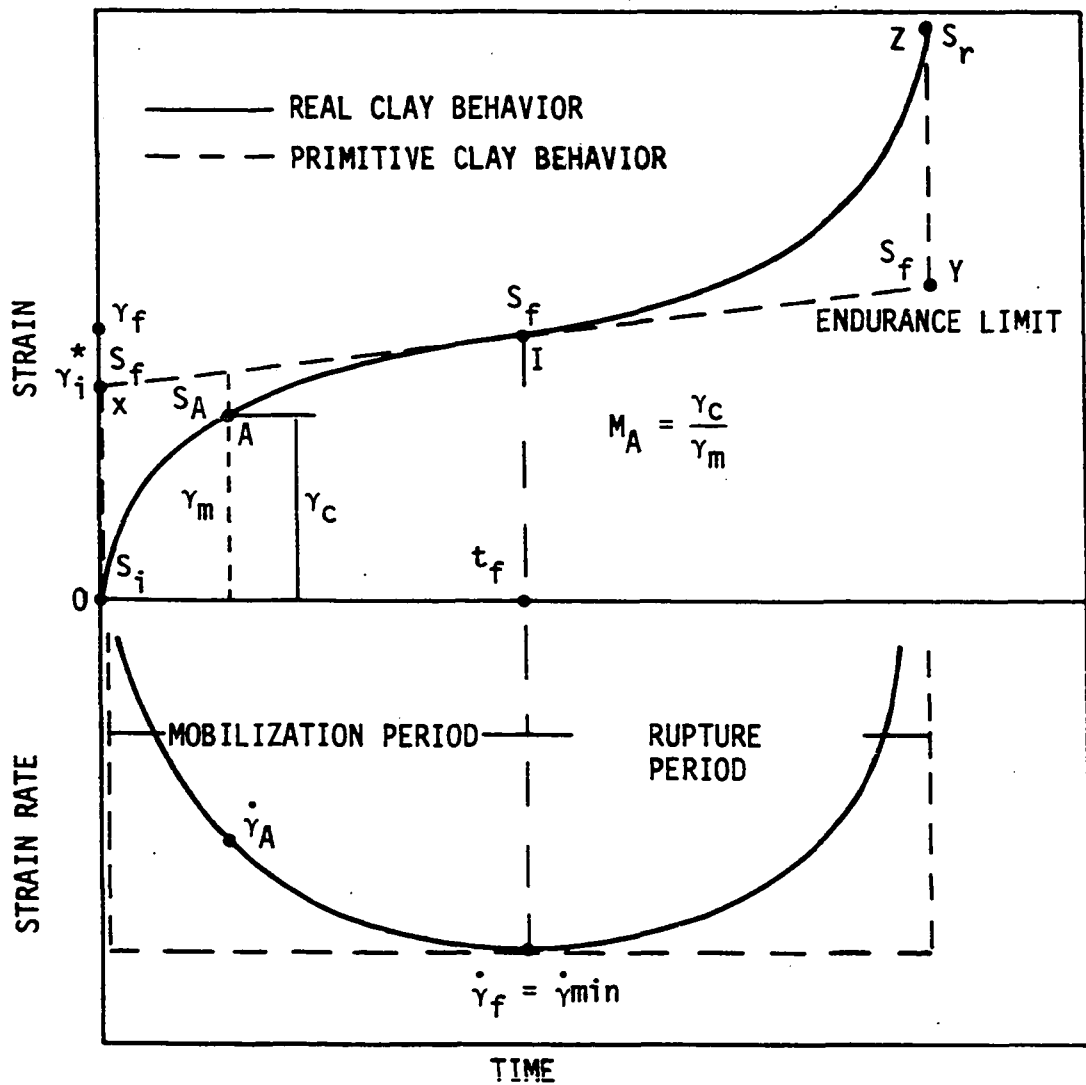
γ_C : CREEP STRAIN

γ_m : PRIMITIVE MODEL STRAIN

M_A : MOBILIZATION RATIO AT "A"

$\dot{\gamma}_f = \dot{\gamma}_{min}$: STRAIN RATE AT INFLECTION POINT

γ_i^* = INITIAL ADJUSTMENT STRAIN

S_i : INITIAL SOIL STRUCTURE

S_f : SOIL STRUCTURE AT FLOW

S_A : SOIL STRUCTURE AT A

S_r : SOIL STRUCTURE AT RUPTURE

γ_f, t_f : TIME AND STRAIN AT I

Figure 2. Primitive model

progressing at constant reference structure. This idealized behavior will be called primitive model. The primitive model shown in Figure 2 is characterized by three reference structure states: initial structure S_i, flow structure S_f and rupture structure S_r. The initial structure S_i is brought to a flow structure S_f when a soil element experiences the initial adjustment strain γ_i^* immediately upon stressing. Structure remains constant at this state until endurance limit, point Y, of the soil is reached. At this point structure S_f changes to a rupture state S_r within an infinite small time. At point I the primitive model coincides with real creep behavior as shown in Figure 2. Two strain ratios are defined to quantize the departure in the behavior of real clay from that of primitive behavior, as follows:

$$M = \frac{\gamma_c}{\gamma_m}$$

$$R = \frac{\gamma_c}{\gamma_m} - 1.0$$

where γ_c and γ_m are real creep and primitive model strains at a given time t, and M and R are mobilization and rupture ratios, respectively. The total creep time is divided into two intervals, mobilization period (from 0 to I in Figure 2) and rupture period (from 0 to Y). The mobilization ratio will be a small fraction at the beginning of the mobilization period and increase to a value of one at the inflection point I. Similarly the rupture ratio will increase from zero at the inflection point to higher fractions as tertiary strains progress. The ratios are defined independently to emphasize the two different behaviors, primary-strain hardening and tertiary-strain softening, respectively. Further, it is assumed that

the flow structure S_f occurring under different shear stresses is the same

for a given material composition and testing condition. In other words

flow structure S_f corresponds to a unique particle arrangement and inter-

action energy state which is independent of the shear stress. Noble (58)

and Marley (43) demonstrated the experimental verification of this assump-

tion. The following quote from fabric studies by Vyalov et al. (91)

states some direct evidences indicating that the structure is independent

of shear stress at flow state.

> The analysis of the structure revealed that independently of the
> size of the load and deformation duration, the failure started
> (authors define failure as the beginning of tertiary creep) when
> the development of the fissures reached to a certain magnitude
> which represents a constant for a given soil.

As noted earlier, the departure of the deformational behavior of the

soil corresponding to a point on the real creep curve from that of the

constant rate flow model (primitive model) can be attributed to the dif-

ference between the structure of the soil at that point and the reference

structure (primitive model). The absolute value of mobilization ratio at

that particular point is selected as a quantitative measure of this struc-

tural difference. Thus on the strain time curves of a clay-water system

at various shear stresses points of equal mobilizations will correspond to

the point of identical structures. To establish the shear stress-creep

rate relationships and to determine flow volumes β' independent of struc-

ture effects, the creep rates at point of equal mobilizations must be

compared as illustrated in Figure 3. Similarly on creep curves obtained

at various temperatures and fixed level of shear stress, the strain rates

at equal mobilization ratios should be compared to determine activation

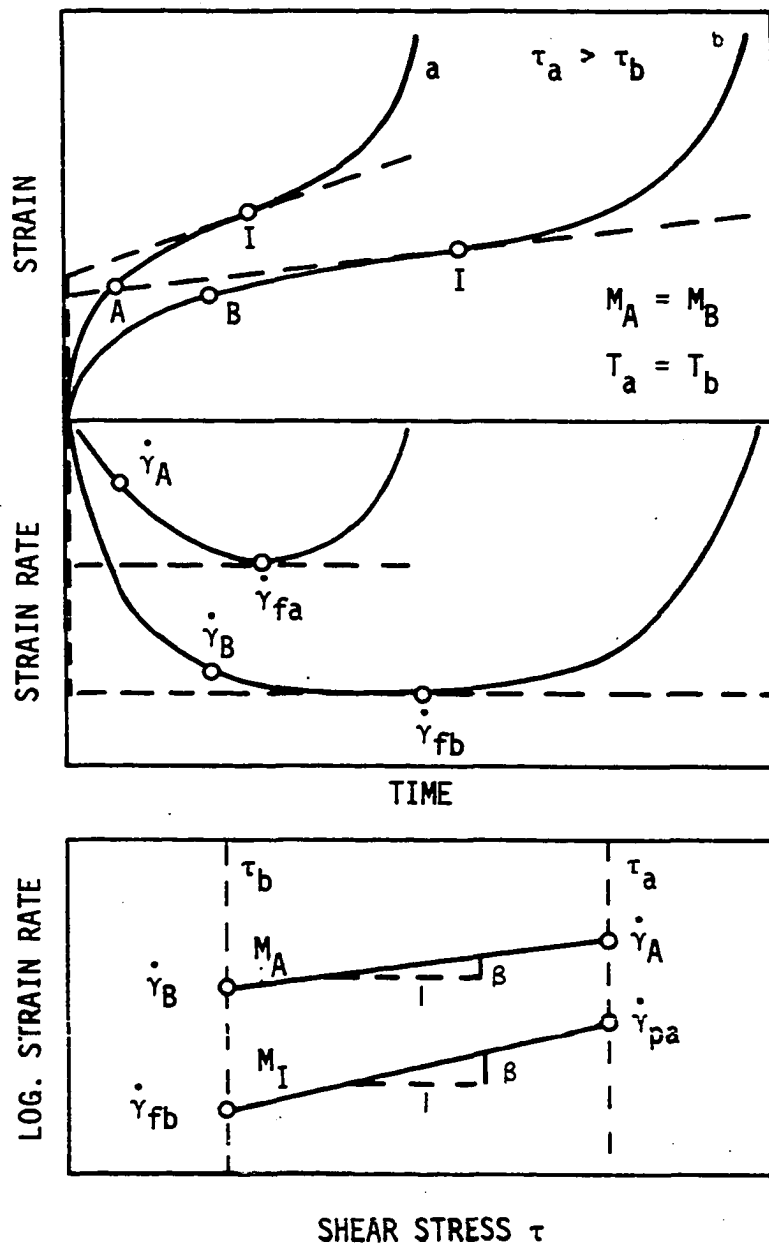enthalpies, ΔH^*, as shown in Figure 4.
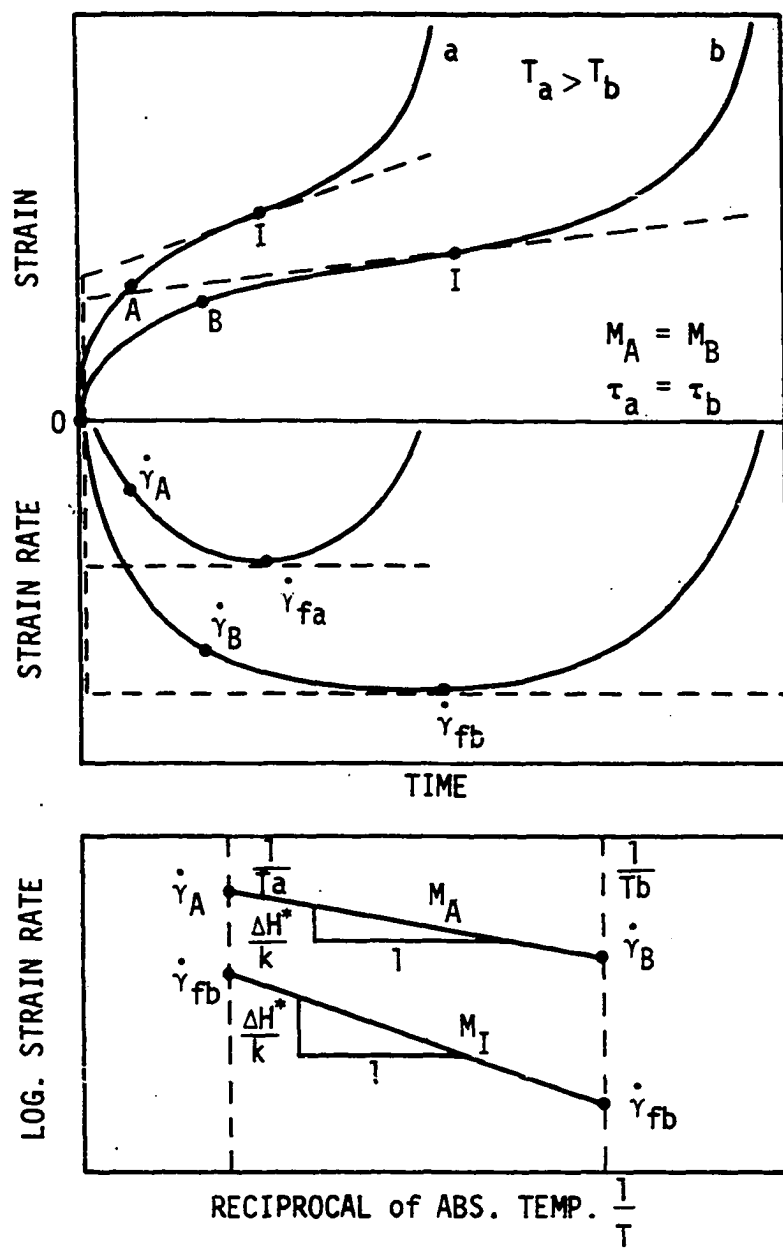
Figure 3. Determination of flow volumes

Figure 4. Determination of activation enthalpies

The hypothesis proposed is summarized below:

1. Under a given stress and temperature the strain predicted by the rate process theory is equal to the real strain experienced by a clay water system at the inflection point of the deformational history (creep curve). This describes the creep curve predicted by the rate process theory.

2. Deviations of strain time behavior of a clay water system from that predicted the rate process theory is due to structural rearrangements which occur during the deformation of the clay water system.

3. Under any two different stresses (temperature constant) or at any two different temperatures (stress constant) the two strains experienced by a clay water system at identical structures are directly proportional to respective strains predicted by the rate process theory. The coefficient of proportionality is defined as the mobilization or rupture ratio.

This hypothesis has been verified by the experimental results.

METHODS OF INVESTIGATION

Materials Tested

Two different clays were tested in the experimental program. The first, montmorillonite, was obtained from Ward's Natural Science Establishment, Inc., New York. This clay is known as Wyoming Bentonite and is essentially sodium montmorillonite with minor amounts of feldspar and quartz. The second, Grundite clay, collected from Morris, Illinois, consists of mainly illite with minor amounts of kaolinite (92). The clays were sieved through a number 200 standard sieve and only finer fraction was used to prepare test specimens. The properties of clays are summarized in Table 1.

Table 1. Properties of clays

Property	Grundite	Bentonite
Liquid limit, %	58.6	515
Plastic limit, %	28.4	51
Shrinkage limit, %	19.3	
Percent finer than 2 micrometers	72.2	
Mineralogical composition	Illite with minor amounts of kaolinite	Predominantly sodium montmorillonite

Shear Apparatus

One of the basic requirements of rate process theory is simultaneous determination of stresses and strains in a soil specimen subjected to large deformations under the action of externally applied loads. This requirement cannot be met by employing standard soil testing techniques, namely, triaxial and direct shear testing. Both testing methods have limitations arising from indeterminate state of stresses and strains at large deformations (83,75,37).

In the present work simple shear test was selected as a method of testing which met the requirement of uniform strain application and its accurate measurement. Early investigations have shown that simple shear apparatus is capable of satisfying this requirement over a wide range of deformations (62,65,66,14,8,26,33). In this study the apparatus originally designed by Hartwell (33) was modified and used in creep testing. A picture and the diagrammatic representation of the apparatus are shown in Figures 5 and 6, respectively.

The mechanical details of the apparatus is shown in Figure 6b. The basic features are the following: The normal load in the form of a suspended weight is applied to (1) through a guide system (3). Guide system is composed of two cylindrical shafts rigidly mounted to the base plate (6). Two bushing bearings (4) are fixed to the ends of the yoke (2) so that the shaft and the bearings ensure vertical alignment and constrain the loading plate to move vertically without any friction. With this system tilting and the tipping of the loading plate (1) is securely prevented.
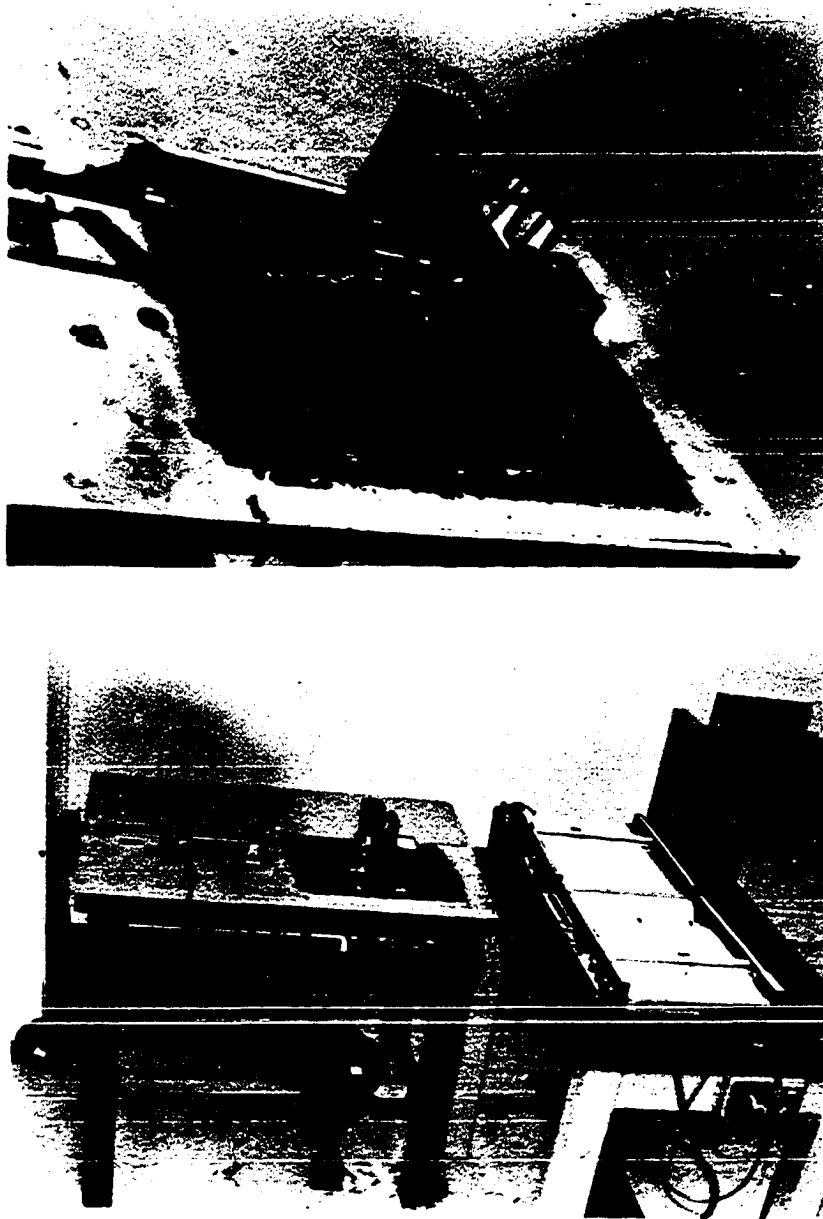
Figure 5. Simple shear apparatus

(a)   DIAGRAMATIC REPRESENTATION
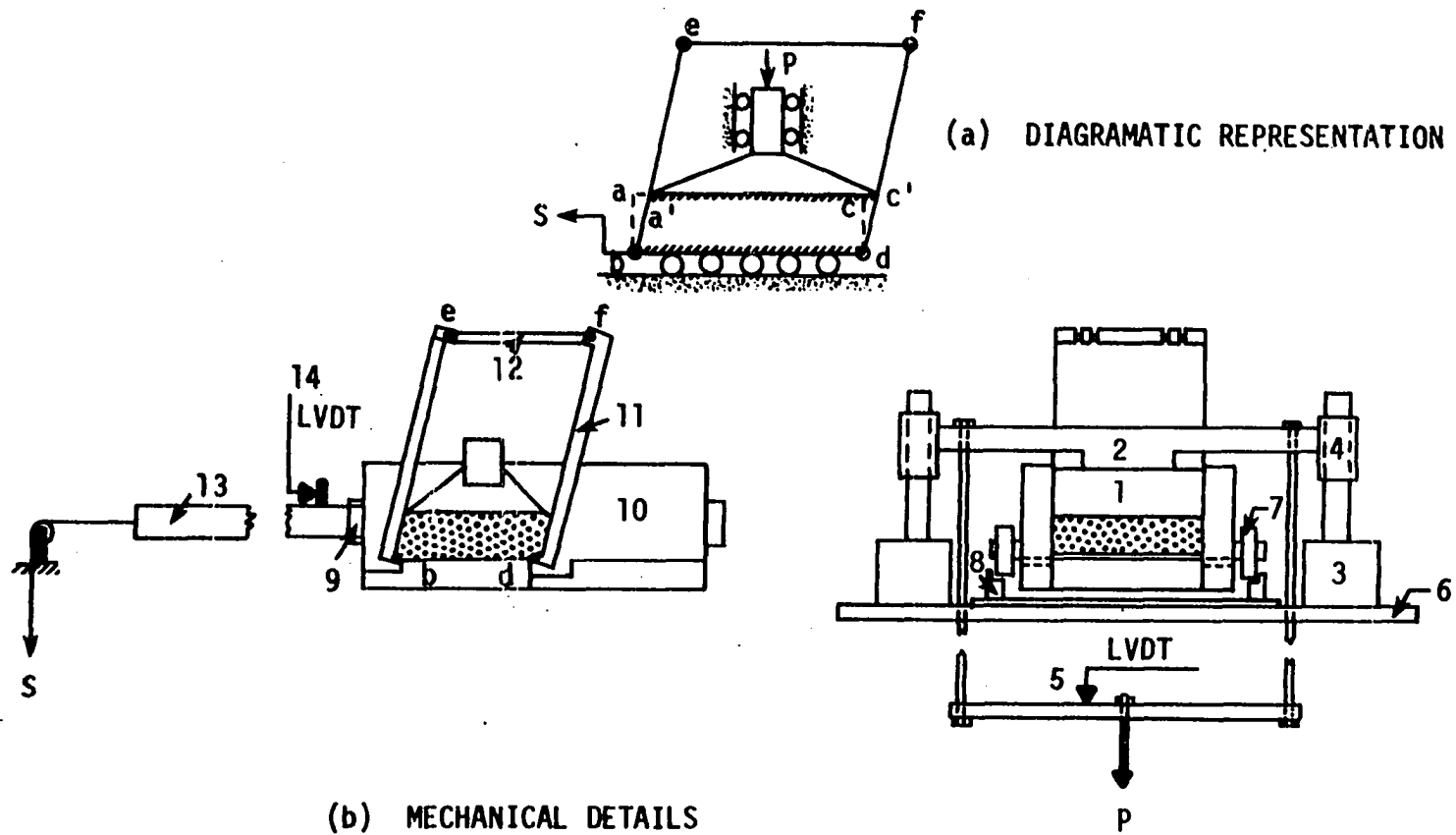
(b)   MECHANICAL DETAILS

Figure 6.   Mechanical details of the apparatus

The volume changes of the specimen is monitored by the vertical displacement of (1) by means of a linear variable differential transformer, LVDT (5), mounted on the normal load frame. The frictionless roller bearings (7) are mounted on the sides of the shear box, to move the box in horizontal plane and alignment in the direction of shear loading is achieved by tracks (8). Shear load is applied through a rod (13) connected to the lateral brace (9) in form of suspended weights. Shear displacement is monitored by means of a LVDT attached to the shear load rod.

The side walls (10) and the shear gates (11) are made of chrome plated steel and covered with Teflon to minimize friction on the shear box-soil interfaces.

The shear gates (11) are assembled to the shear box by means of hinges at b and d, as shown in Figure 6b. Adequate friction between the specimen and the bottom and top plate of the shear box, which is necessary to transfer the shear loads to the specimen, was achieved as follows. The loading plate (1) was machined with a series of sharp ribs one millimeter high, transverse to the shear direction and bottom plate was covered with coarse sand paper.

Clearances between the side walls, and load plate and shear gates were allowed so that no frictional contact would be made during shear.

Specimens were maintained at constant temperature by controlling the temperature of the air around the shear box. The system consisted of a double layered insulated asbestos housing, two heating elements, a fan and a solid state temperature controller accurate within ±0.5°C.

Figure 7 shows a modeling clay specimen which experienced 0.263 $\frac{in}{in}$ shear strain under constant normal and shear stresses of 10.0 psi and 2.7 psi, respectively. Uniform deformations were achieved throughout the specimen except a small portion at the bottom. A thin zone experienced relatively less deformations than the rest of the specimen. This non-uniformity was introduced by the hinges at b and d in Figure 6b imposing an unstrained dead zone at the bottom. This limitation of the apparatus was considered to be outweighed by the advantage of the uniformity of the strains throughout the large portion of the specimen.

Although the strains are uniform in simple shear testing, the stress conditions within the specimen are not completely known (23,42,65). An attempt was made to investigate the stress conditions in simple shear. Four contact pressure transducers were mounted on the shear box. The lateral pressures on the shear gates were measured by transducers a and b located at mid-height of the specimen, as shown in Figure 8. Bottom pressures were monitored by means of transducers c and d located in the base plate, at one-third of the base length from the ends. A series of constant strain rate tests were run with a kaolinite sample and the typical stresses measured are shown in Figure 8.

In Figure 8b the pressures recorded on shear gates are plotted as a function of applied shear strains. The lateral stresses increased con-tinuously to magnitudes in excess of applied normal stress of 10 psi at high strains. Figure 8c shows the recorded pressures at the base of the specimen. The magnitudes of the incremental stresses were in the order of 10 to 30 percent of the applied normal stress of 10 psi.

normal stress : 10.0 psi
shear stress : 2.7 psi
shear strain : 0.263 in/in
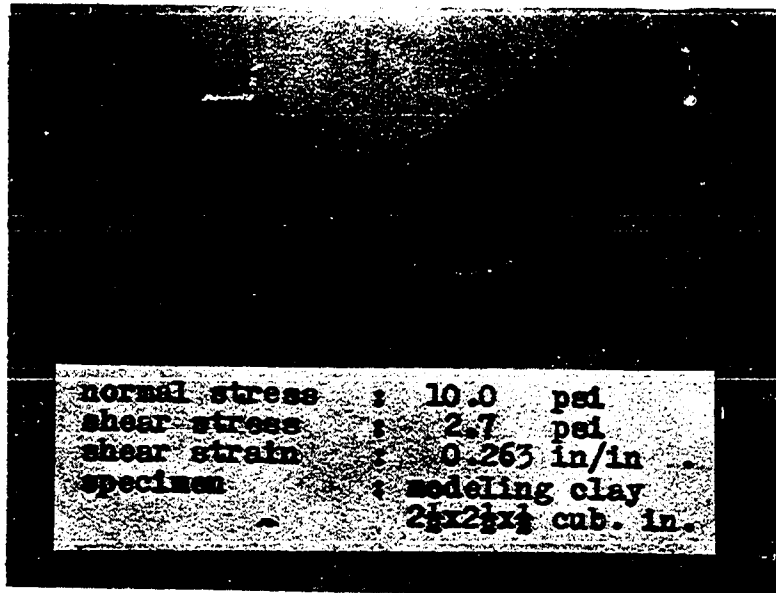specimen : modeling clay
2½x2½x¼ cub. in.
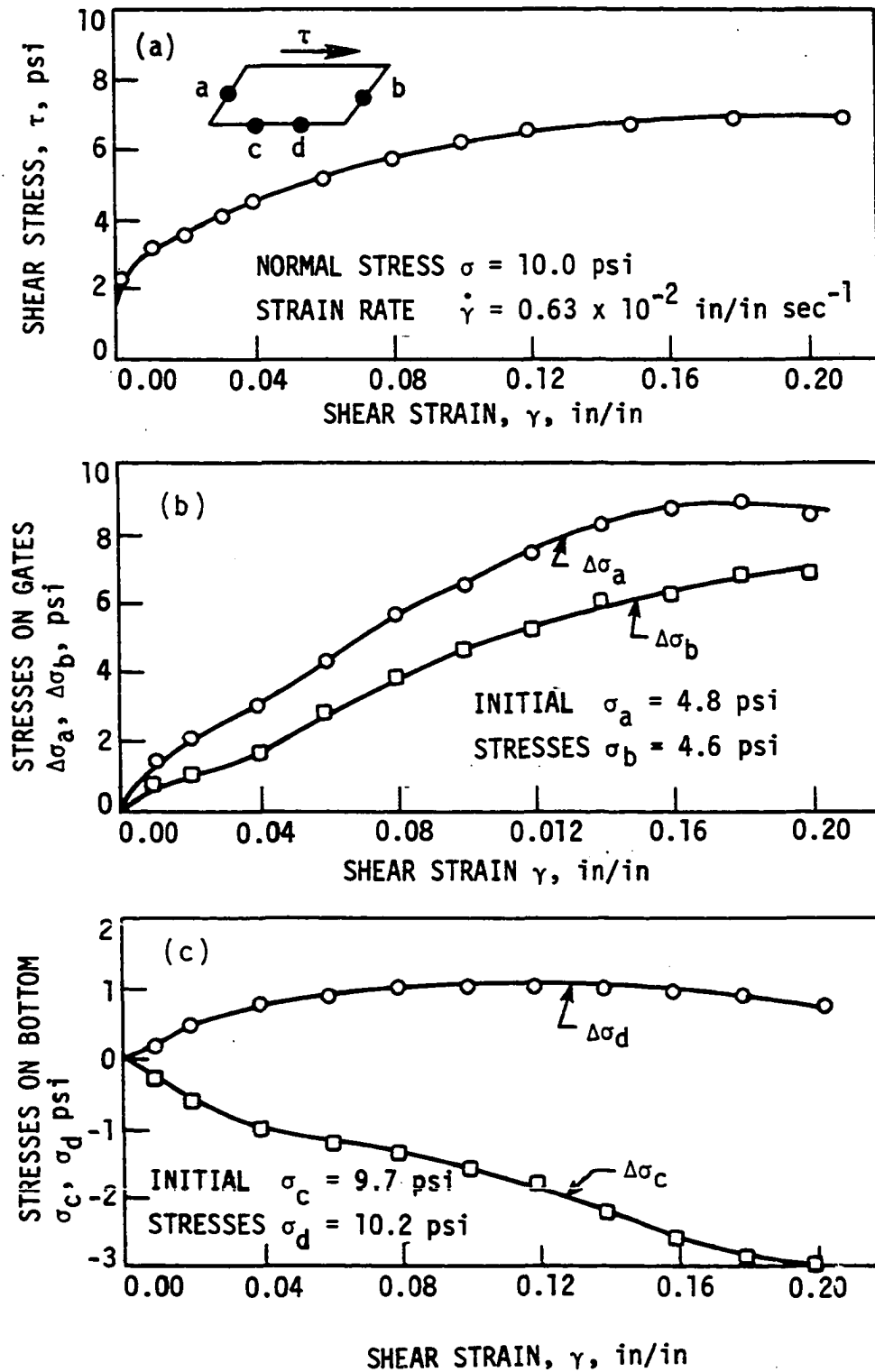
Figure 7. Deformations in simple shear

Figure 8. Stress conditions in simple shear

The relatively high stresses measured on the shear gates suggested that the shear deformations are imposed by the combined effect of the applied shear stress on the horizontal plane and the normal stresses developing on the shear gates. This observation further implies that the idealized simple shear conditions do not exist in simple shear testing of soils. The stress conditions within specimens approach the triaxial state of stresses as suggested by Duncan et al. (23).

The different magnitudes of pressures suggested a nonuniform normal stress distribution along the bottom of the specimen. Roscoe et al. (67) measured the stresses on all soil-shear box interfaces by employing extensive instrumentation and their results indicated that all the boundary stresses are actually nonuniform in the simple shear test. These observations are in agreement with the results of mathematical solutions employing linear elastic (65) and nonlinear elastic (23,42) models for the simple shear boundary conditions. Due to the nonexistence of complimentary shear stresses along the shear gates the moment equilibrium of the specimens is not maintained. As a result, stress nonuniformities develop along the boundaries of the specimens to assist in maintaining the equilibrium as shown in Figure 9. The magnitudes of the nonuniform stresses are proportional to the sample height as illustrated in Figure 10, since the unbalanced moment is the product of the sample height and the magnitude of applied shear force. To reduce the magnitude of unbalanced moment and therefore the nonuniformity of stresses, the specimen heights were reduced to 1/2 inch.
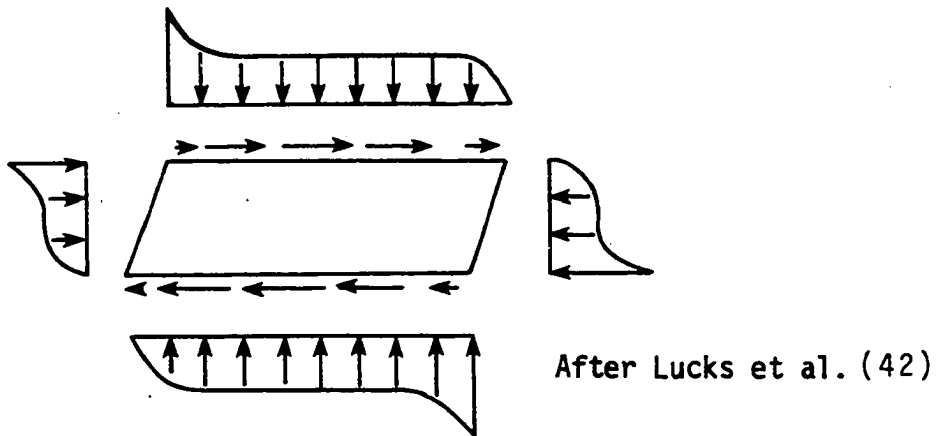
After Lucks et al. (42)

Figure 9. Stress distribution at simple shear boundaries

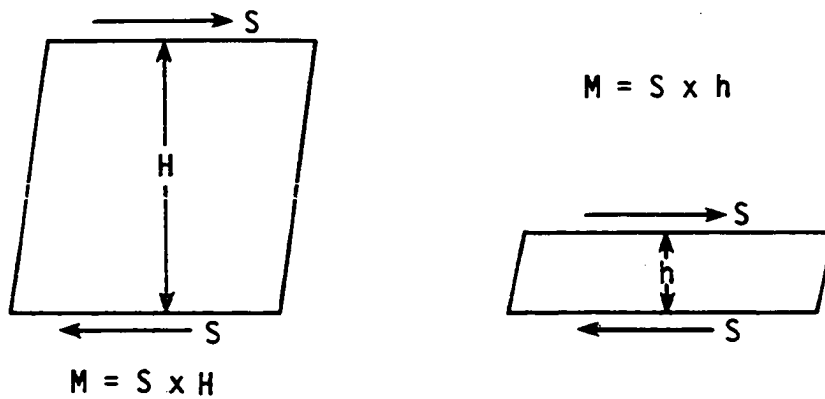$M = S \times h$

$M = S \times H$

Figure 10. Unbalanced moment in simple shear loading

Because of the complexity of the stresses developing along simple shear boundaries an accurate stress analysis is difficult to perform. However mathematical solutions for the particular boundary value problems suggest that the nonuniformities are localized and large portions of the specimens are under uniform stress conditions (65,67,42). For the purpose of the present work, simultaneous measurement of stresses and strains in only one direction was sufficient to describe the stress-strain-time relationships of the soils. Therefore no further attempt was made to investigate entire state of stresses and strains. In the analysis of the test results, the externally applied shear force was considered to result in a uniformly distributed shear stress on the horizontal planes; the stress-strain-time relationship of the specimens were characterized by this stress and the measured shear strains in the horizontal direction.

Testing Procedure

Clay samples which were originally sieved through number 200 standard sieve put through a number 80 sieve to eliminate lumps which might form during storage. The proper amounts of dry powder thus prepared and distilled water were mixed to obtain clay pastes at a predetermined moisture level. Water was added gradually while the samples were kneaded by hand. For lower moisture content specimens, water was added in excess of the amount predetermined. The excess moisture was then evaporated by air drying and kneading. This procedure eliminated the uneven moisture distribution. The moist batches were placed into polyethylene bags and cured at 100 percent relative humidity for at least 48 hours prior to
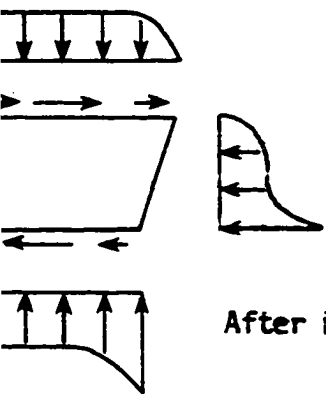
After Lucks et al. (42)

...ution at simple shear boundaries
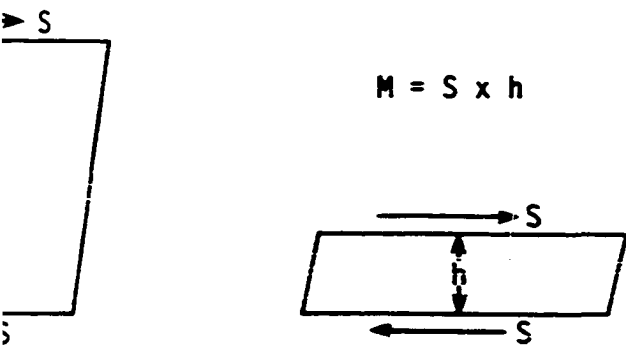
$M = S \times h$

...ment in simple shear loading

Bec...
shear bo...
However ...
suggest ...
specimer...
of the p...
only one...
lationsh...
vestigat...
test res...
in a uni...
stress-s...
this str...

Cla...
sieve pu...
during s...
tilled w...
level. .
For lowe...
amount p...
drying a...
distribu...
cured at...

UMI

testing. Predetermined weights of specimens were then removed and kept individually in plastic bags. The moisture contents of the specimens were determined, and the ones having moisture contents deviated approximately ±0.5 percent from the average moisture content of the particular test series were discarded to minimize moisture variations.

Before each test, the clearances along the hinges and between the side walls and shear gates of the shear box were covered with lubricated aluminum foil strips. This was necessary to prevent extrusion of the specimens during testing and to control drainage conditions.

The individual test specimens were kneaded by hand prior to molding into the shear box to eliminate possible thixotropic hardening effects. Molding was followed by an application of 15 psi normal pressure for 5 minutes to seat the specimens. After this step, the load and loading plate were removed, and the clay extruded through the clearances between loading plate and side walls of the apparatus was cleaned to eliminate friction development.

Prior to the application of normal stress the LVDT's monitoring the horizontal and vertical deformations of the specimens were calibrated mechanically by means of an ames dial. A lab lift (jack) was used for the application of the shear loads and care was taken not to impose impact effect to the specimens during the instantaneous application of the shear loads.

The shear deformations were recorded continuously on a Houston Omnigraphic Model 3000 strip chart recorder having a chart speed range of 0.06-24.00 inches per minute. A Houston Omnigraphic Model 2000 X-Y

recorder was used to record vertical deflections to compute volume changes against horizontal deformations.

The testing temperatures were limited to the range 10°C-65°C because of the following reasons. During preliminary tests, considerable moisture losses (in the order of 4 to 5% of the dry weight of the clay) were observed when the specimens were heated to temperatures above 65°C, and testing temperatures beyond this temperature were not employed. To obtain testing temperatures lower than the room temperature cold nitrogen gas was circulated in the asbestos housing unit surrounding the shear box. The temperature of the nitrogen gas was lowered by circulating it through liquid nitrogen prior to entering into the asbestos housing unit. At temperatures lower than 10°C, difficulties were met in supplying nitrogen gas and liquid nitrogen continuously during testing. Therefore 10°C was taken as the lower limit for the testing temperatures. Direct measurements of temperatures of the clay pastes placed in the shear box (specimens were covered by a thick film of grease on the top to prevent evaporation) showed that 105-120 minutes of initial heating was sufficient for the specimens to equilibriate with the highest testing temperature of 65°C. The equilibration time of 150 minutes was then adopted for all temperature ranges.

Experimental Program

The total of 111 creep tests were divided into two series B and C. In B series 35 tests were run on bentonite clay. In this series moisture content was kept constant and shear stress and testing temperature were

varied to study temperature and stress dependency of the creep rates. The C series includes 76 creep tests performed on Grundite clay. This series is divided into 5 groups C.1 to C.5 each corresponding to different moisture contents. Within each group all testing conditions were the same except shear stress and temperature. The test series and groups are summarized in Table 2.

Table 2. Test series

Series	Clay	Normal stress σ, psi	Average moisture content, M.C. % dry weight
B	Bentonite	6.0	70.5
C.1	Grundite	6.0	33.0
C.2	Grundite	6.0	35.6
C.3	Grundite	6.0	41.1
C.4	Grundite	6.0	46.0
C.5	Grundite	6.0	52.1

Difficulties were met with bentonite clay due to its highly thixo-tropic nature. Time and temperature dependency of thixotropic behavior presented difficulties in determination of strain rates at various tem-peratures for this clay. Although flow volume β' for the montmorillonite could be determined with confidence, the other parameters A and ΔH^* could not, due to variation of structure with temperature (accelerated thixo-tropic hardening with increasing temperature). This could be remedied by curing all the samples at the highest test temperature until the attain-

ment of constant structure. However ΔH* determined in this way would apply to thixotropically hardened montmorillonite. A study of thixotropic hardening mechanism of montmorillonite should be undertaken first. Because of time limitations this study was not undertaken. For these reasons discussion of montmorillonite is put in Appendix A as a separate entity. To formulate the rate process theory for stable clay water systems the main thrust of the work was aimed at Grundite-Illite clay which seemed to be free of these problems.

Scanning Electron Microscopy Studies

SEM studies require that the clays or soils be dry when they are placed in the instrument. The observations are significant only if the solid state is observed in the same condition at which it exists when the water is present. Clay water systems are colloidal systems and the removal of the water phase without disturbing the original fabric is a formidable problem (89,25). Among the techniques available which include oven-drying, vacuum-drying, air-drying, substitution-drying, super-critical drying and freeze drying, freeze drying has been shown to result in least sample disturbances (89,25). In the present investigation the freeze drying technique described by Tovey et al. (89) and Erol et al. (25) was selected as the method of specimen preparation for SEM studies.

In this method, isopentane which is first cooled down to its freezing point of -160°C is used as the freezing medium. This was achieved by immersing glass jars filled with isopentane in liquid nitrogen and keeping them in liquid atmosphere for about 10 minutes. Then small pieces of clay

water mixes (approximately 1 gram) placed in small aluminum dishes were immersed into this cold isopentane. To assure complete freezing, the specimens were kept in isopentane for approximately 2 minutes. Direct measurements by Tovey et al. (89) indicate that the specimen temperatures of -150°C can be achieved within 15 seconds after the specimens were immersed in isopentane.

Sublimation was achieved in a Virtis freeze drying apparatus in which the samples were held under a vacuum of 2 to 5 x 10^{-4} torr at a temperature of -60°C for 24 to 48 hours. The freeze dried samples were then fixed on the stubs and coated first with carbon and then with gold about 200 to 300 Å thick in a Danton vacuum evaporator.

Peeling technique described by Dides (76) was employed to eliminate the presence of loose particles, which may obscure the original fabric features from surfaces. For this purpose an adhesive tape was applied to the surface of the specimens approximately 100 times.

A model JSM-U3 scanning electron microscope was used at an accelerating voltage of 25 KV throughout the study.

RESULTS, ANALYSIS, AND DISCUSSION

Method of Analysis

A finite number of data points were selected from continuously re-corded charts to represent the deformation versus time curves recorded in all creep tests. These points were chosen in such a manner that the portion of the time deformation data which was defined by two successive data points was approximately a straight line. By this approximation to the continuously recorded curve it was possible to calculate the first derivative of the shear strain with respect to time as follows:

$$\dot{\gamma}_{(2i+1)/2} = \frac{\gamma_{i+1} - \gamma_i}{t_{i+1} - t_i} \qquad \text{(Eq. 3)}$$

where t_i and t_{i+1} are the time, and γ_i and γ_{i+1} are the strains corre-sponding to two successive points on the recorded curve. Then the strain rate at the time $(t_i + t_{i+1})/2$ or at the strain $(\gamma_i + \gamma_{i+1})/2$ is given by $\dot{\gamma}_{(2i+1)/2}$. A 9100 B Hewlett-Packard computer was employed to obtain printout values of the time versus strain and the strain rate versus time and strain.

This method is an approximation since the slope of the strain versus time curve is computed for an increment of the curve and reported as the strain rate at a point. However by choosing data points at proper time intervals, the precision of the calculations can be made adequate for the intended purpose. Figure 11 shows the data scatter from the smooth curve thus illustrating the magnitude of reading errors involved in the proce-dure described. For all creep tests, it was possible to fit continuous
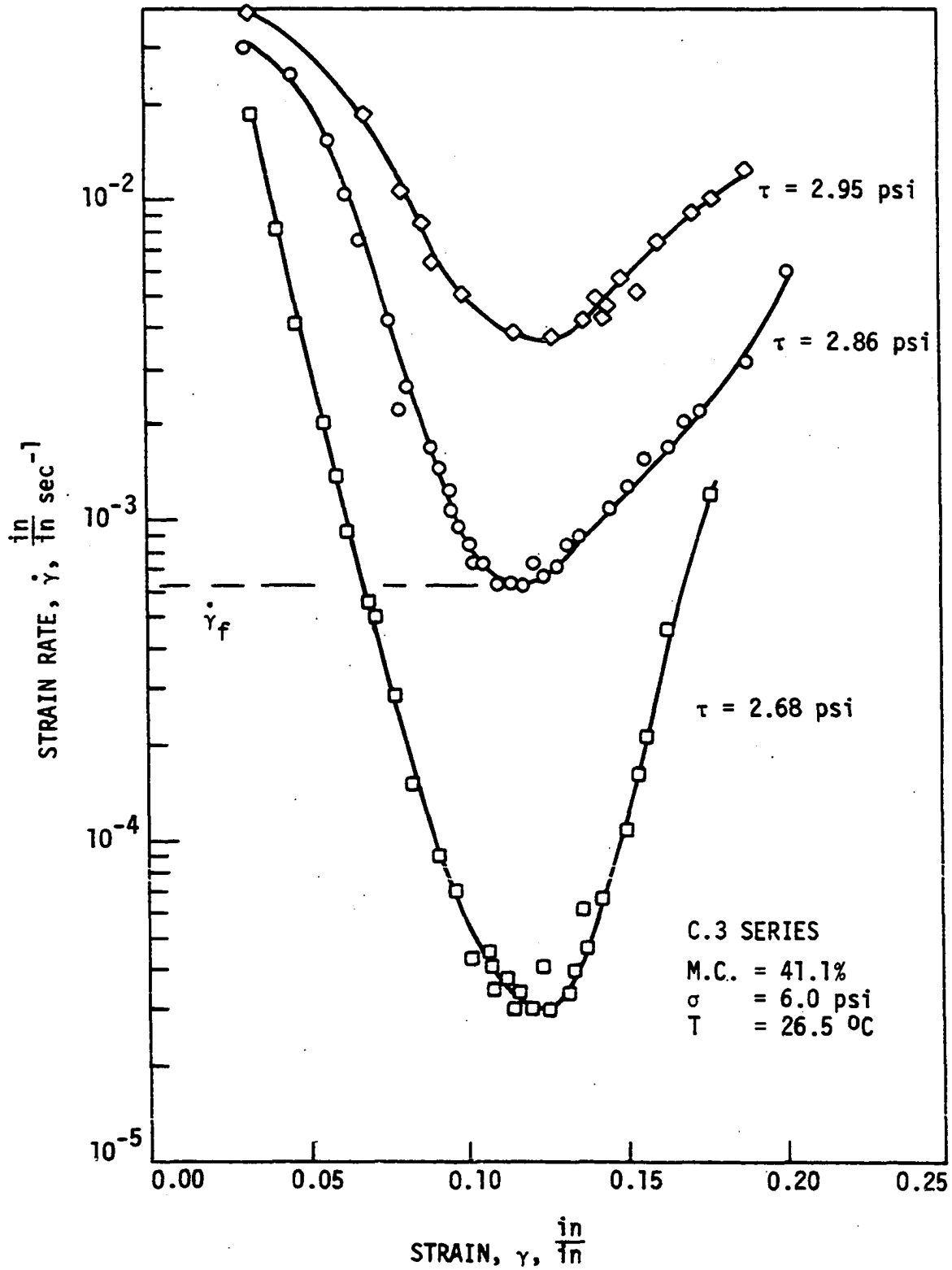
Figure 11. Typical strain rate versus strain plots

curves to the calculated data points by eliminating the few scattered points which reflected the reading errors.

The time versus strain, the logarithm of strain rate versus strain and the logarithm of strain rate versus logarithm of time plots were then made and used as the primary data for further analysis. Because of the large number of tests and very large number of individual data points obtained for each test, it is not practical to include all of the primary data from all tests in either tabular or graphical form, only tables of observed quantities and representative graphs have been included for each type of analysis.

The minimum strain rates, $\dot{\gamma}$, which occurred in tertiary creep curves, were determined from the minima of log $\dot{\gamma}$ versus γ plots as shown in Figure 11. Two different γ_f (the strain corresponding to $\dot{\gamma}_f$ on creep curves) were determined independently. First, the strain magnitudes corresponding to minimum strain rates on log $\dot{\gamma}$ versus γ plots were found as shown in Figure 11. Secondly, values of γ_f were determined by using strain-time curves on which approximately linear segments were observed around inflection points (approximate tangent to the curve) and the strains corresponding to the centers of these segments were taken as the second approximation for γ_f. The averages of the two, which appeared to be close to each other in most of the tests, were taken as representative values for γ_f. Table 3 shows the agreement between two procedures followed to determine γ_f values in C.4 series.

Table 3. γ_f values in C.4 series

Test No.	γ_f, in/in, from γ vs. t plots	γ_f, in/in, from Log $\dot{\gamma}$ vs. γ plots	γ_f, in/in average
C.4.1	8.53×10^{-2}	8.50×10^{-2}	8.52×10^{-2}
C.4.2	9.35×10^{-2}	9.15×10^{-2}	9.20×10^{-2}
C.4.3	8.00×10^{-2}	7.60×10^{-2}	7.80×10^{-2}
C.4.4	9.40×10^{-2}	9.00×10^{-2}	9.20×10^{-2}
C.4.5	6.15×10^{-2}	6.20×10^{-2}	6.18×10^{-2}

The time of occurrence of the minimum strain rates were determined by reading the time corresponding to γ_f on the strain time plots. The primitive model strains corresponding to a given time t were then calculated by the following relationships:

$$\gamma_m = \gamma_i^* + \dot{\gamma}_f \, t \qquad \text{(Eq. 4)}$$

$$\gamma_i^* = \gamma_f - \dot{\gamma}_f \, t_f \qquad \text{(Eq. 5)}$$

where t_f is the time of occurrence of γ_f (and $\dot{\gamma}_f$), γ_i^* is the primitive model initial strain at zero time and γ_m is the primitive model strain at time t. Combining Equations 4 and 5, the following relationship is obtained:

$$\gamma_m = \gamma_f - \dot{\gamma}(t-t_f) \qquad \text{(Eq. 6)}$$

Mobilization ratios M and rupture ratios R were found by taking ratios of the experimental creep strains, γ_c, to primitive model strains, γ_m calculated from Equation 6. The ratios M and R were plotted against the strains for each test. Then it was possible to determine the time, strain

and strain rates for a particular value of M (or R) ratio. Typical M or R versus strain curves are shown in Figure 12.

The strains and strain rates in the initial portion of the creep curves were found to be affected by the uncontrollable experimental errors involved in the instantaneous application of the creep shear stress. Therefore the mobilization ratios smaller than 0.30 were affected by these experimental errors. In addition, the strains progressed rapidly and subsequently the strain rates were high and difficult to evaluate during late tertiary creep deformations. Due to these facts the mobilization ratios of 0.4-1.0 and rupture ratios of 0.0-0.3 were considered in the analysis of the test results.

Test Results

In both B and C series tests which were run using bentonite and grundite clay respectively, both the terminal and tertiary creep be-haviors, depending on the stress level, were observed within the 24 hours of shearing time allowed for the specimens. Typical time deformation curves as examples of the terminal and tertiary creeps are shown in Figure 13.

For the tertiary creep curves logarithm of strain rates corresponding to the same M and R ratios were plotted against shear stresses and are shown in Figures 14 to 21 for the C series. The slopes of the straight lines on these plots are equal to the coefficient β in Equation 1. The Figures 21 to 27 show the plots of log strain rates at equal M and R ratios versus reciprocal of absolute temperatures for C.1, C.3 and C.4
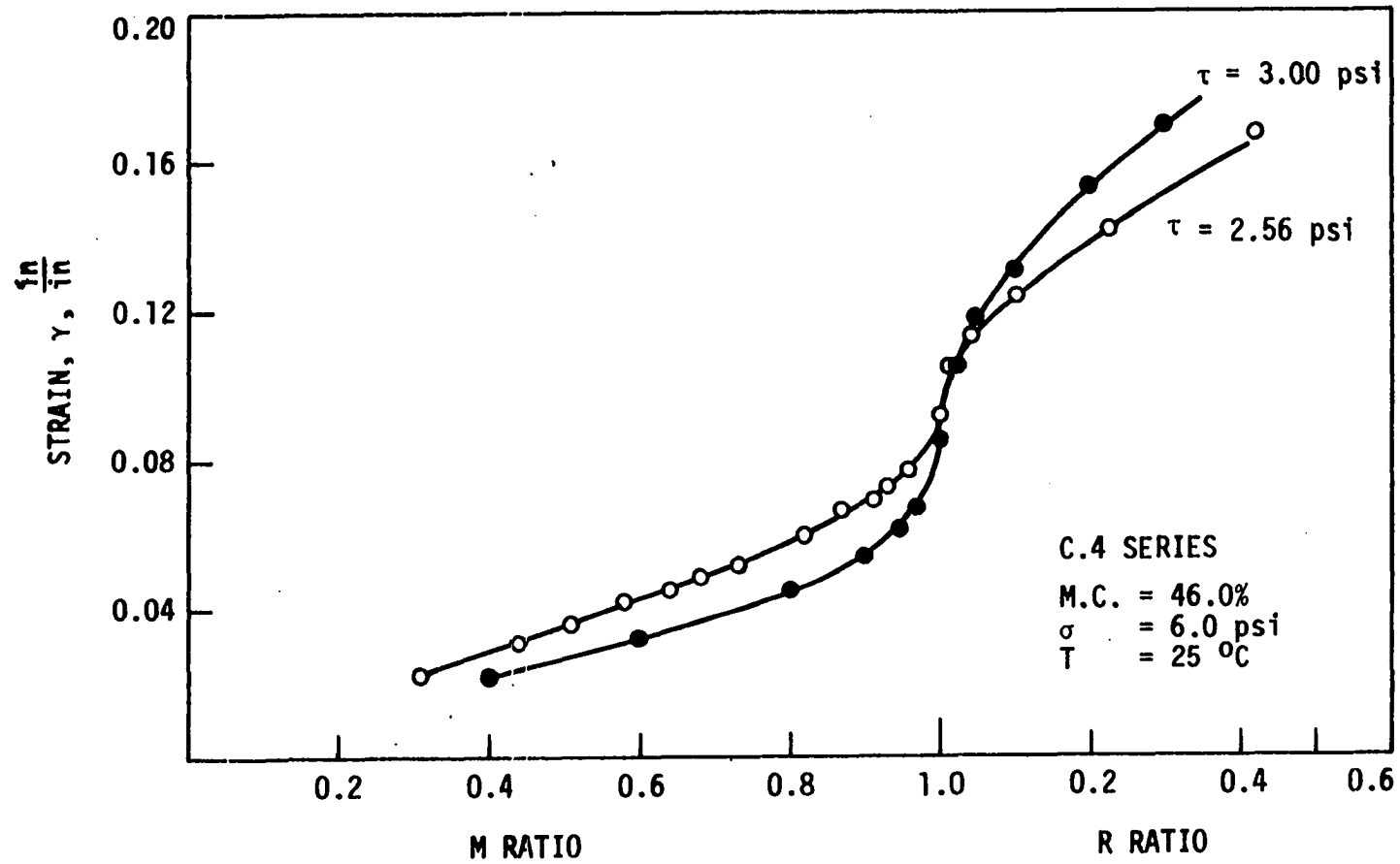
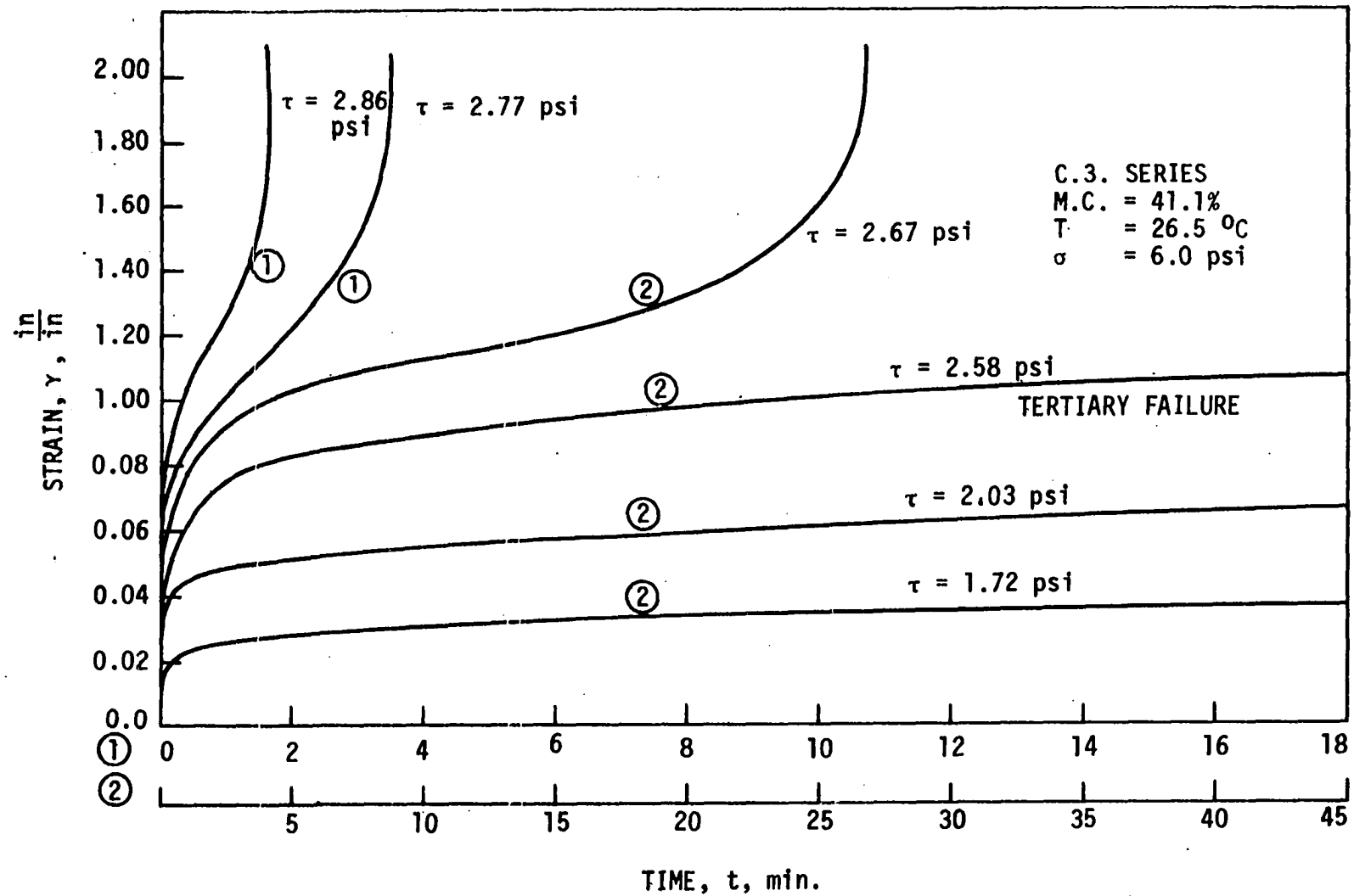Figure 12.   Typical mobilization-rupture ratios versus strain plots

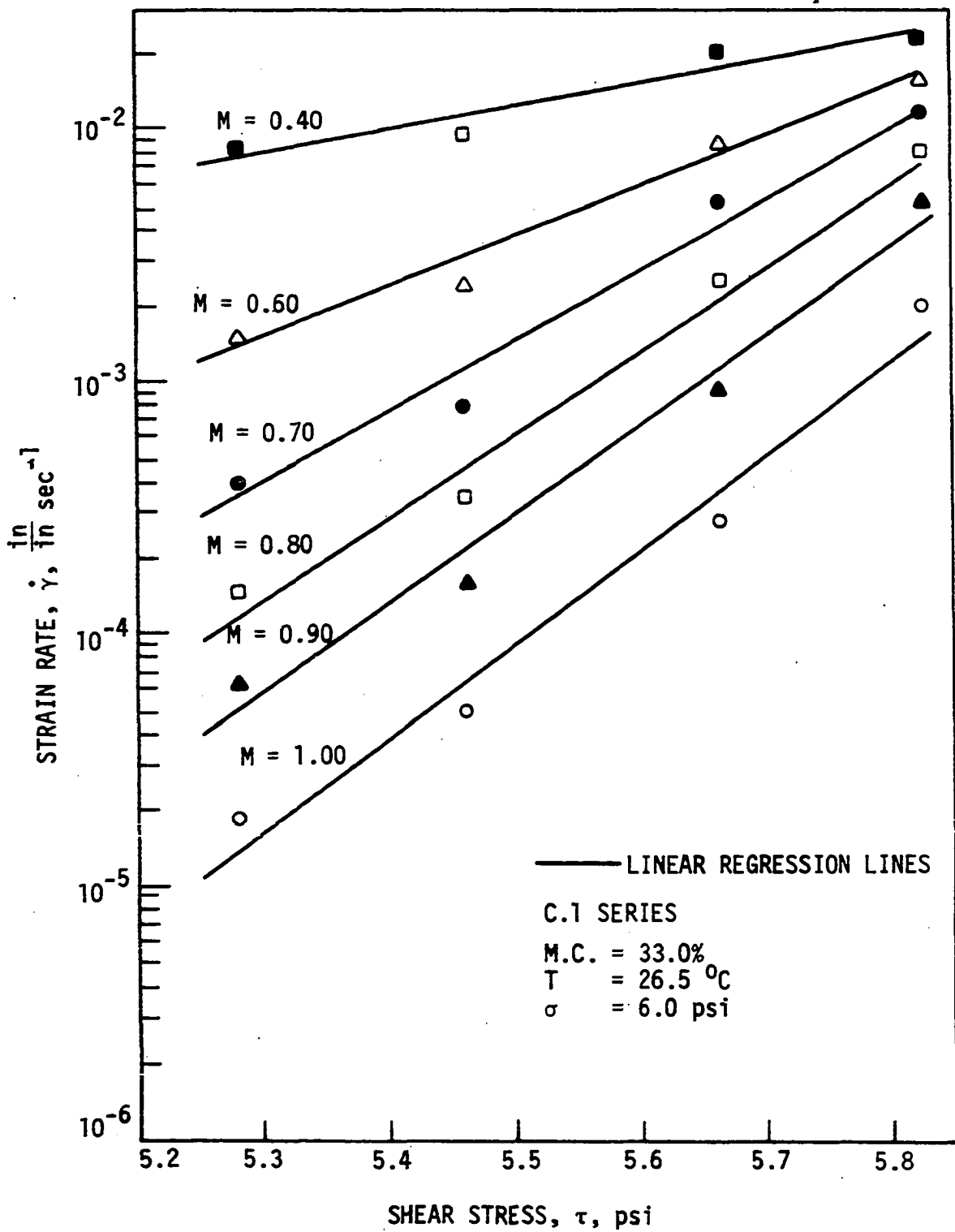Figure 13. Time deformation curves of Grundite clay, C.3 series

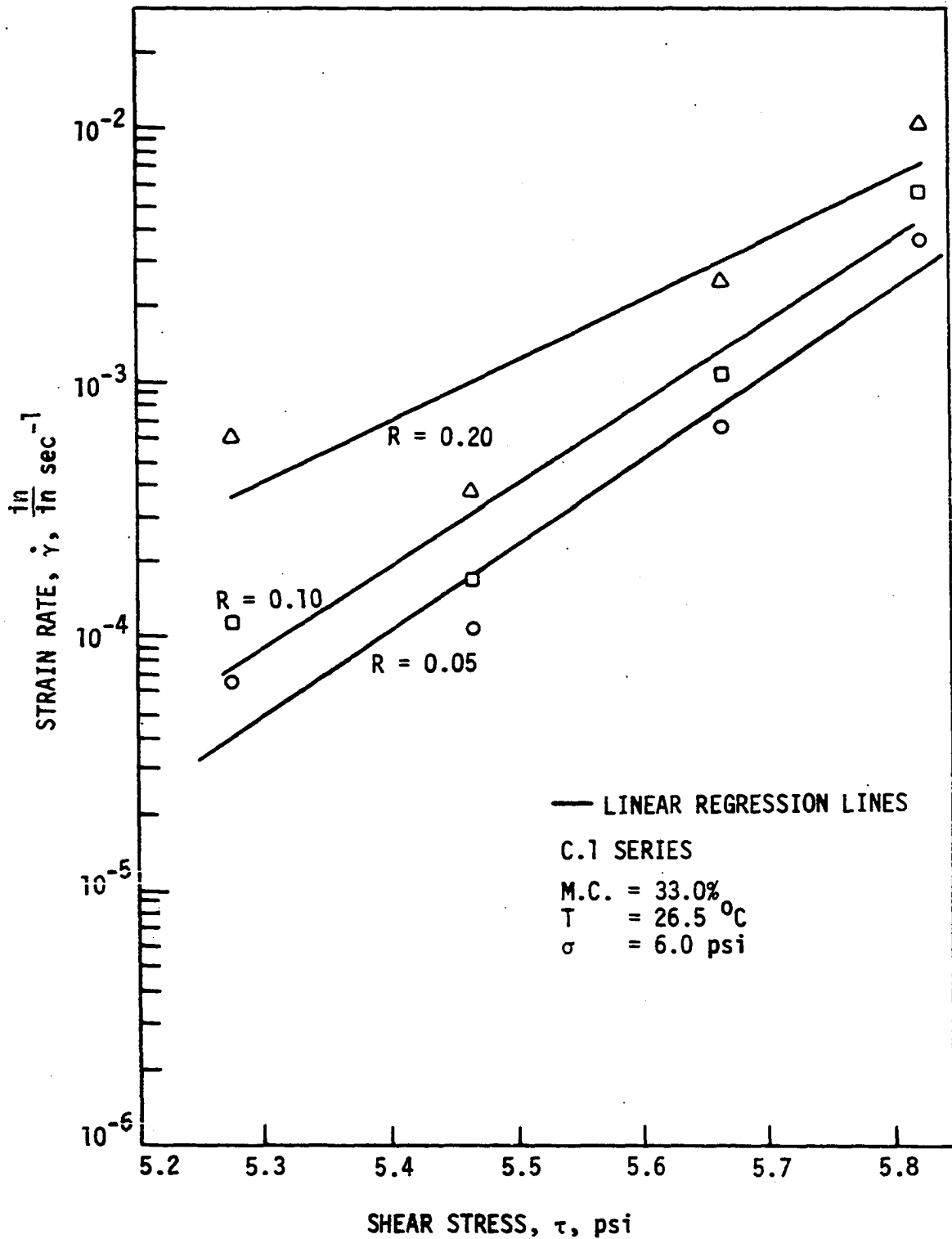Figure 14. Plots of shear stress τ versus strain rate γ̇ at various mobilization ratios M for C.1 series

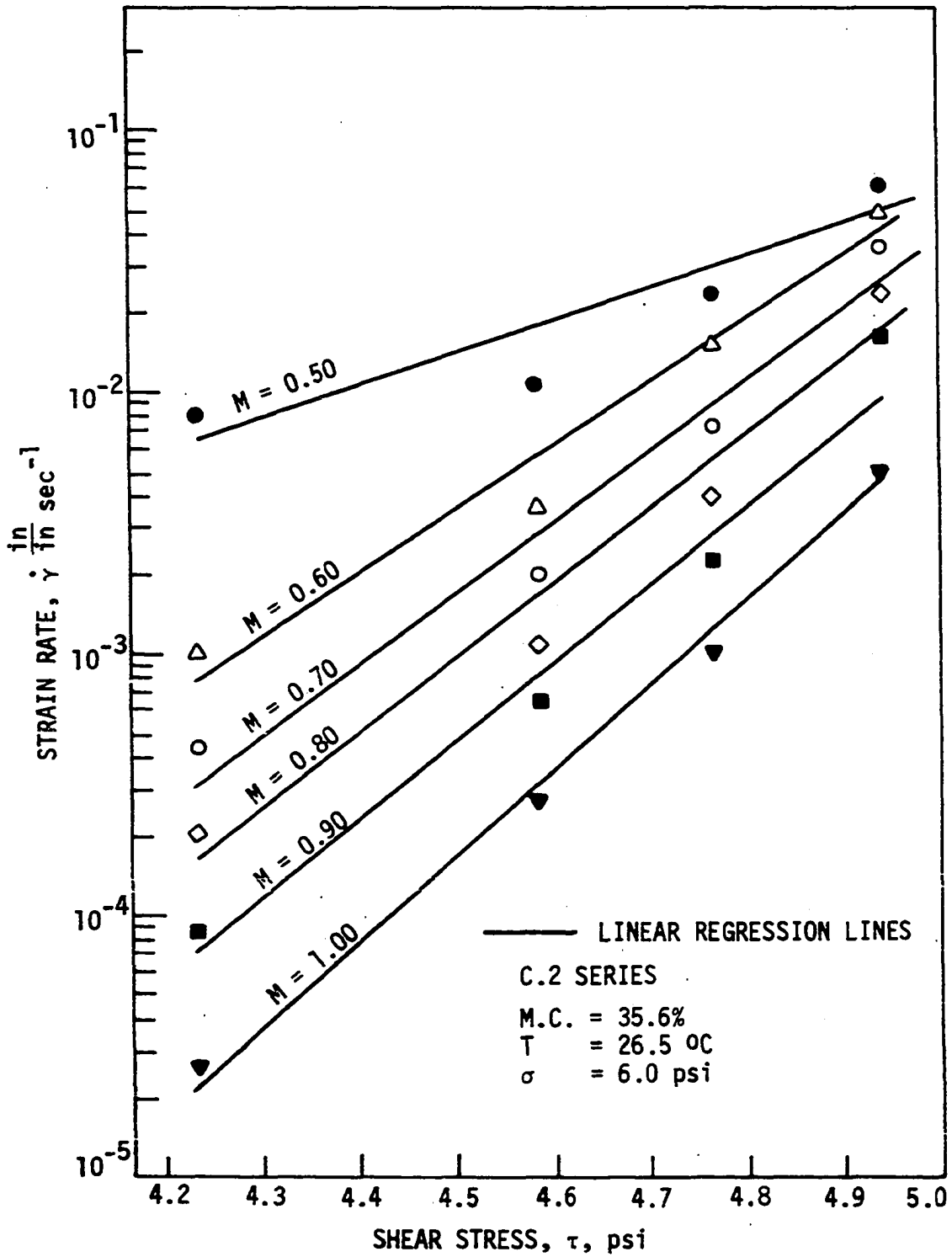Figure 15. Plots of shear stress τ versus strain rate γ̇ at various rupture ratios R for C.1 series

Figure 16. Plots of shear stress τ versus strain rate γ̇ at various mobilization ratio M for C.2 series

Figure 17. Plots of shear stress τ versus strain rate γ̇ at various rupture ratios R for C.2 series

Figure 18. Plots of shear stress τ versus strain rate γ̇ at various mobilization ratios M for C.3 series
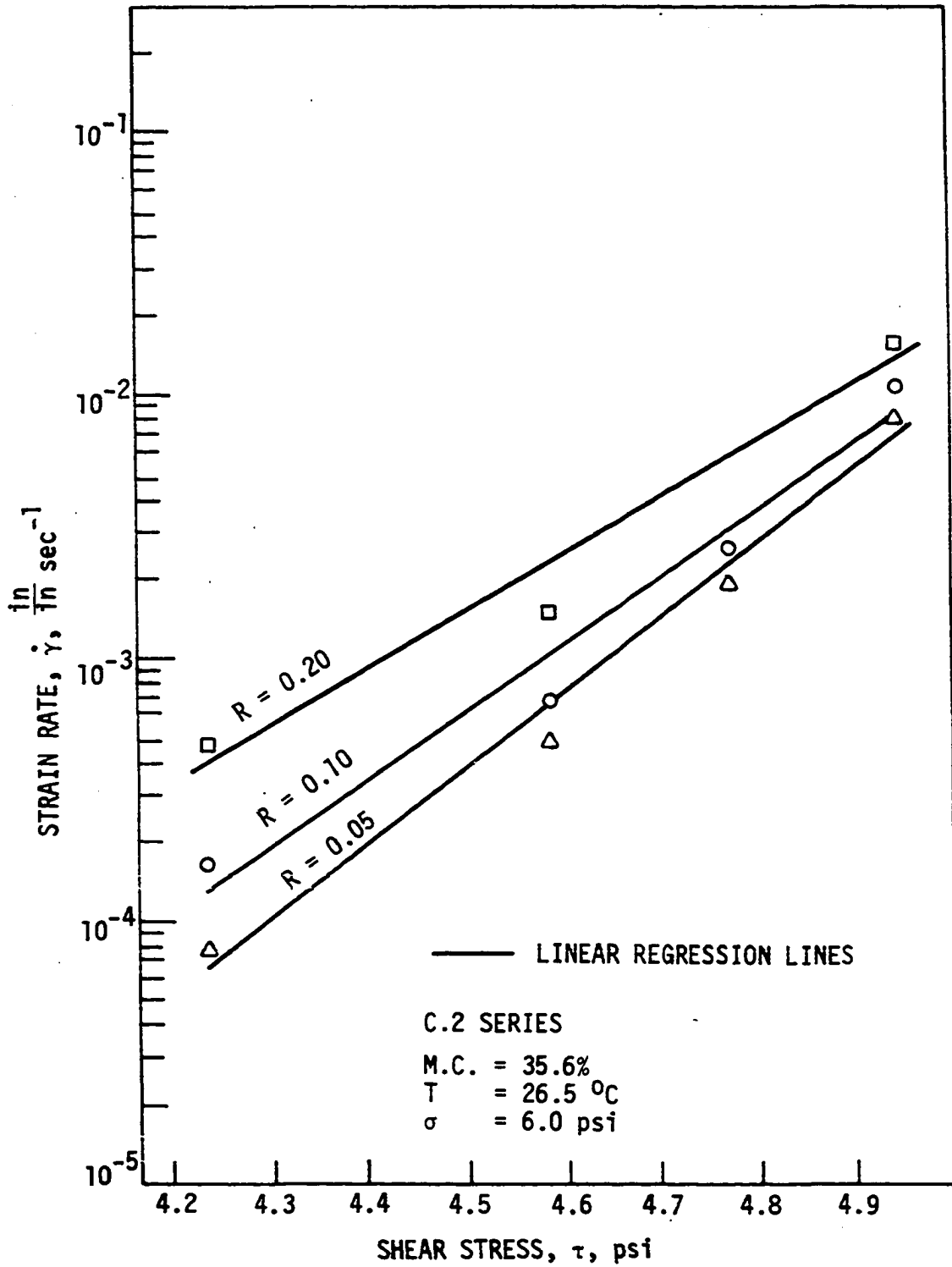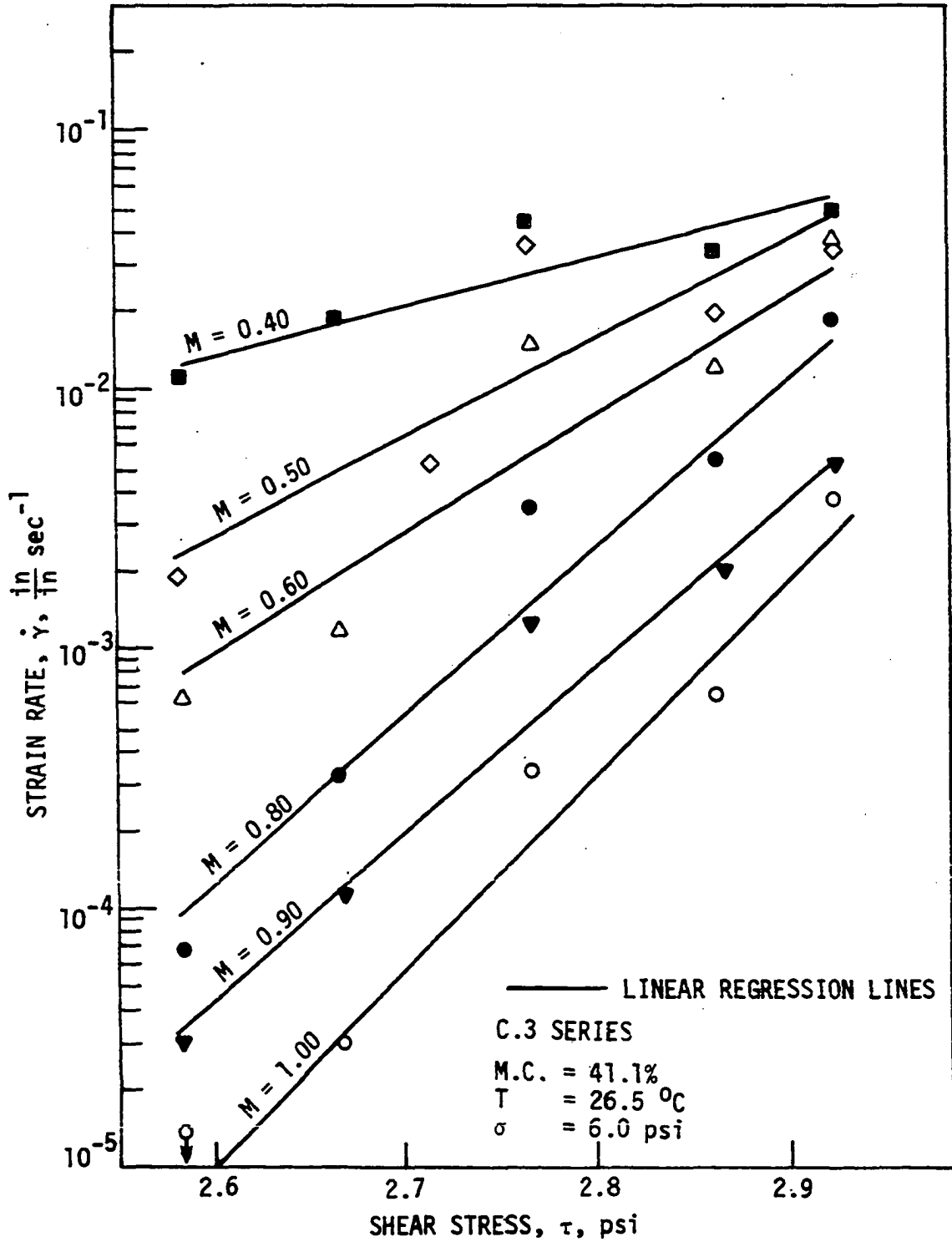
Figure 19. Plots of shear stress τ versus strain rate ẏ at various rupture ratios R for C.3 series
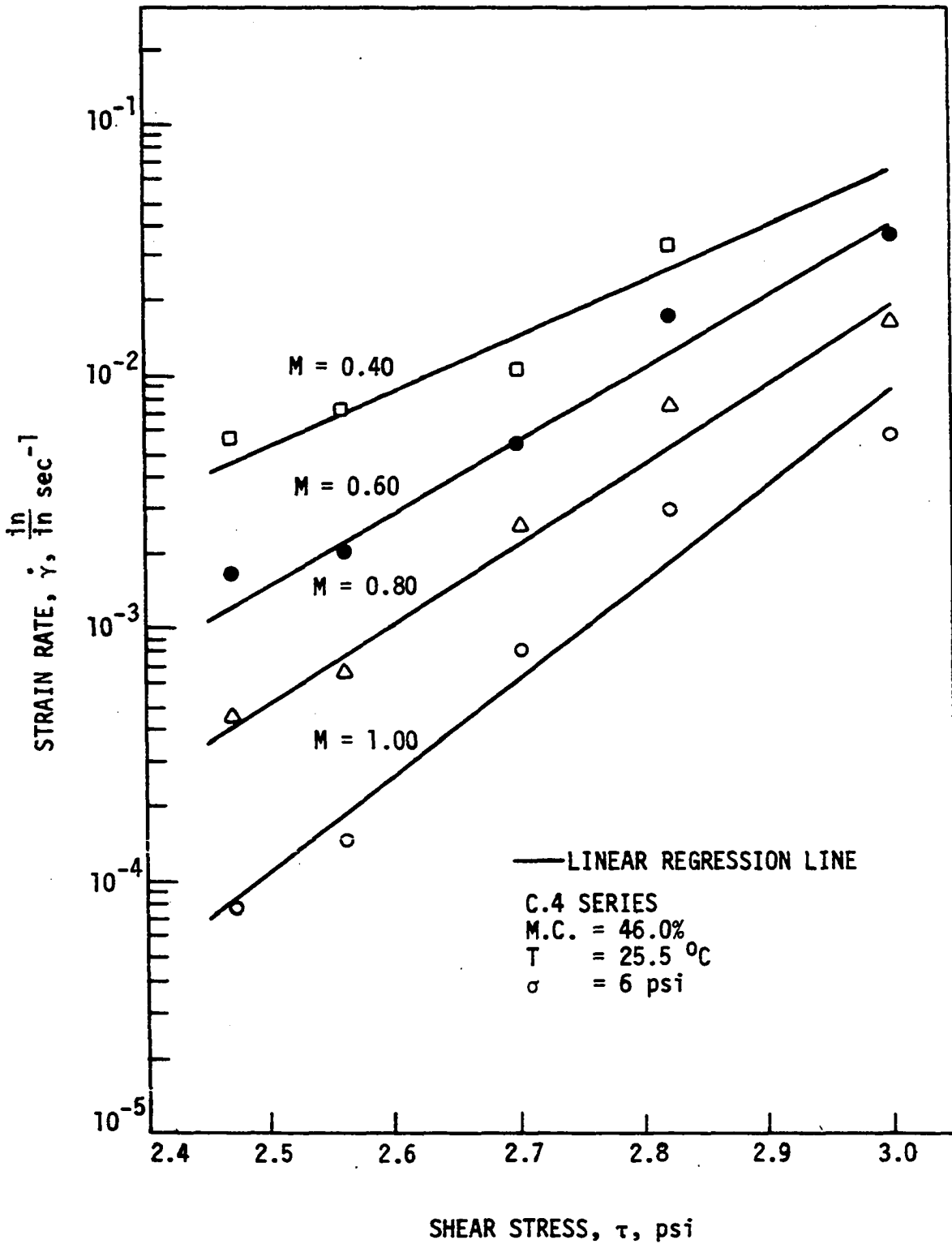
Figure 20. Plots of shear stress τ versus strain rate γ̇ at various mobilization ratios M for C.4 series

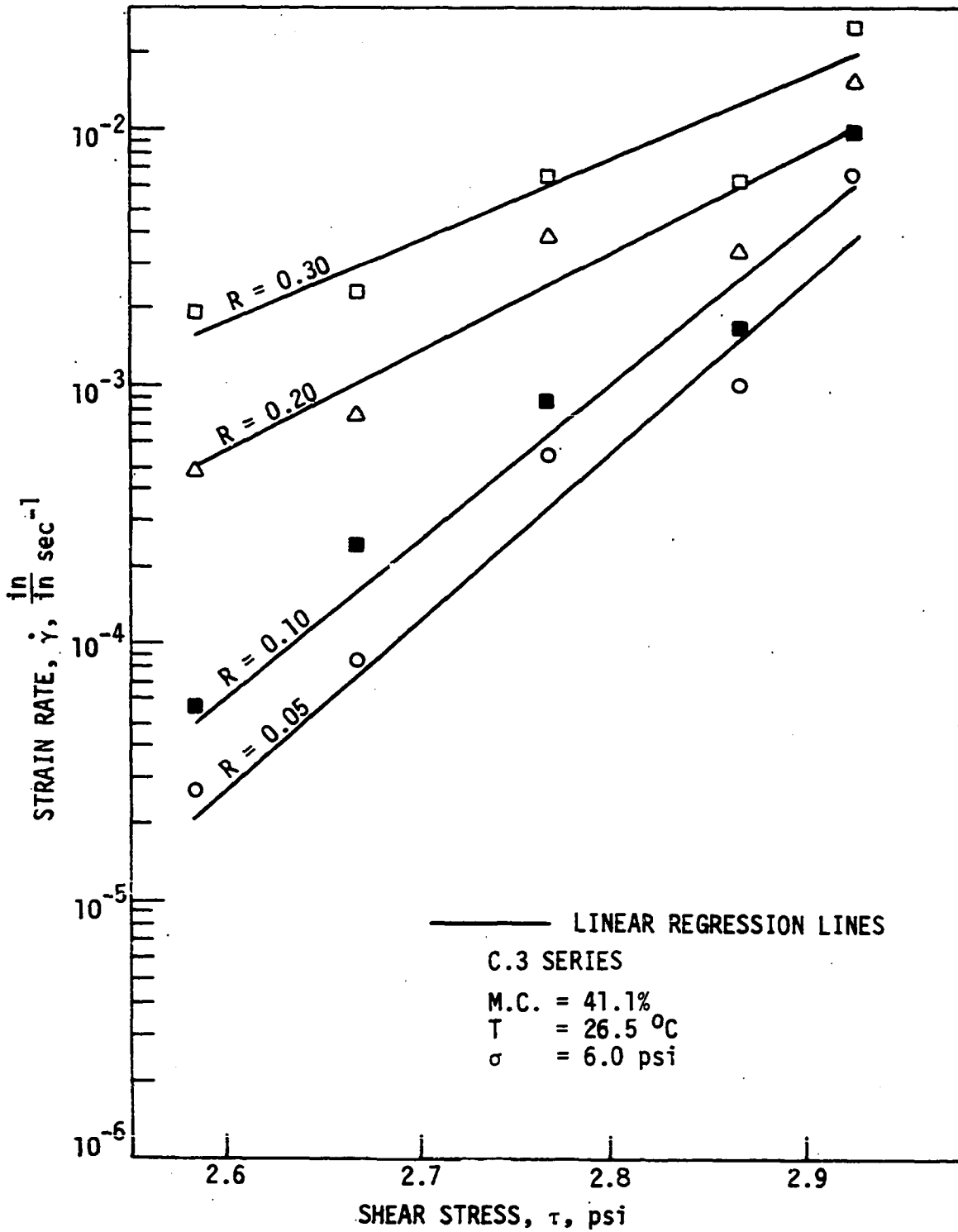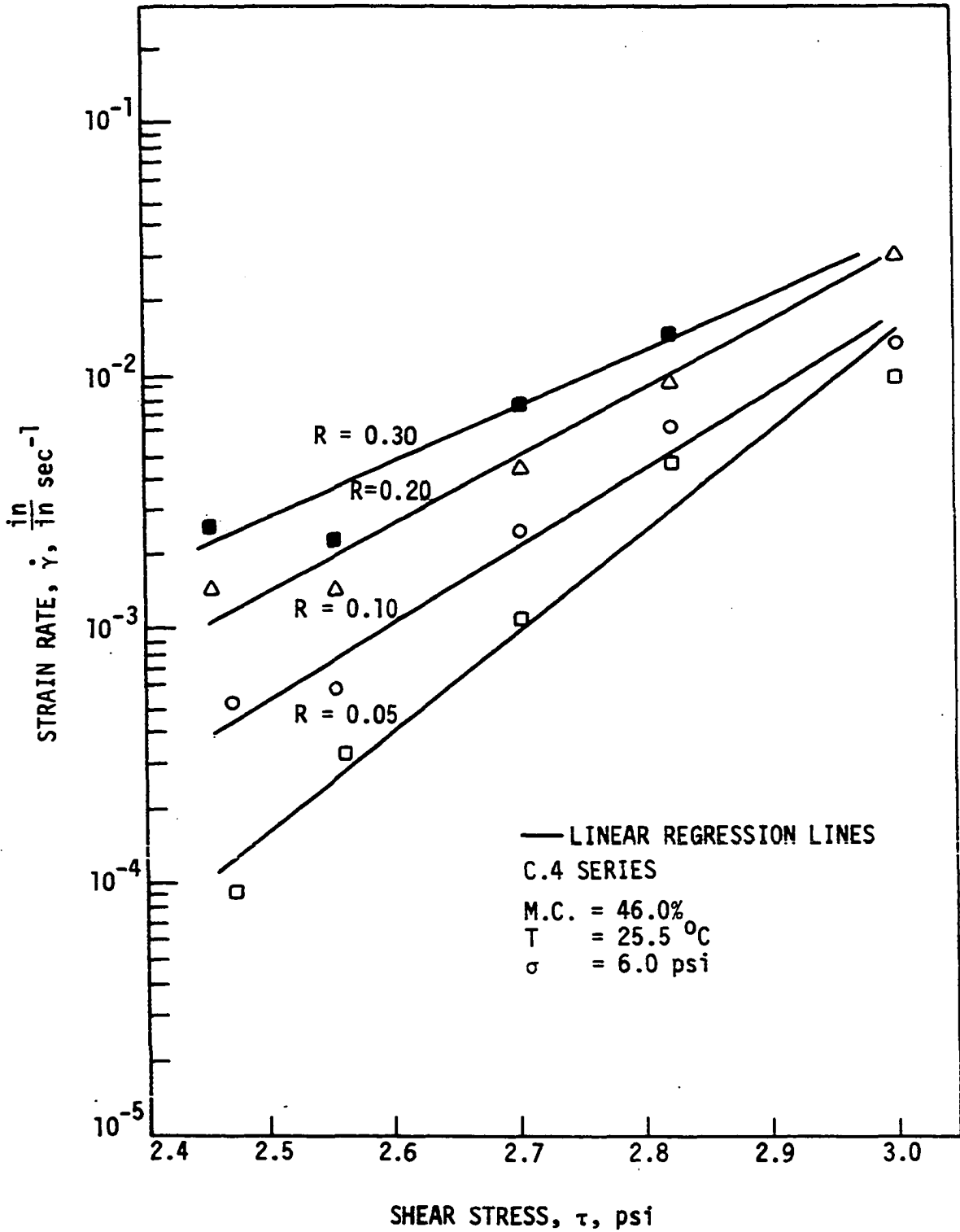Figure 21. Plots of shear stress τ versus strain rate γ̇ at various rupture ratios R for C.4 series

Figure 22. Plots of reciprocal of absolute temperature $\frac{1}{T}$ versus strain rate $\dot{\gamma}$ at various mobilization ratios M for C.1 series

Figure 23. Plots of reciprocal of absolute temperature $\frac{1}{T}$ versus strain rate $\dot{\gamma}$ at various rupture ratios R for C.1 series

Figure 24. Plots of reciprocal of absolute temperature $\frac{1}{T}$ versus strain rate $\dot{\gamma}$ at various mobilization ratios M for C.3 series

Figure 25. Plots of reciprocal of absolute temperature $\frac{1}{T}$ versus strain rate $\dot{\gamma}$ at various rupture ratios R for C.3 series
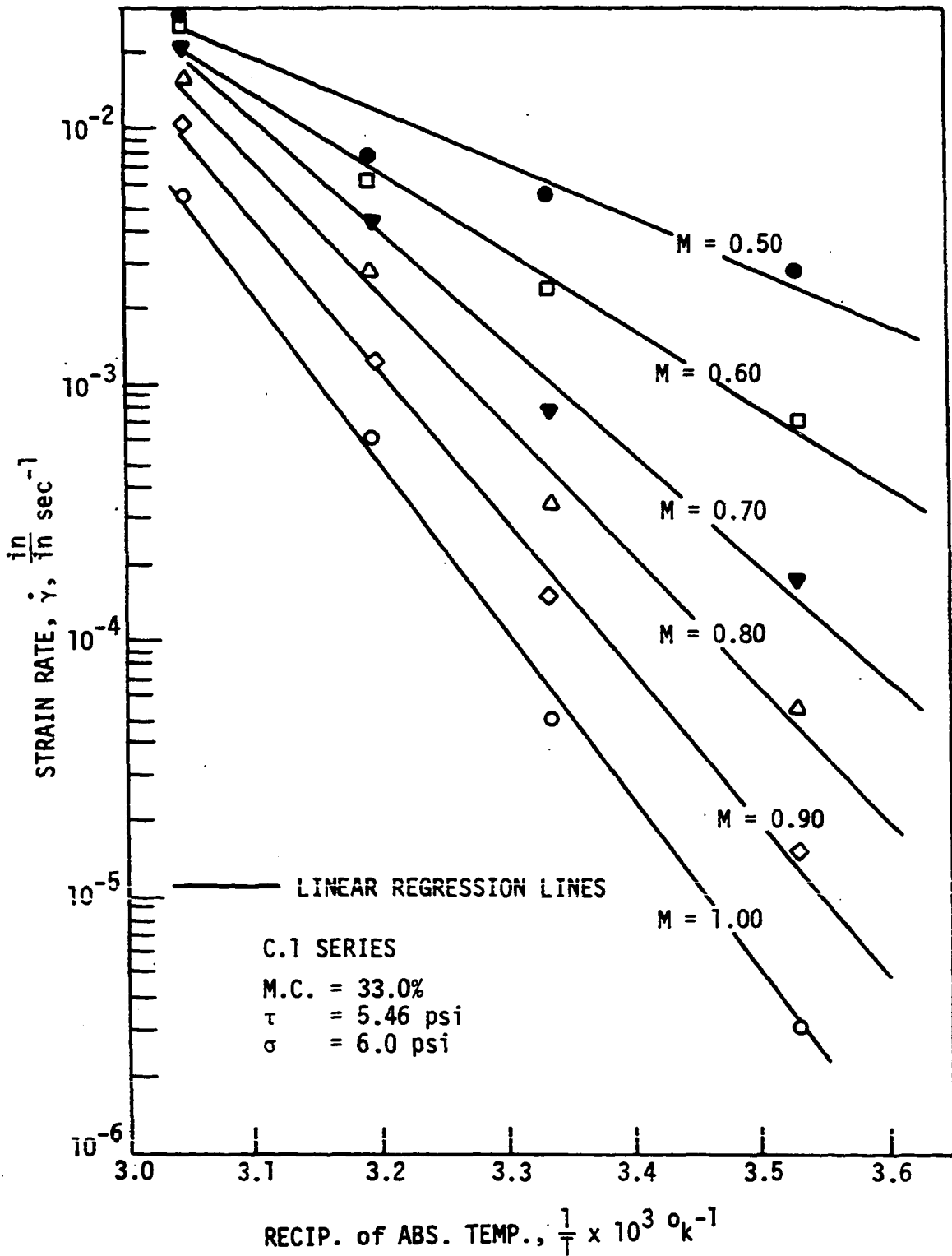
Figure 26. Plots of reciprocal of absolute temperature $\frac{1}{T}$ versus strain rate $\dot{\gamma}$ at various mobilization ratios M for C.4 series
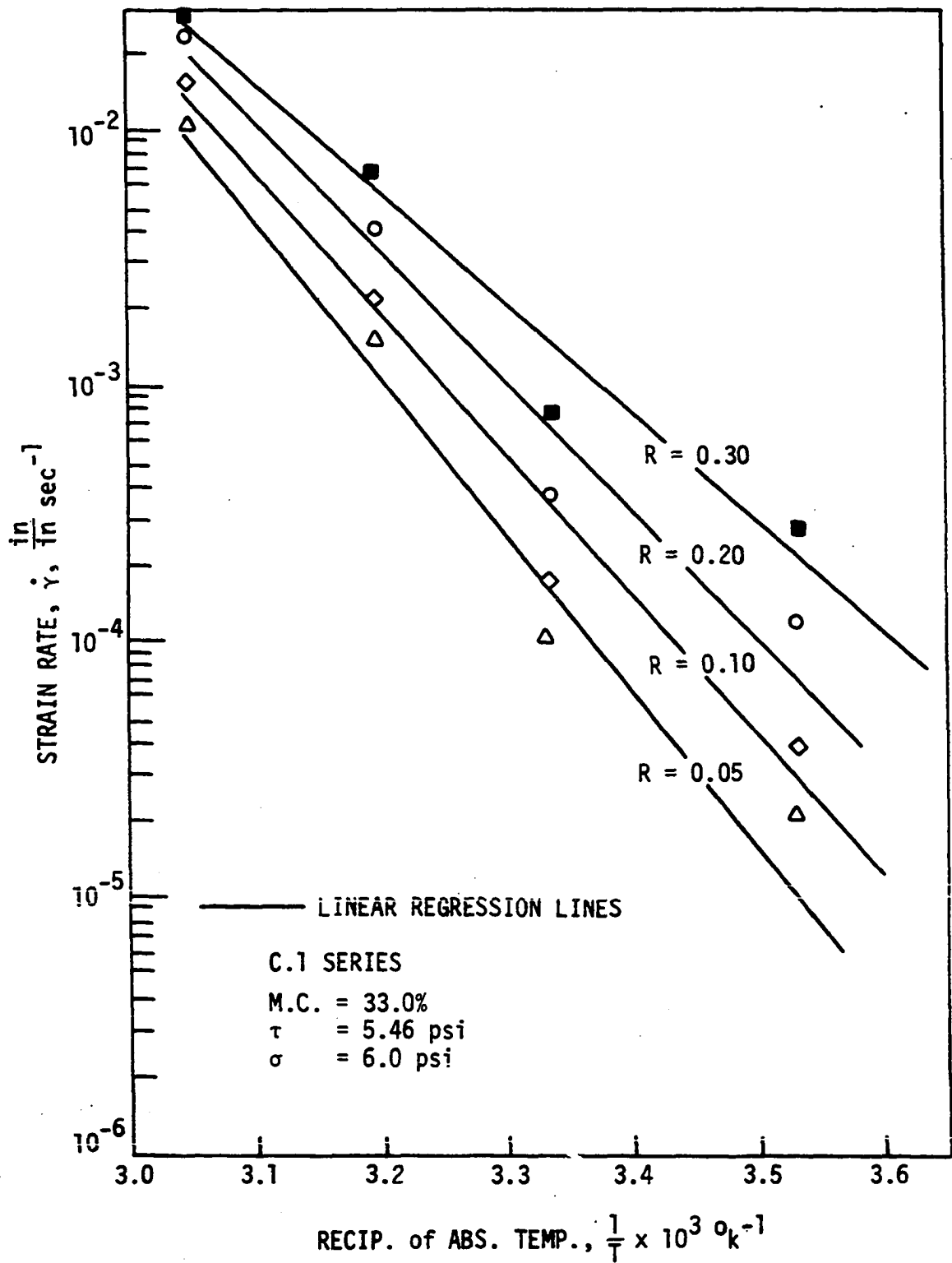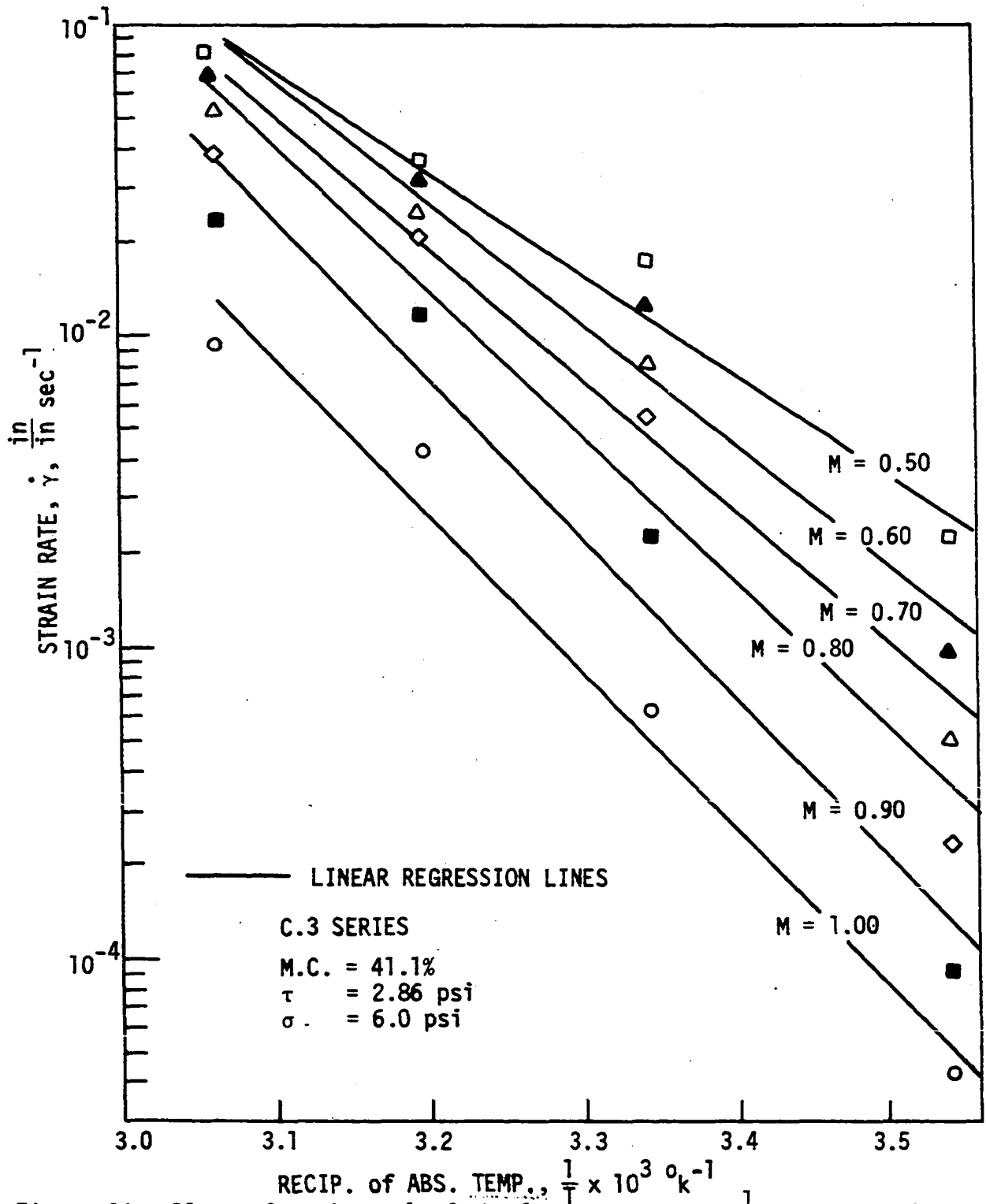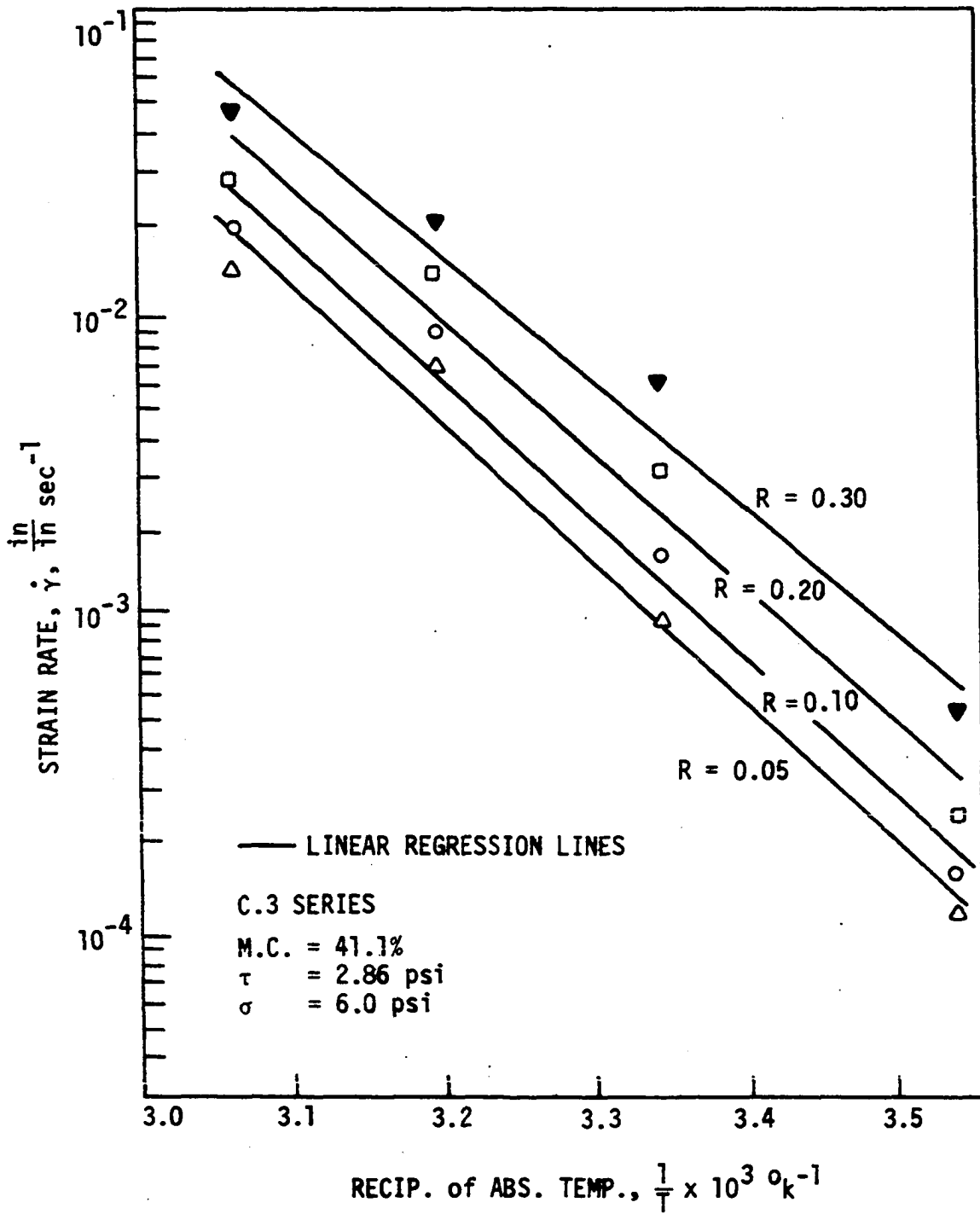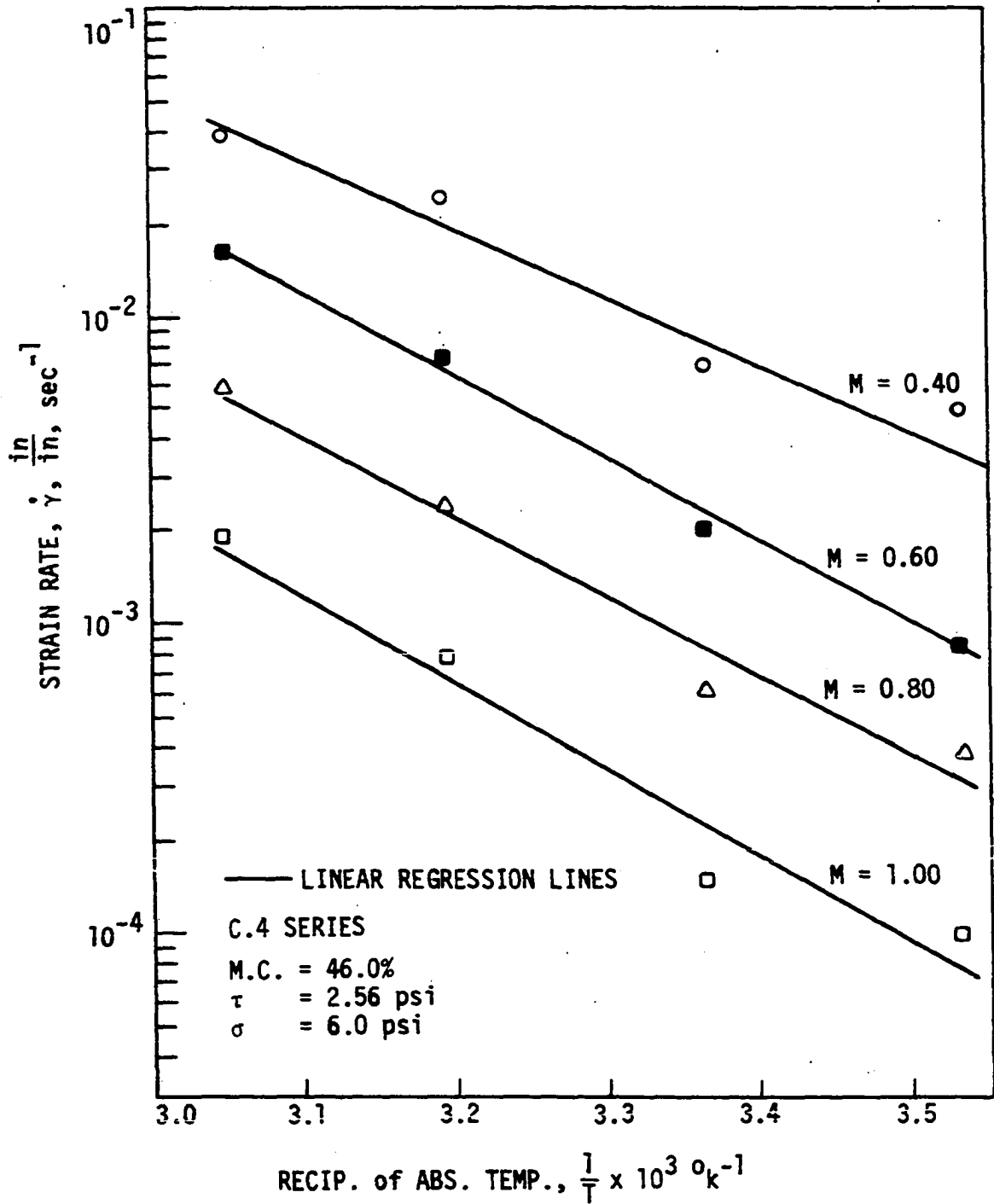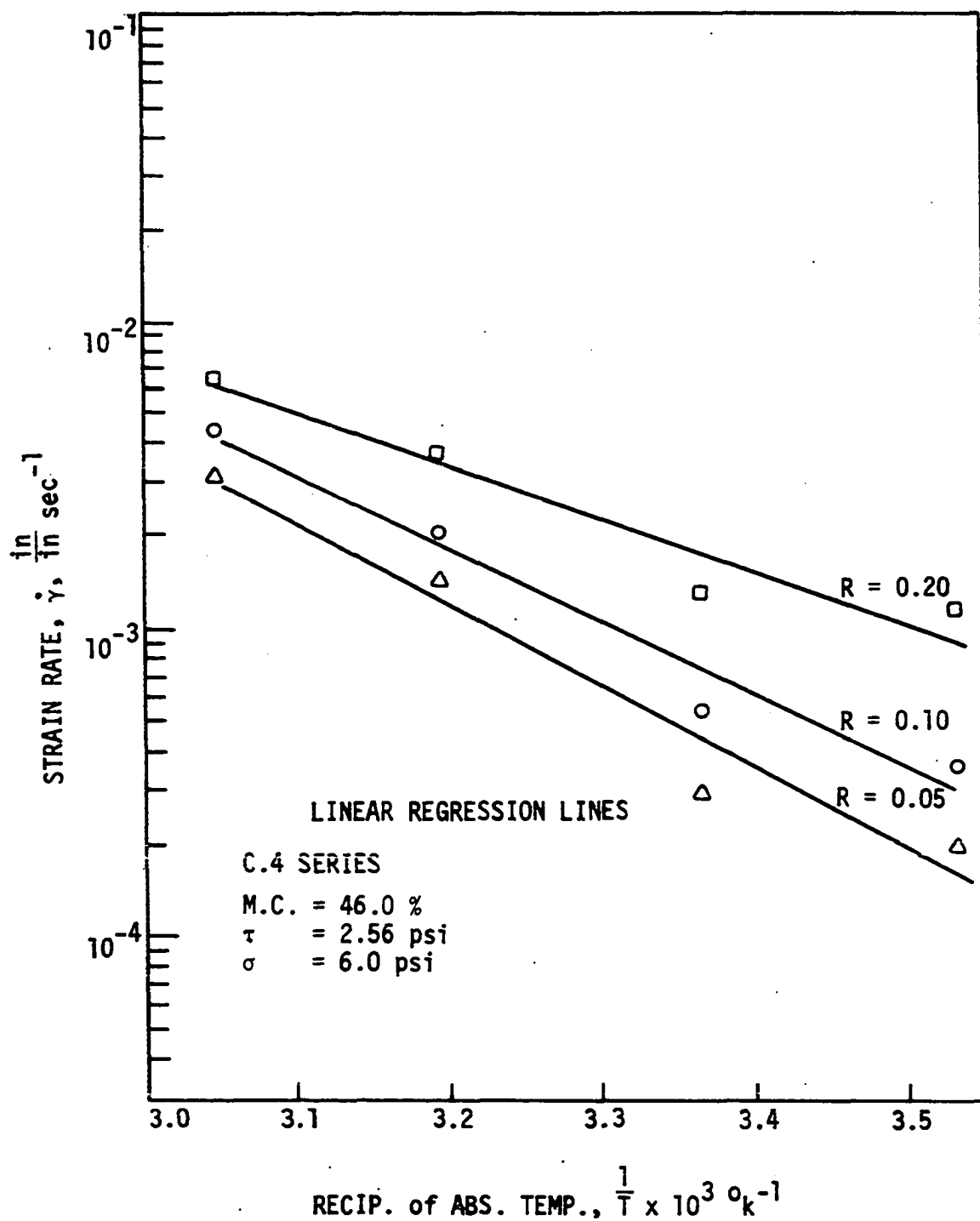
Figure 27. Plots of reciprocal of absolute temperature $\frac{1}{T}$ versus strain rate $\dot{\gamma}$ at various rupture ratios R for C.4 series

group tests. The tests included in these plots were run at different temperatures and at a fixed level of shear stress, therefore the slope of the straight lines gives the value of $\frac{\Delta H^*}{k}$ in Equation 1.

The best fitting straight lines to the experimental points were found by least squares regression analysis and the results of the analysis are summarized in Tables 4 to 7. In the present investigation, the basic assumption made was the occurrence of equivalent soil structures at points of equal mobilization and rupture ratios. This assumption is supported by the linearity of the log $\dot{\gamma}$ versus τ and log $\dot{\gamma}$ versus $\frac{1}{T}$ plots shown in Figures 14 to 21 and high correlation coefficients, r (close to 0.99 in most cases), given in Tables 4 to 7. Relatively low values of r (0.92-0.95) corresponding to M and R values of 0.4-0.5 and 0.2 to 0.3, respectively, reflected the limitation of the method employed to calculate the strain rates. The time intervals between the successive data points were kept small so that for highly curved portions a closer approximation to linearity could be achieved. The error in strain rate is equal to the ratio $\frac{\delta\gamma}{\Delta t}$ where $\delta\gamma$ is the reading error in strains and Δt is the time interval between two successive data points. Since magnitude of $\delta\gamma$ is the same for all points, smaller time intervals resulted in higher ratios of $\frac{\delta\gamma}{\Delta t}$.

For each mobilization and rupture ratio, the flow volumes β', activation enthalpies ΔH^* and proportionality constants A were calculated from the slope and intercept values listed in Tables 4 to 7. These values are given in Tables 8 and 9. The values of β', ΔH^* and log A were then plotted against the M and R ratios and are shown in Figures 28 to 32.

Table 4. C.1 series creep parameters

| M or R | Regression analysis | | | | | |
| | log $\dot{\gamma}$ vs. τ | | | log $\dot{\gamma}$ vs. 1/T | | |
	Slope β	Intercept C_1	Corr. Coeff. r	Slope $\Delta H^*/k$	Intercept C_2	Corr. Coeff. r
M=0.40	0.935	-5.049	0.968	-1.149×10^3	3.902	0.872
0.50	1.458	-8.147	0.979	-2.112×10^3	6.829	0.970
0.60	2.043	-11.665	0.980	-3.267×10^3	10.324	0.991
0.70	2.922	-16.895	0.984	-4.358×10^3	13.568	0.994
0.80	3.390	-19.845	0.993	-5.174×10^3	15.937	0.995
0.90	3.527	-20.924	0.989	-5.856×10^3	17.835	0.998
1.00	3.725	-22.522	0.989	-6.858×10^3	20.642	0.997
R=0.05	3.282	-19.696	0.989	-5.827×10^3	16.957	0.985
0.10	3.218	-19.112	0.972	-5.527×10^3	15.258	0.983
0.20	2.441	-14.382	0.894	-4.914×10^3	13.763	0.978

Table 5. C.3 series creep parameters

| | Regression analysis | | | | | |
| | log $\dot{\gamma}$ vs. τ | | | log $\dot{\gamma}$ vs. 1/T | | |
M or R	Slope β	Intercept C_1	Corr. Coeff. r	Slope $\Delta H^*/k$	Intercept C_2	Corr. Coeff. r
M=0.40	1.848	-4.667	0.928	-2.407×10^3	8.367	0.967
0.50	3.588	-0.859	0.925	-3.284×10^3	11.048	0.984
0.60	4.664	-13.115	0.958	-3.935×10^3	13.027	0.978
0.70	5.660	-16.178	0.973	-4.302×10^3	14.059	0.978
0.80	6.453	-18.655	0.980	-4.753×10^3	15.362	0.970
0.90	6.861	-20.170	0.986	-5.208×10^3	16.535	0.977
1.00	7.394	-22.221	0.990	-5.114×10^3	15.794	0.989
R=0.05	6.212	-18.668	0.991	-4.600×10^3	14.374	0.991
0.10	5.642	-16.741	0.994	-4.531×10^3	14.292	0.991
0.20	3.579	-10.463	0.915	-4.478×10^3	14.329	0.985
0.30	2.968	-8.446	0.964	-4.139×10^3	13.459	0.986

Table 6. C.4 series creep parameters

| M or R | Linear regression analysis | | | | | |
| | $\log \dot{\gamma}$ vs. τ | | | $\log \dot{\gamma}$ vs. $1/T$ | | |
	Slope β	Intercept C_1	Corr. Coeff. r	Slope $\Delta H^*/k$	Intercept C_2	Corr. Coeff. r
M=0.40	2.080	-5.447	0.928	-2.189×10^3	7.309	0.988
0.50	2.477	-6.698	0.958	-2.342×10^3	7.564	0.978
0.60	2.748	-7.637	0.990	-2.703×10^3	8.481	0.997
0.70	3.020	-8.599	0.991	-2.648×10^3	8.080	0.991
0.80	3.184	-9.239	0.988	-2.561×10^3	7.567	0.984
0.90	3.459	-10.202	0.982	-2.709×10^3	7.799	0.974
1.00	3.793	-11.436	0.984	-2.785×10^3	7.749	0.974
R=0.05	3.892	-11.537	0.983	-2.641×10^3	7.540	0.978
0.10	2.888	-8.488	0.984	-2.350×10^3	6.792	0.982
0.20	2.411	-6.902	0.983	-1.707×10^3	5.006	0.963
0.30	2.359	-6.550	0.956			

Table 7. C.2 and C.5 series creep parameters

| M or R | log $\dot{\gamma}$ vs. τ for C.2 series | | | log $\dot{\gamma}$ vs. τ for C.5 series | | |
	Slope β	Intercept C_1	Corr. Coeff. r	Slope β	Intercept C_1	Corr. Coeff. r
M=0.40	-	-	-	2.541	-2.885	0.937
0.50	1.256	-5.496	0.920	3.089	-3.758	0.978
0.60	2.427	-11.369	0.983	3.935	-5.038	0.998
0.70	2.715	-12.872	0.982	4.553	-6.025	0.999
0.80	2.897	-14.064	0.982	5.123	-6.954	0.999
0.90	3.148	-15.488	0.986	5.592	-7.758	0.999
1.00	3.211	-16.223	0.996	6.199	-8.900	0.997
R=0.05	2.860	-14.290	0.992			
0.10	2.559	-12.706	0.987			
0.20	2.165	-10.576	0.974			
0.30	-					

Linear regression analysis

Table 8. Creep parameters

M or R	C.1 series, M.C. = 33.0%				C.3 series, M.C. = 41.1%			
	β' 10^6 Å^3	$(\beta')^{1/3}$ Å	$\Delta H*$ Kcal mol^{-1}	Log A	β' 10 Å	$(\beta')^{1/3}$ Å	$\Delta H*$ Kcal mol^{-1}	Log A
M=0.40	1.29	109	5.26	-1.218	2.56	137	11.01	3.360
0.50	2.02	126	9.66	-1.106	4.96	171	15.02	1.085
0.60	2.83	141	14.95	-0.797	6.45	186	18.06	-0.001
0.70	4.40	159	19.94	-2.369	7.83	199	19.68	-1.837
0.80	4.69	167	23.67	-2.599	8.92	207	21.75	-2.811
0.90	4.88	170	26.79	-1.405	9.49	212	23.83	-2.811
1.00	5.15	173	31.37	-0.337	10.23	217	23.39	-5.174
R=0.05	4.54	166	26.66	-0.273	8.63	205	21.04	-3.335
0.10	4.45	164	25.29	-0.689	7.80	198	20.73	-1.637
0.20	3.38	145	22.47	-1.993	4.95	170	20.49	4.465
0.30					4.11	160	18.94	5.351

Table 9.   Creep parameters

M or R	C.4 series, M.C. = 46.0% β' 10^6 $\overset{o}{A}^3$	$(\beta')^{1/3}$ $\overset{o}{A}$	ΔH^* Kcal mol^{-1}	Log A	C.2 series M.C. = 35.6% β' 10^6 $\overset{o}{A}^3$	$(\beta')^{1/3}$ $\overset{o}{A}$	C.5 series M.C. = 52.1% β' 10^6 $\overset{o}{A}^3$	$(\beta')^{1/3}$ $\overset{o}{A}$
M=0.40	2.88	142	10.2	1.851			3.52	152
0.50	3.43	151	10.71	1.108	1.73	120	4.27	162
0.60	3.80	156	12.37	1.373	3.36	150	5.44	185
0.70	4.18	161	12.11	0.224	3.80	156	6.30	192
0.80	4.40	164	11.72	-0.704	4.01	159	7.09	192
0.90	4.79	169	12.39	-1.172	4.36	163	7.74	198
1.00	5.25	174	12.74	-2.153	4.44	164	8.58	205
R=0.05	5.38	175	12.08	-2.730	3.96	158		
0.10	3.99	159	10.75	-0.653	3.54	152		
0.20	3.34	149	7.81	0.997	3.00	144		
0.30	3.26	148						

66

Figure 28. Plots of mobilization ratio M and rupture ratio R versus (a) flow volume β', (b) activation enthalpy ΔH*, and (c) log of coefficient A for C.1 series (M.C.=33.0%, normal stress= 6.0 psi)

Figure 29. Plots of mobilization ratio M and rupture ratio R versus (a) flow volume β', (b) activation enthalpy ΔH*, and (c) log of coefficient A for C.3 series (M.C.=41.1%, normal stress= 6.0 psi)
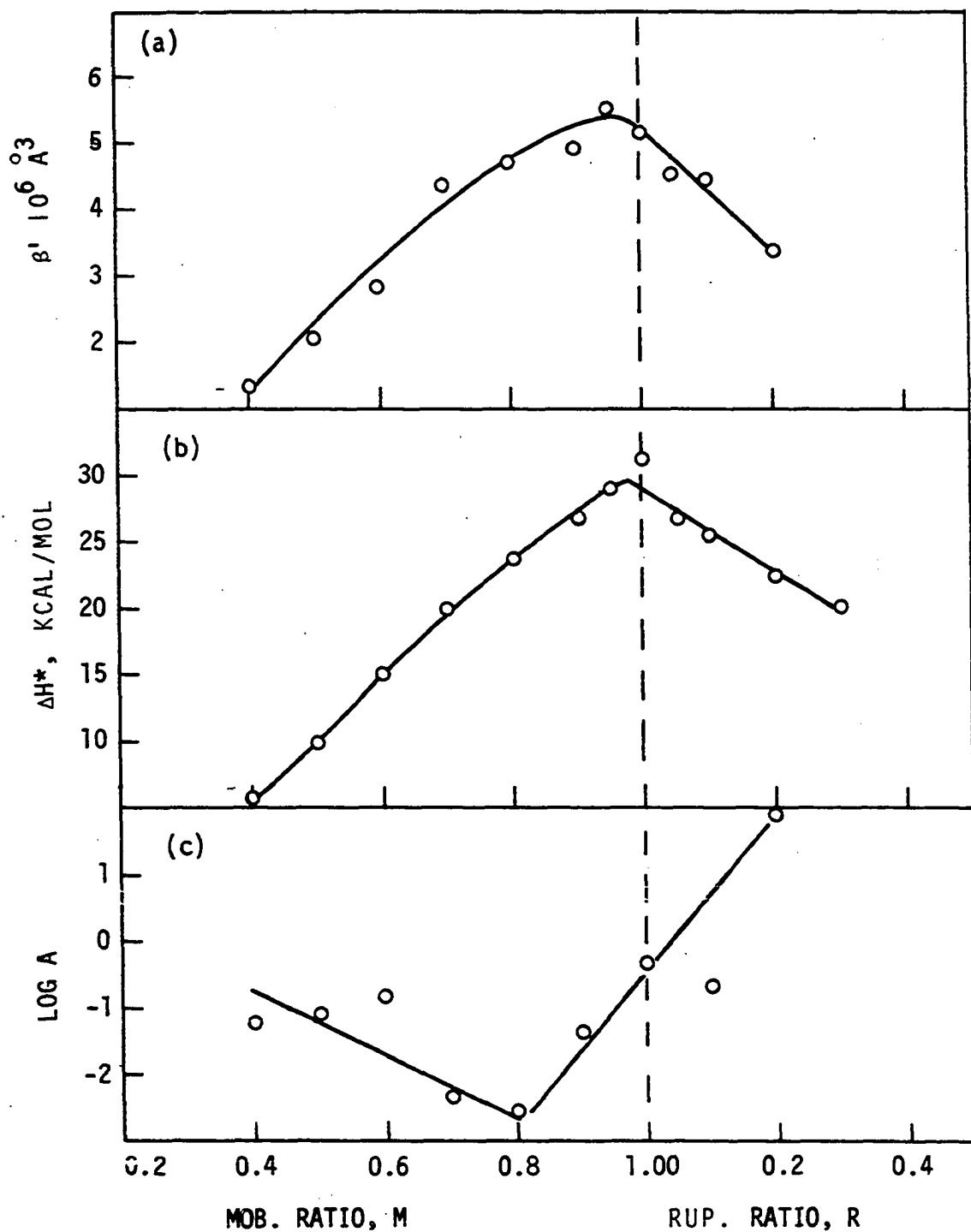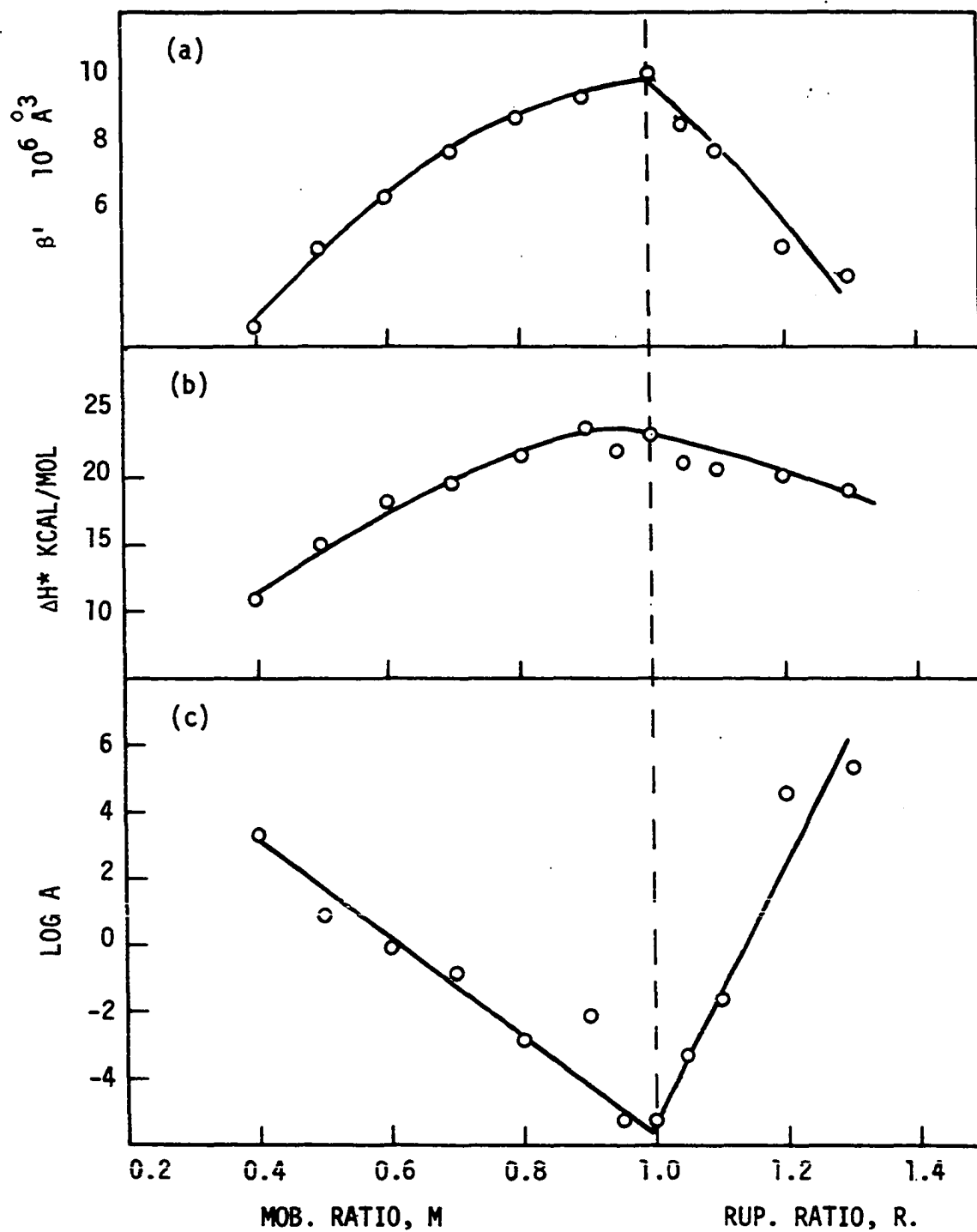
Figure 30. Plots of mobilization ratio M and rupture ratio R versus (a) flow volume β', (b) activation enthalpy ΔH^*, and (c) log of coefficient A for C.4 series (M.C.=46.0%, normal stress= 6.0 psi)

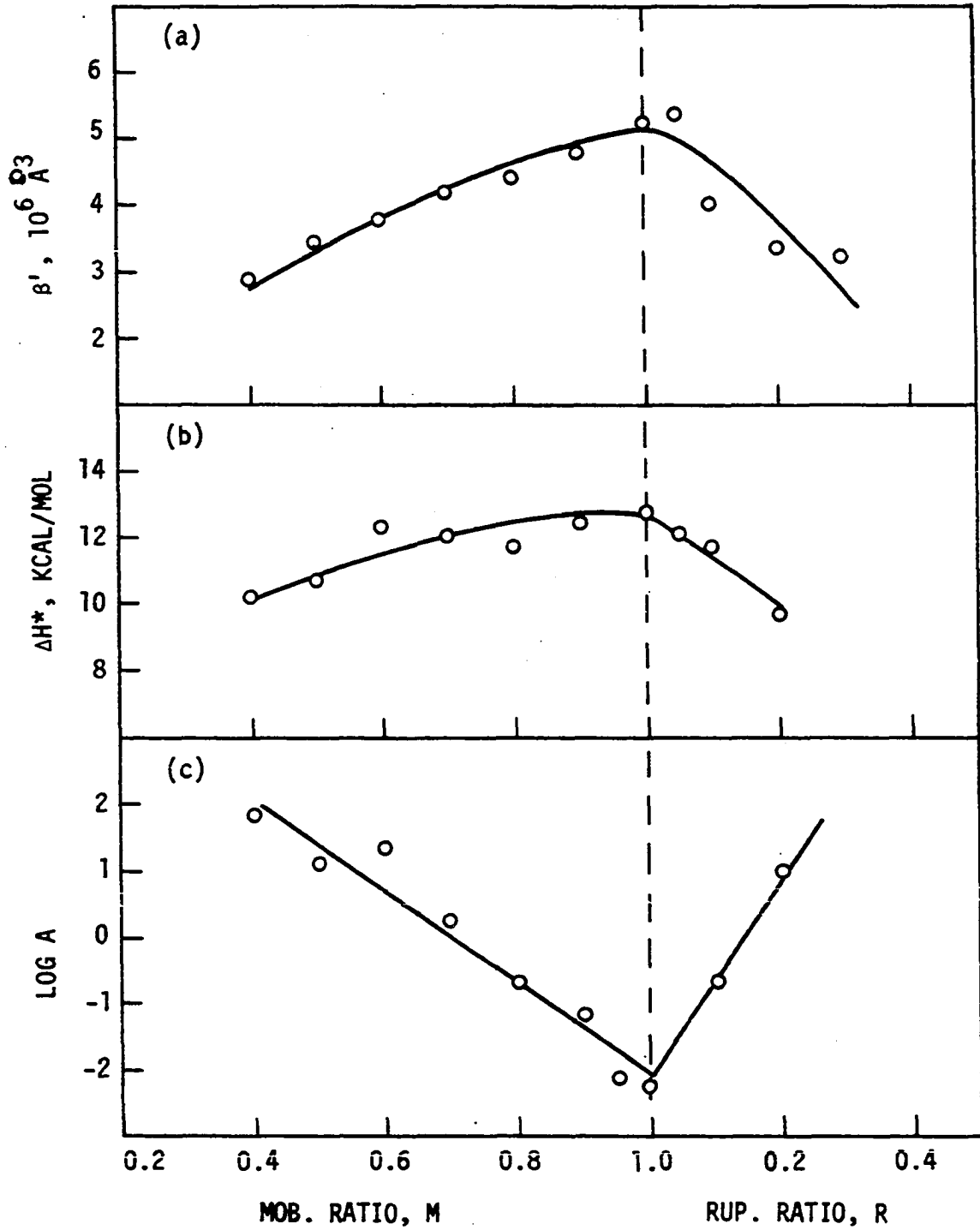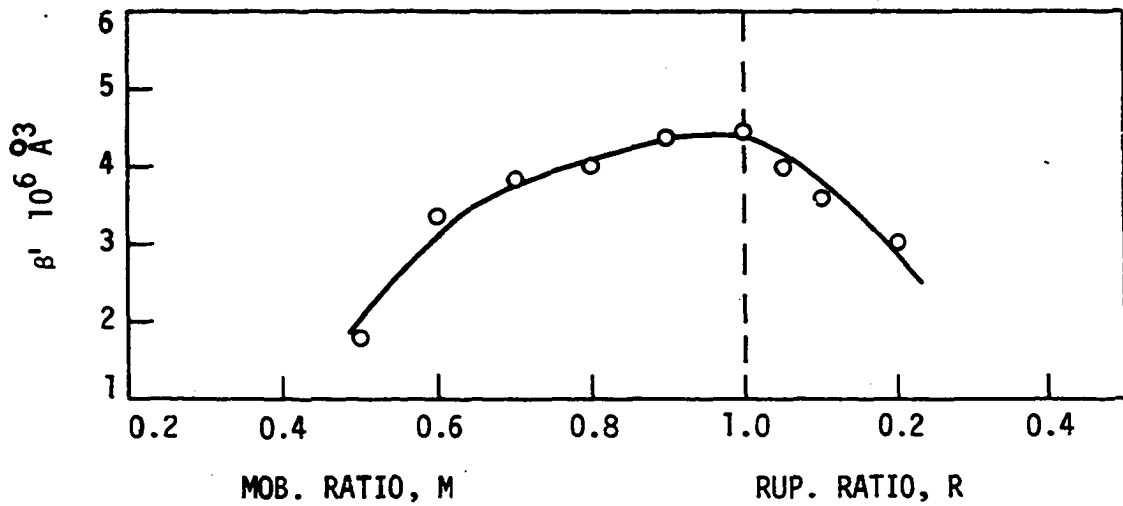Figure 31.   Plot of mobilization ratio M and rupture ratio R versus flow
volume β' for C.2 series (M.C.=35.6%, normal stress=6.0 psi)
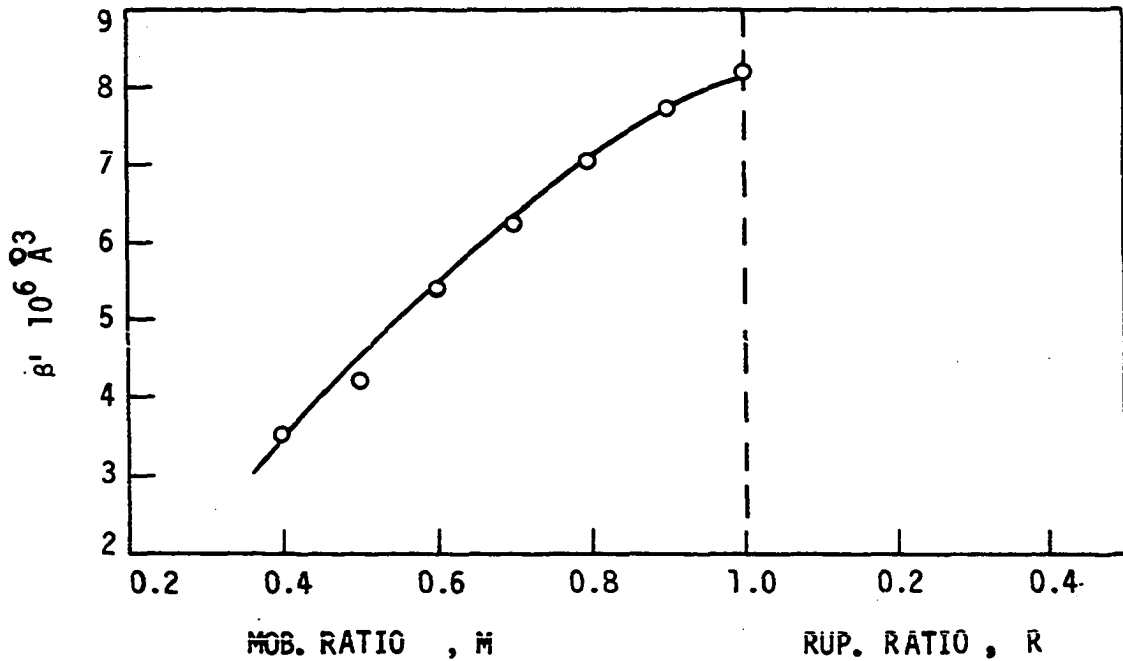

Figure 32.   Plot of mobilization ratio M and rupture ratio R versus flow
volume β' for C.5 series (M.C.=52.1%, normal stress=6.0 psi)

Since only room temperature tests were run in C.2 and C.5 series tests, it was not possible to calculate ΔH^* and log A values, therefore only M (or R) versus β' plots are given for these series (Figures 31 and 32).

Variation of Rate Process Parameters

Mobilization and rupture ratios versus flow volumes β', activation enthalpies ΔH^* and log of proportionality constant A plots shown in Figures 28 to 32 indicate that these parameters vary with progressive creep deformations. The variation of these parameters with respect to M and R ratios showed consistent trends. In mobilization period, flow volumes and activation enthalpies increased with increasing M ratios. This trend was followed by decreases in β' and ΔH^* in the rupture period after showing a peak at mobilization ratio of 1.0. Variation of log A with M and R ratios followed a reverse trend showing first a decrease then an increase in mobilization and rupture periods, respectively, exhibiting a minimum at mobilization ratio of 1.0 with only one exception. In C.1 series minimum log A value occurred around M ratio of 0.30 as shown in Figure 28. This deviation from the general trend observed in other series may be due to data scatter which in case of computation of A is further amplified due to inclusion of two sets of data for determining the values of A from the intercepts and slopes of log $\dot{\gamma}$ versus τ and log $\dot{\gamma}$ versus $\frac{1}{\tau}$.

The changes in rate process parameters A, ΔH^*, and β' with deformation show that the structure can be characterized by changes in these parameters. The parameters β', ΔH^* and A are related to size, strength and arrangement of bonds, respectively. These observed trends appear to be

logical in light of expected structural variations and are in complete agreement with direct SEM observations of Vyalov et al. (91) and Foster (28) as discussed earlier in section on fabric studies (p. 13). In clay water systems the structural changes include particle movements and change in particle orientations as expected due to particulate nature of soils. As particles move relative to each other changes in interaction of particles including the phases adsorbed by them are expected. Interference of adsorbed layers and possible variations in interparticle distances may cause change in interaction energies between clay surfaces and influence the bond energies which would then appear as a change in activation enthalpies. Change in particle orientations would affect the entropy of the system which would be reflected as a variation in parameter A. Decrease in this parameter in mobilization period indicate a change in the structure towards a more orderly state which can be interpreted as an increase in degree of particle orientations. The reorientation of clay particles resulting in alignment of the basal planes in the shear direction as reported by Vyalov et al. (91) correspond to a minimum entropy state, in steady flow stage. The interpretation of the minimum value of A at mobilization ratio of 1.0 is in agreement with direct observations. Changes in particle arrangements and orientations influence the flow mechanism and caused the observed variations in activation enthalpies ΔH^* and flow volumes β' as discussed earlier in the section on fabric studies (p. 13).

The possibility of variation in activation energies and proportionality constants has been noted but not formulated by previous investigators (22,52,95,28,19,63,30,85) due to lack of a diagnostic criteria for

structure. Hence a structure function was introduced to the rate process equation without much success. Dorn (22) who introduced the concept of structure function also states:

> In general both A and ΔF (free energy of activation) might depend on the instantaneous stress and structure. Consequently, any change in creep rate during a constant stress isothermal creep test must be ascribed to change in A and ΔF which are due to the substructural changes arising during creep itself.

Foster (28) employed rate process theory to study shear behavior kaolin clay and reported variations in activation energies from 16 to 21 kcals per mole at different stages of shear deformations, and interpreted this observation by stating: "Once creep is active surface roughness would contribute to the resistance to further displacement of the moving particles." Zaretskii and Vyalov (95) considered two parameters to characterize the structural changes which influence the activation energies of soils: particle orientation and intensity of microfractures in clay fabric, their effect being an increase and decrease in activation energies. These authors were able to show some evidences for these structural changes in a previous publication which included SEM studies of soil fabric at various stages of deformations (91). Rehbinder (63) notes the possibility of isothermal decrease in the entropy of clay-water systems due to the inevitable orientation of axes or of anisometric particles or chain-like aggregates in the direction of shear in the process of deformation. None of the previous investigators, however, took the problem in its totality and analyzed possible variations in all three parameters.

The occurrence of highest absolute values of ΔH* and β' and lowest value of log A at mobilization ratio of 1.0 as found in this study is

significant in clarifying the meaning of flow structure or critical structure. Soil structure is most resistive to deformation at the mobilization ratio of 1.0 as indicated by minimum strain rates occurring at this point. The test results showed that, at this point, the structure has its most strongly bonded, most orderly arranged and most textured state.

The present knowledge of flow mechanism and character of bonding in clay soils is still in a hypothetical stage. It is hoped that further investigations which should include direct measurements of fabric and its variation with deformations, will make expressing the rate process parameters in terms of a fabric parameter possible and clarify the deformation and failure mechanism in clay soils.

Comparison of Terminal and Tertiary Behavior

In tertiary creep curves the time, t_M, corresponding to points of equal mobilization ratios were plotted against shear stresses as shown in Figure 33 for C.1 series. The straight lines best fitting these points were obtained by regression analysis. The assumed straight line relationships were justified by high values of correlation coefficients obtained. Figure 34 shows log time for mobilization ratio of 1.0 (inflection point) versus shear stress plots which are reproduced from the tertiary failures published by Murayama et al. (56), Noble (58) and Campanella et al. (17). It is interesting to note that linearity of these plots are in complete agreement with the behavior observed in Figure 33. The straight lines shown in Figure 33 were then extrapolated to estimate the time for equivalent mobilization ratios, t_M, on terminal creep curves corresponding to
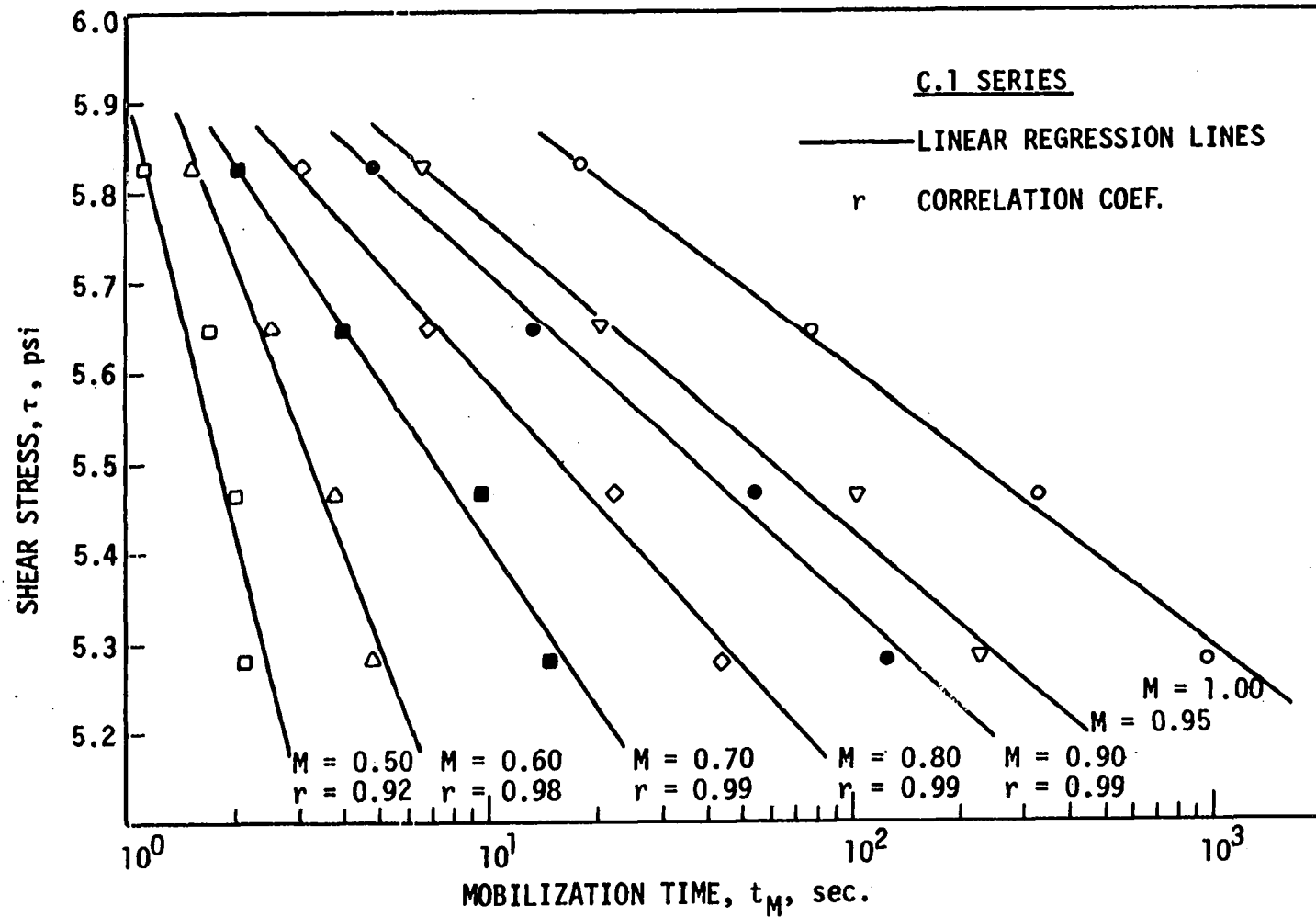
Figure 33. Plots of mobilization time t_M versus shear stress τ plots at various mobilization ratios M for C.1 series (M.C.=33.0%, normal stress=6.0 psi)
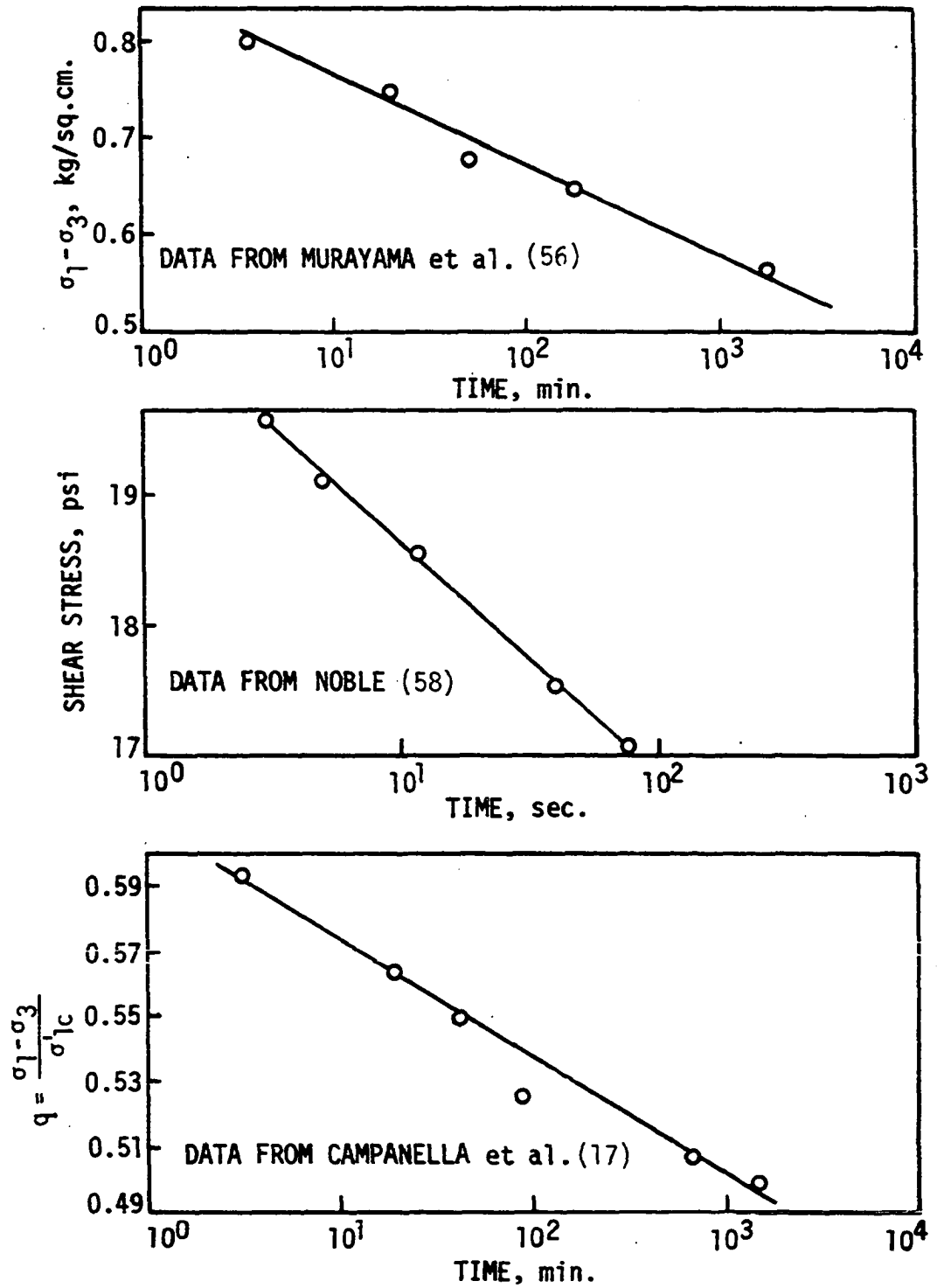
Figure 34. Plots of mobilization time t_M at mobilization ratio of 1.0 versus shear stress for various clays

lower stresses. Strain rates corresponding to the predicted t_M were then determined from the experimental log $\dot{\gamma}$ versus log t plots of terminal creep curves.

The results are reported for C.1 series. In other test series, similar trends were obtained. These are given in Appendix B.

Figures 35 and 36 show the plots of log strain rate versus shear stress for mobilization ratios of 0.5 to 1.0. Equivalent mobilization ratios were either directly found when tertiary behavior occurred or were obtained as described above (from shear stress versus log t_M plots by extrapolation). Linear regression analyses were run to obtain best fitting straight lines to all data points within the stress range 4.0 to 5.9 psi as shown in Figures 35 and 36. This will be referred to be as the combined analysis. The results of combined analyses are summarized in Table 10. The flow volumes β' calculated for C.1 series tertiary creep curves (given in Table 8) are also included in Table 10 to compare tertiary and terminal behavior. The β' values obtained from tertiary behavior and combined data appeared to be in agreement. When the combined data is used, due to increased number of data points included in the analysis, a better statistical distribution is obtained as demonstrated by the higher correlation coefficients shown in Figures 35 and 36.

The almost perfect overlap of log strain rate versus shear stress relationships of both tertiary and terminal creep ranges in the stress range (4.0-5.9 psi) considered suggests that one flow mechanism governs the total creep behavior. In other words, at constant mobilization ratios the structure or fabric of the material remains independent of stress level since the continuity of log $\dot{\gamma}$ versus τ is maintained. The SEM

Figure 35. Plots of log strain $\dot{\gamma}$ versus shear stress τ combining tertiary and terminal stress levels at mobilization ratios M of 0.5 and 0.6 (C.1 series, M.C.=33.0%, normal stress=6.0 psi)
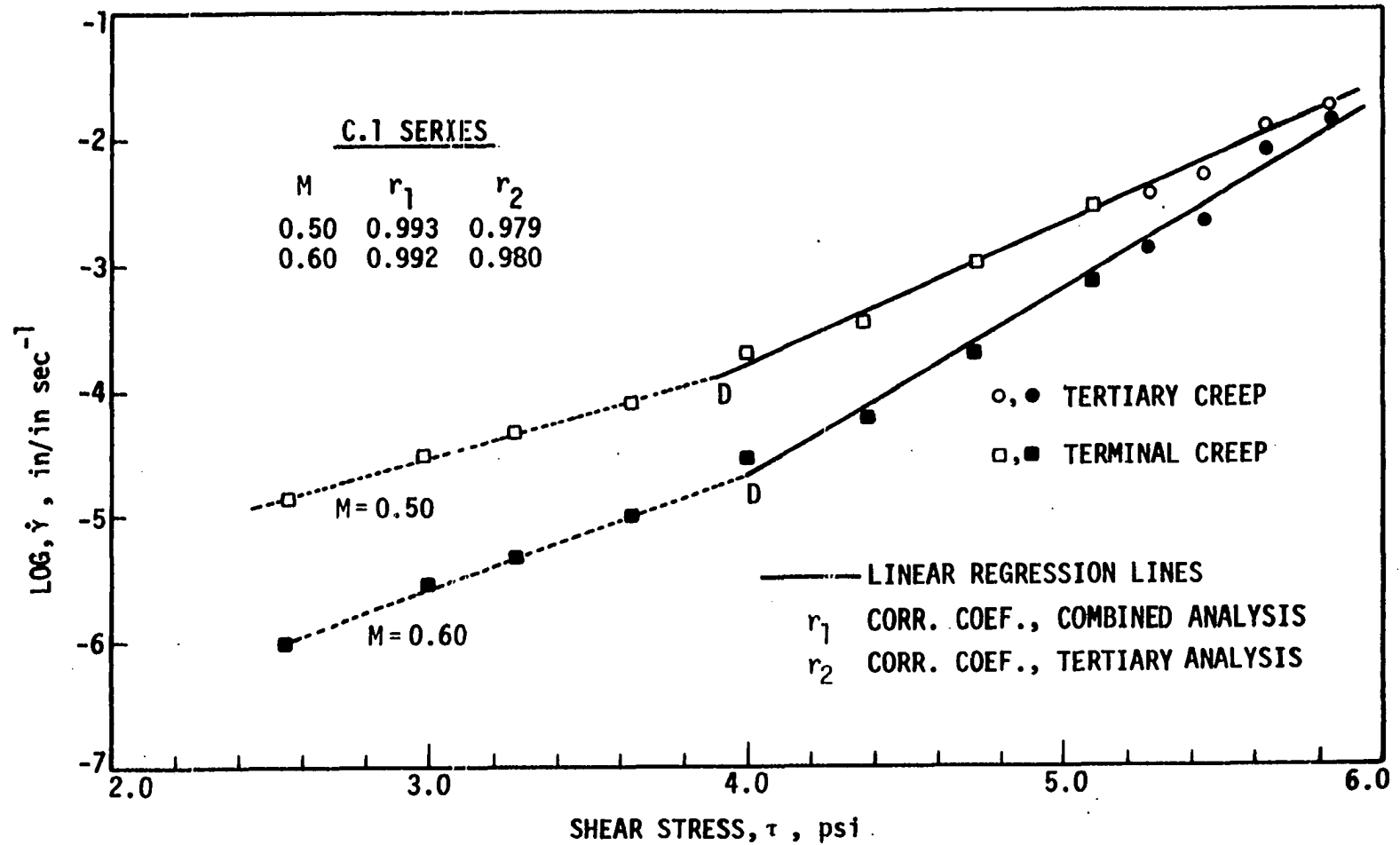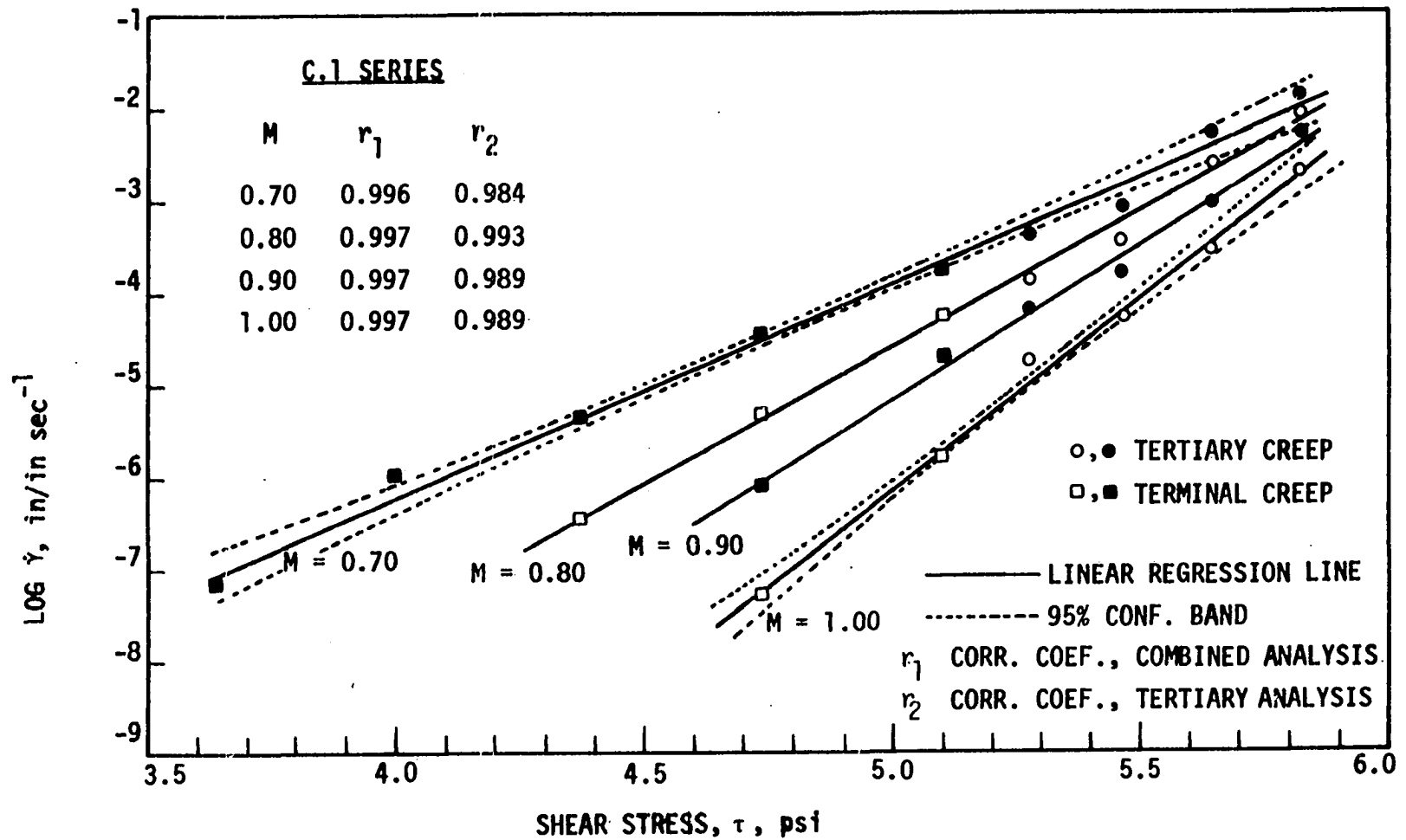
Figure 36. Plots of log strain rate $\dot{\gamma}$ versus shear stress τ combining tertiary and terminal stress levels at mobilization ratios M of 0.7 to 1.00 (C.1 series, M.C.=33.0%, normal stress= 6.0 psi)

Table 10. C.1 series combined linear regression analysis and β' values obtained from tertiary data

| M | Log $\dot{\gamma}$ versus τ | | | β'_o 10^6 $\overset{o}{A}^3$ | $(\beta')^{1/3}_o$ $\overset{o}{A}$ | β'^a_o 10^6 $\overset{o}{A}^3$ |
	Slope β	Intercept C_1	Corr. Coeffi. r			
0.5	1.1012	-6.1630	0.993	1.52	115	2.02
0.6	1.4996	-8.6727	0.992	2.07	127	2.83
0.7	2.2928	-13.3736	0.996	3.17	147	4.40
0.8	2.9320	-17.2627	0.997	4.06	159	4.69
0.9	3.3458	-19.8798	0.997	4.63	167	4.88
1.0	4.1365	-24.8126	0.997	5.72	179	5.15

[a]β' calculated from tertiary creep curves only.

observations by Vyalov et al. (91) on shear induced fabrics are in com-plete agreement with the above statements. These authors report that changes in the structures are identical for terminal creep and for primary portion of tertiary creep. This behavior also suggests that the terminal creep curves may eventually show tertiary failures if longer time periods were allowed for shearing. Time extrapolations (Figure 33) indicated that the shear time of 24 hours allowed for the specimens was not long enough to observe tertiary failures (mobilization ratio of 1.0) in all terminal creep curves obtained except two which were run at shear stresses of 4.73 and 5.10 psi. The time predicted for the occurrence of inflection points was within 24 hours for these tests, but specimens did not show tertiary failures. A possible explanation for this behavior may be the dilatation of the material which may constitute under confining pressure an addi-

tional energy (compressional free energy) barrier to be surmounted at successive stages of deformation. This increase in activation energy and subsequent decrease in number of bonds having thermal energies which can surmount the increased activation energy would result in a decrease in strain rate. It should be noted here that when the magnitude of the compressional free energy exceeds that of mechanical energy supplied by shear stress $(\beta'\tau)$ potential for flow in the direction of shear completely ceases resulting in the termination of the deformations. Dilatation would be reflected as a tendency for an increase in the volume of the specimen. In the present work however very small volume changes were also affected by partial drainage of the specimens which appeared as an instrument limitation. As the result of partial drainage consolidation may take place causing additional structure changes unaccounted for in the analysis given above. This effect may result in an additional deceleration of the deformation but would not completely terminate it. Since partial drainage was not allowed and was not expected and volume changes were small to be detected proper measures were not taken to detect these effects in the present study.

At stress intensities close to tertiary stress range in Figures 35 and 36 no distinct change in strain rate versus shear stress behavior which would indicate discontinuity of tertiary behavior was observed. This observation is in agreement with the rate process theory adopted which does not define stress limits for terminal and tertiary type behavior. Further modifications on the apparatus to improve drainage control and long term creep tests may be necessary to obtain direct evidences for the continuity of the behavior in future work.

The systematic deviation of the data points at low stress levels (<4.0 psi) from the combined regression line corresponding to higher stress levels (>4.0 psi) as shown in Figure 35 may be attributed to the approximations involved in time extrapolations. If however time extrapolations are assumed to be valid, the systematic deviation can be explained on the basis of structural changes due to consolidation and compressional energy effects discussed above. When the deviation is approximated by another straight line as shown by dotted lines on Figure 35, two slopes would define two different β' values. The values of β' determined from the two linear segments, then, reflect the structural variation due to stress levels. It can then be stated that below a critical stress level corresponding to the intercept D of the two linear segments (Figure 35) the magnitude of structure parameter β' will never reach the critical value defined by the tertiary behavior. This may be part of the reason for termination of creep deformations at lower stress intensities.

<div align="center">Time Dependency of Structural Changes</div>

The rate of structural changes is dependent on stress level and the time necessary to reach a given mobilization increases as stress intensity decreases. This can be demonstrated by β' versus time plots as shown in Figure 37. On this figure dashed lines which belong to terminal creep curves were constructed by extrapolating the straight lines on Figure 33 to lower (<5.10 psi) stress levels and the solid lines correspond to tertiary curves. This figure indicates that at constant time of shear the flow volumes are smaller at lower stress intensities. This means the criteria
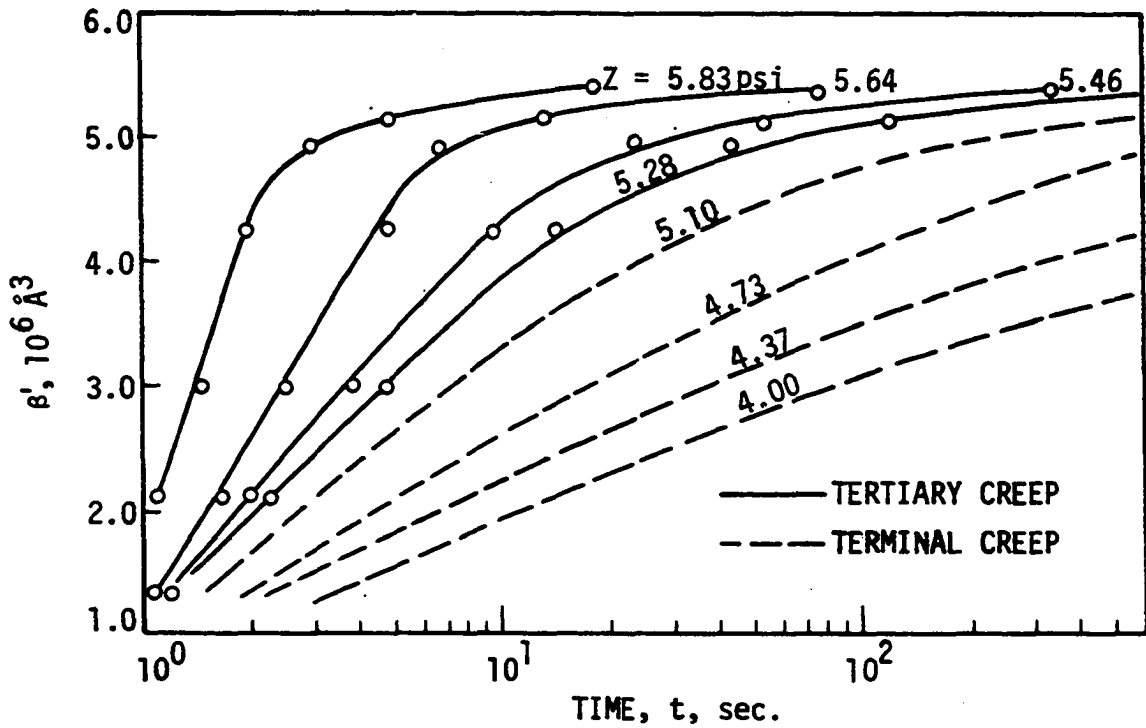
Figure 37. Plots of flow volume β' versus time t at various stress levels
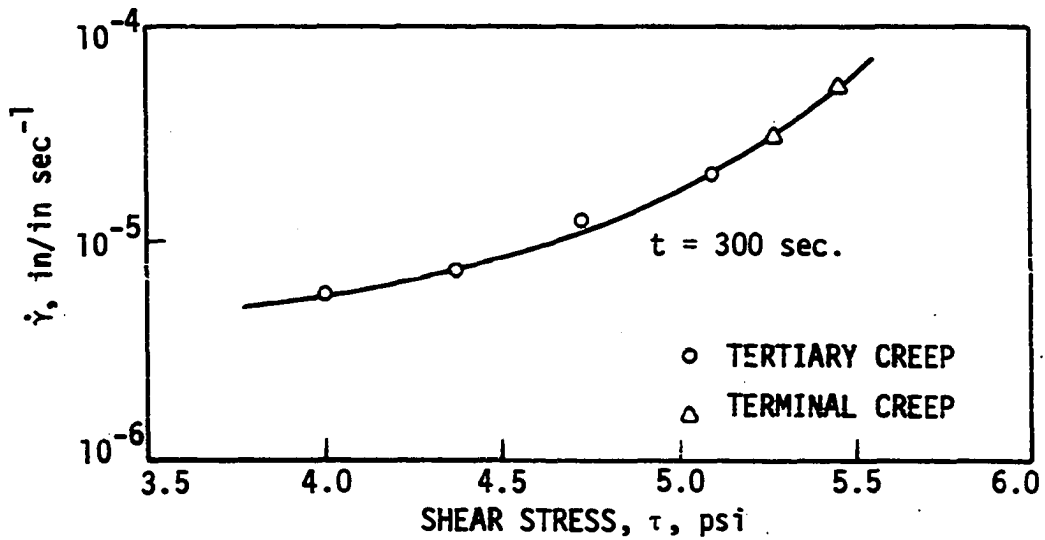(C.1 series, M.C.=33.0%, normal stress=6.0 psi)

Figure 38. Plots of log strain rate $\dot{\gamma}$ versus shear stress τ at constant
time of shear of 300 seconds (C.1 series, M.C.=33.0%, normal
stress=6.0 psi)

of constant time of shear to locate the points of equivalent structures as
suggested by Mitchell et al. (52) could not reveal linear log $\dot{\gamma}$ versus
shear stress plots. To demonstrate this, the strain rates measured at
shear time of 300 seconds on the experimental creep curves were plotted
against shear stresses and are shown in Figure 38. The slope of the log
$\dot{\gamma}$ versus τ curve in Figure 38 decreases with stress intensities suggesting
smaller β' values at lower stresses. This observation is in agreement
with the time dependency of structural changes shown in Figure 37.

Creep Parameters-Moisture Relationships

The magnitude of activation enthalpies computed at inflection points
were in the order of 31.4, 23.4, 12.7 kcals per mole at moisture contents
of 33.0, 41.1 and 46.0 percent by dry weight of clay, respectively. This
decrease in activation enthalpies with increasing moisture contents indi-
cates a decrease in magnitude of net particle interaction energies. The
decrease in bond energies can be attributed to the fact that, as moisture
content of the system increases the distance between interacting clay
surfaces increases. Due to the increased distance between surface force
fields, weaker interactions are expected at higher moisture contents.
Some of the reported activation energies for clay water systems are given
in Table 11.

These values lie within the range of 4 to 50 kcals per mole which
corresponds to the activation energies of water and metals. The different
magnitudes of the values reported reflect differences in mineralogy,
moisture state and other properties of clay water systems, and measurement
techniques employed in testing.

Table 11. Activation energies for creep of various soils

Material	Activation energy kcals per mole	Reference
Illitic clay	34-40	(52)
Kaolinite clay, slurry	2-8	(19)
Montmorillonite pastes	20-26	(64)
Natural clay	12-29	(58)
Natural clay	2.8	(4)
Kaolinite clay	16-21	(28)

The summary of rate process parameters are given in Table 12. According to the derivation of Equation 1 flow volume β' is the product of average bond area times the average distance moved by a bonding unit. If the average bond area and the distance traveled were in the same order of magnitude as suggested by previous investigators (59), then cubic root of flow volumes reveals the length of one side of flow volume. The cubic root of flow volumes varies within the range of 163-205 $\overset{o}{A}$. These figures suggest that the average volume occupied by a flow unit is in the order of size of clay particle.

The variation of flow volumes with moisture content do not show a systematic trend. This behavior suggests that flow volumes, β', are not affected significantly to show either increasing or decreasing trends when moisture content of the clay water pastes varies between liquid limit and plastic limit of the clay water system. Chaudry (18) reports flow volumes

Table 12. Summary of rate process parameters

Series	M.C. %	β'_i $\overset{\circ}{A}^3 \times 10^6$	$(\beta'_i)^{1/3}$ $\overset{\circ}{A}$	ΔH^*_i Kcal/mol	Log A_i	$\frac{\Delta\beta'}{\Delta M}$ [a]	$\frac{\Delta(\Delta H^*_i)}{\Delta M}$ [a]	$\frac{\Delta \log A}{\Delta M}$ [a]
C.1	33.0	5.15	173	31.4	-0.34	7.7	41.7	-4.8
C.2	35.6	4.44	163	-		4.6		
C.3	41.1	8.63	205	23.4	-5.17	13.3	24.3	-13.3
C.4	46.0	5.25	174	12.7	-2.15	3.6	4.3	-6.7
C.5	52.1	7.74	198	-		8.2		

[a] Values of $\frac{\Delta\beta'}{\Delta M}$, $\frac{\Delta(\Delta H^*)}{\Delta M}$ and $\frac{\Delta \log A}{\Delta M}$ were found from the slopes of the curves in Figures 18 to 22. The data points on these figures were approximated by straight lines. β_i, ΔH^*_i and log A_i are the values of rate process parameters at mobilization ratio of 1.0 (at inflection point).

in the order of 100-150 x 10^{6^1} $\overset{\circ}{A}^3$ which are considerably higher than 4.5-8.5 x 10^6 $\overset{\circ}{A}^3$ obtained in the present study. In Chaudry's work the moisture contents were in the order of twice the liquid limit of the clays and clay water systems were in liquid state. Considering this fact, it can be noted that significant changes in flow volumes are expected over wide range of moisture variations.

It is noted that the highest and lowest magnitudes of β_i' and log A_i occur at mid-range of moisture content as given in Table 12. This behavior may be interpreted as follows: Since β_i' and A_i are related to bonding geometry, and entropy and therefore the degree of orderliness of the system, the clay paste at the mid-range of moisture content has the most textured and ordered structure as compared to the other moisture contents studied.

The ΔH^* vs. M, β' vs. M and log A vs. M plots shown in Figures 18 to 22 were approximated by straight lines and slope of these lines are given in Table 12. These slopes reflect the characteristics of soil structure at different moisture contents. Zero slope (a horizontal line on ΔH^*, β' and log A vs. M plots) corresponds to a material having a constant structure or its behavior is not affected by the structure. If this condition is analogous to a viscous flow and the material having no variation in structure could be represented by a viscous material, then the steepest slopes can be considered as representing most structure sensitive

---

[1]An error was found in Chaudries' computations. Chaudries corrected flow volumes were found to be in the order of 100-200 x 10^7 $\overset{\circ}{A}^3$ which is even higher than the values he first reported (T. Demirel, personal communication, 1977).

material. It is interesting to note that the steepest slopes occurred at the mid-range of moisture contents studied as given in Table 12. This observation suggests that most structure sensitive material is the one having its moisture content at the mid-range. SEM studies show indications confirming the above statement as will be discussed in the following section.

Fabric Characteristics

Electron micrographs showing the fabric of grundite clay pastes at 33, 41 and 52 percent moisture contents are shown in Figures 39a, 39b and 39c, respectively. Fabric is characterized by particle assemblages or aggregates and continuous pores surrounding them. The details of individual aggregates for three moisture contents are shown in Figures 40a, 40b and 40c. The aggregates consist of individual platy particles with irregular geometries. There is a dominant face to face orientation of the particles within the aggregates as clearly shown in Figures 40b and 40c. Thin and curly nature of individual particles indicates that the particular clay is not well crystallized.

Comparison of the fabrics, shown in Figures 40a, 40b and 40c, reveals that there is a tendency of denser arrangement of the particles in aggregates with decreasing moisture contents. At lowest moisture content (33 percent) fabric reflects a granular character resulting from very close spacing of particles within aggregates (Figure 39a) and details of individual particles cannot be clearly seen in Figure 40a. As moisture content increases aggregates disappear and association of individual particles within the particle assemblages becomes looser.

89

(a)
M.C. = 33%

50 μm

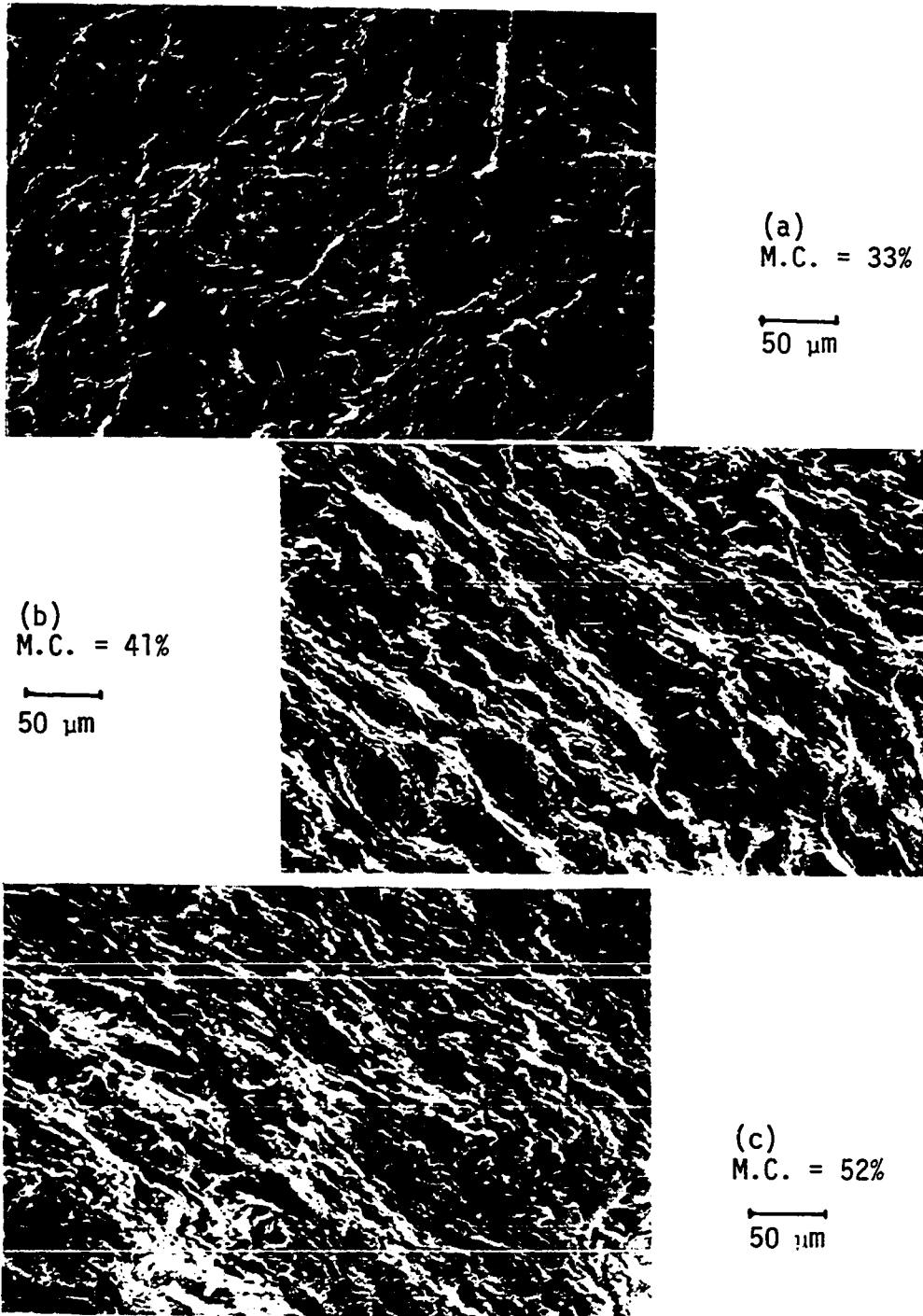(b)
M.C. = 41%

50 μm

(c)
M.C. = 52%

50 μm

Figure 39. Fabric of Grundite clay at low magnifications (200X)

(a)
M.C. = 33%

50 μm

(b)
M.C. = 41%

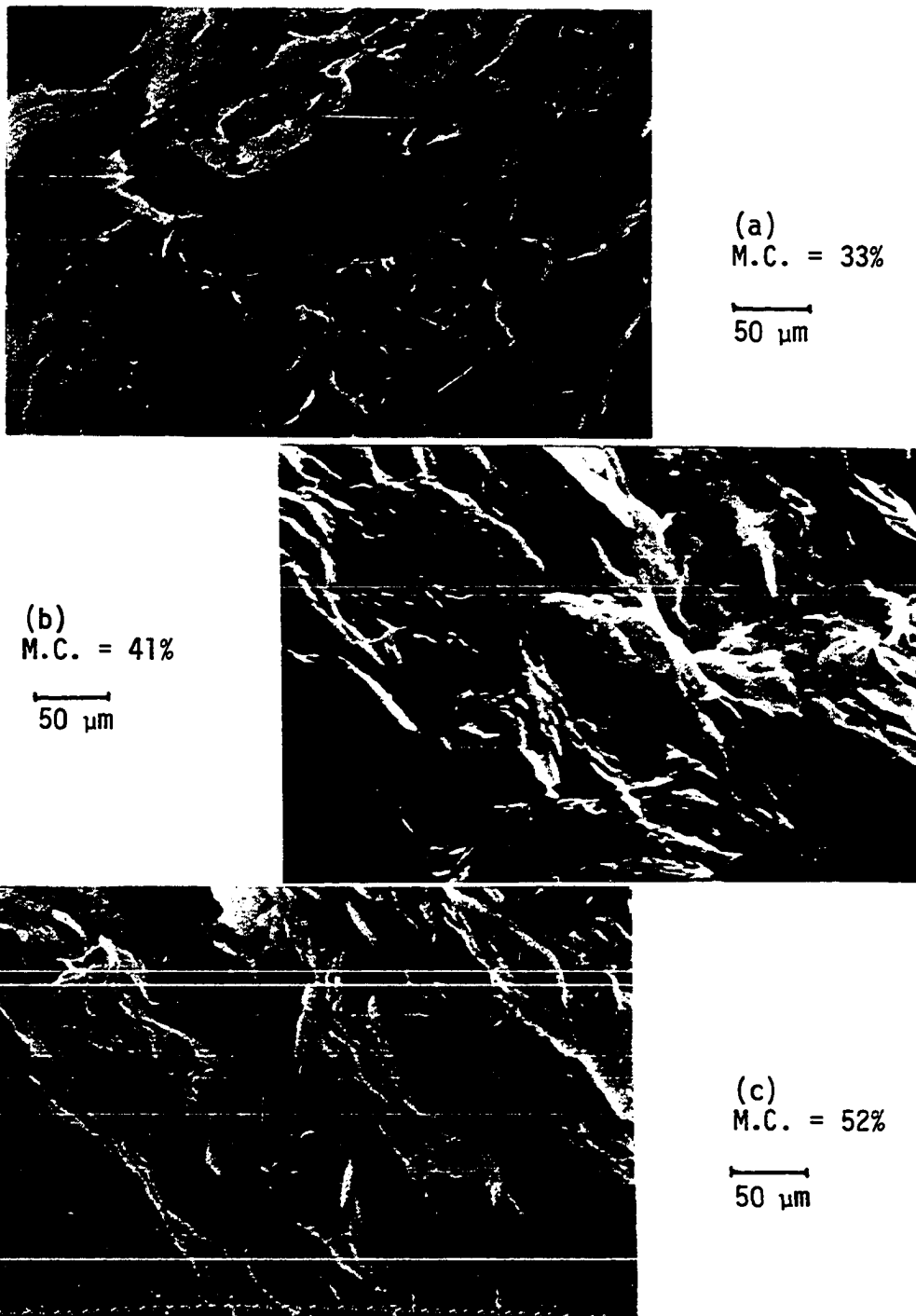50 μm

(c)
M.C. = 52%

50 μm

Figure 40.   Fabric of Grundite clay at high magnifications (4000X)

Soil structure is expected to be related to both characteristics of individual grains or particle assemblages and arrangement of these assemblages. At the lowest moisture content (33 percent), although the particles are densely arranged within grains, the granular nature of the fabric leads to the formation of large pores which appear as discontinuities among the grains (Figure 39a). At the highest moisture content (52 percent), both particle spacing within the particle assemblages and spacing among particle assemblages themselves are increased due to increase in water content (Figures 39c and 40c). Fabric characteristics of intermediate water content can be replaced in between those two from the viewpoint of particle association within particle assemblages and spacing among the particle assemblages as indicated by Figures 39 and 40. This may be part of the reason why intermediate moisture content behaves as the most structure sensitive material, which is indicated by the steepest slopes of ΔH^*, β' and log A vs. M plots, as compared to other moisture contents studied.

SUMMARY AND CONCLUSIONS

In order to incorporate the structural variations into the rate process theory a primitive or ideal clay-water system is defined by a linear strain-time relationship implicit in the rate process equation. The deviations of the real clays strain-time curve from linear strain-time behavior of primitive model is attributed to the structural changes which accompany the deformation of real clay. To measure the structural changes quantitatively, two strain ratios are defined: (i) mobilization ratio, (ii) rupture ratio, and it is demonstrated that equivalent mobilization or rupture ratios correspond to identical soil structures on experimental creep curves. The method of analysis made by following this line of reasoning yielded the following observations:

1. The fundamental soil parameters ΔH^*, β' and A, which were treated as material constants in previous studies, were found to be structure dependent. Since these parameters are related to bond strength, bond size and degree of orderliness of the system, their variation gives the most quantitative picture of structure and structural variations.

2. The strain hardening behavior was found to be characterized by an increase in flow volume and activation enthalpy and a decrease in activation entropy up to the inflection point of strain versus time plots (tertiary creep curves). These structural changes were followed by reverse trends in strain softening portion of creep curves and structural parameters β', ΔH^* and A attained their maximum and minimum values at the inflection point. These trends demonstrated that, at the inflection point

structure attains the coarsest texture, mostly strongly bonded and most orderly mode of particle arrangement.

3. The comparison of tertiary and terminal creep behavior revealed that the structural changes are independent of stress level. In other words, the structure and the structural changes were found to be identical for the primary portion of both terminal and tertiary creep curves irrespective of the magnitude of shear stress. This is supported by the SEM observation of others. This observation suggested the possibility of long term tertiary failures at stress levels considerably less than that of exhibiting short term tertiary failures.

4. The concept of occurrence of identical structures at equivalent time of shear was shown to be invalid for the clays studied. The rate of structural changes were shown to be stress dependent as such, lower the stress intensity slower is the rate.

5. The activation enthalpies were found to be dependent on moisture content. Decreasing bond energies with increasing moisture contents demonstrated the role of water phase as a bonding agent in clay water systems and contradicted the idea of existence of solely covalent or ionic type bonds.

6. The slopes of ΔH^*, β' and $\log A$ versus mobilization ratio plots were considered to reflect the sensitivity of the material behavior to structural changes. Experimental results revealed that the mid-range of moisture content between the liquid and plastic limit of the clay pastes has the most structure sensitive character.

Tests on Bentonite clay revealed that thixotropic hardening itself being a rate process was affected by temperature and thus at higher temperatures initial structures became different than those at lower temperatures which made determination of activation enthalpies impossible in the present study. It is suggested for future studies that all samples be heated to highest temperature and cured to a stable structure, then be brought down to desired test temperatures for testing.

Review of simple shear and the experimental work of this study showed that stress-nonuniformities develop along boundaries of specimens tested in simple shear. It is demonstrated that if sample thickness is reduced, the error introduced by the stress-nonuniformities may be negligible.

REFERENCES

1. Abdel-Hady, M. and M. Herrin. 1966. Characteristics of soil-asphalt as a rate process. ASCE, Journal of Highway Div., Proc. 92(HW1): 49-69.

2. Alymore, L. A. and J. P. Quirk. 1960. Domain or turbostratic structure in clays. Nature 187: 1046.

3. Andersland, O. B. and I. Al Nouri. 1970. Time dependent strength behavior of soils. ASCE, Journal of Soil Mech. Found. Div., Proc. 96 (SM4): 1249-1265.

4. Andersland, O. B. and A. G. Douglas. 1970. Soil deformation rates and activation energies. Geotechnique 20(1): 1-16.

5. Anderson, D. M. and P. F. Low. 1958. The density of water adsorbed by lithium, sodium and potassium bentonite. Soil Science Soc. of Am. Proc. 22: 99-103.

6. Arthur, J. R. F., R. G. James and K. H. Roscoe. 1964. The determination of stress fields during plane strain of sand mass. Geotechnique 14: 283-308.

7. Arulanandan, K., C. K. Shen and R. B. Young. 1971. Undrained creep behavior of a coastal organic silty clay. Geotechnique 21(4): 359-375.

8. Atakol, K. and H. G. Larew. 1970. Dynamic shearing resistance of dry Ottawa sand. ASCE, Journal of Soil Mech. Found. Div., Proc. 9(SM2): 705-720.

9. Barden, L. 1971. Examples of clay structure and its influence on engineering behavior. Proc. Roscoe Memorial Symposium, Cambridge Univ., pp. 195-205.

10. Barden, L. and G. R. Sides. 1970. Engineering behavior and structure of compacted clay. ASCE, Journal of Soil Mech. Found. Div., Proc. 96(SM4): 1171-1200.

11. Barklay, L. M. and D. W. Thompson. 1969. Electron microscopy of sodium montmorillonite. Nature 222: 263.

12. Bazant, Z. P., K. Ozaydin and R. J. Krizek. 1975. Micromechanics m model for creep of anisotropic clay. ASCE, Journal of Engr. Mech. Div., Proc. 101(EM1): 57-78.

13. Bjerrum, L. and T. C. Kenney. 1967. Effect of structure on the shear behavior of normally consolidated quick clays. Proc. of Geotech. Conf. 2: 19-27.

14. Bjerrum, L. and A. Landva. 1966. Direct simple shear tests on a Norwegian quick clay. Geotechnique 16(1): 1-20.

15. Borst, R. L. and F. J. Shell. 1970. The effect of thinner on the fabric of clay muds and gels. Soc. Petrol. Engrs. of AIME, SPE 3110: 1-10.

16. Calladine, C. R. 1971. A microstructural view of the mechanical properties of saturated clay. Geotechnique 21(4): 391-415.

17. Campanella, R. G. and Y. P. Vaid. 1974. Triaxial and plane strain creep rupture of an undisturbed clay. Canadian Geotechnical Journal 11(1): 1-10.

18. Chaudry, T. I. 1973. Rate process theory as applied to clay slurries. M.S. thesis. Iowa State University, Ames, Iowa.

19. Christensen, R. W. and J. S. Kim. 1969. Rheological model studies in clay. Clays and Clay Mins. 17(2): 83-94.

20. Collins, K. and A. McGown. 1974. The form and the function of microfabric features in a variety of natural soils. Geotechnique 2: 223-254.

21. Demirel, T. 1962. Adsorption of water vapor by sodium and calcium montmorillonites. Ph.D. thesis, Iowa State University, Ames, Iowa.

22. Dorn, J. E. 1957. The spectrum of activation energies for creep. In Creep and recovery, pp. 255-283.

23. Duncan, J. M. and P. Dunlop. 1969. Behavior of soils in simple shear tests. Proc. 7th Int. Conf. Soil Mech. 1: 101-109.

24. Eichler, J. and J. Kazda. 1965. Two studies of the heterogeneous system of clay soils. Proc. 6th Int. Conf. Soil Mech. 1: 36-40.

25. Erol, O., R. A. Lohnes and T. Demirel. 1976. Preparation of clay type moisture containing samples for scanning electron microscopy. SEM/1976/1, Proc. of Workshop on Techniques for Particulate Matter Studies in SEM, IIT Research Inst., Chicago, pp. 769-776.

26. Finn, W. D. L. and D. J. Pickering and P. L. Bransby. 1971. Sand liquefaction in triaxial and simple shear tests. ASCE, Journal of Soil Mech. Found. Div., Proc. 97(SM4): 639-659.

27. Foster, R. H. 1971. Discussion Session 1. Proc. of Roscoe Memorial Symp., Cambridge University, pp. 108-116.

28. Foster, R. H. 1971. Behavior of kaolin fabric under shear loading at low stress. Proc. of Roscoe Memorial Symp., Cambridge University, pp. 69-80.

29. Foster, R. H. and P. K. De. 1971. Optical and electron microscopic investigation of shear induced structures in lightly and heavily consolidated kaolinite. Clays and Clay Mins. 19(1): 31-48.

30. Garofalo, F. 1965. Fundamentals of creep and creep-rupture in metals. The Macmillan Company, New York, 466 pp.

31. Glasstone, S. K., K. Laidler and H. Eyring. 1941. The theory of the rate processes. McGraw-Hill Book Company, Inc., New York, 611 pp.

32. Gray, D. H. and N. A. Kashmeeri. 1971. Thixotropic behavior of compacted clays. ASCE, Journal of Soil Mech. Found. Div., Proc. 97 (SM1): 193-207.

33. Hartwell, J. F. 1974. Development of a simple shear apparatus for the rate process studies. M.S. thesis, Iowa State University, Ames, Iowa.

34. Kauzmann, W. 1941. Flow of solid metals from the standpoint of the chemical-rate theory. Trans. Am. Inst. Mining and Met. Engs. 143: 57-81.

35. Kellog, C. G. 1972. Residual and time dependent strengths of two lateritic soils. M.S. thesis, Iowa State University, Ames, Iowa.

36. Lambe, T. W. 1960. A mechanistic picture of shear strength in clay. Res. Conf. Shear Strength of Clay Soils, Colorado, pp. 555-580.

37. Lambe, T. W. and R. V. Whitman. 1969. Soil mechanics. Wiley, New York, 553 pp.

38. Leonard, R. A. and P. F. Low. 1964. Effect of gelation on the properties of water in water clay suspensions. Proc. 12th Nat. Conf. Clays and Clay Mins. 13: 311-326.

39. Low, P. F. 1961. Physical chemistry of clay-water interaction. Advances in Agronomy 13: 269-327.

40. Low, P. F. and D. M. Anderson. 1958. The partial specific volume of water in bentonite suspensions. Soil Science Soc. Am. Proc. 22: 22-24.

41. Low, P. F. and J. L. White. 1970. Hydrogen bonding and polywater in clay water systems. Clays and Clay Mins. 18(1): 63-67.

42. Lucks, A. S., J. T. Christian, G. E. Brandow and K. Höeg. 1972. Stress conditions in simple shear test. ASCE, Journal of Soil Mech. Found. Div., Proc 98(SM1): 155-160.

43. Marley, J. J. 1969. Behavior of granular materials under triaxial compression with pulsating deviator stress. Ph.D. thesis, Iowa State University, Ames, Iowa.

44. Martin, R. T. 1962. Adsorbed water on clay: A review. Nat. Conf. Clays and Clay Mins. Proc. 9: 28-70.

45. McKyes, E. and R. N. Yong. 1971. Three techniques for fabric viewing as applied to shear distortion of a clay. Clay and Clay Mins. 19: 289-294.

46. Mesri, G. and R. E. Olson. 1970. Shear strength of montmorillonite. Geotechnique 20(3): 261-270.

47. Mesri, G. and R. E. Olson. 1971. Consolidation characteristics of montmorillonite. Geotechnique 21(4): 341-352.

48. Mitchell, J. K. 1960. Fundamental aspects of thixotropy in soils. ASCE, Journal of Soil Mech. Found. Eng. Div., Proc. 86(SM3): 19-52.

49. Mitchell, J. K. 1964. Shearing resistance of soils as a rate process. ASCE, Journal of Soil Mech. Found. Engr. Div., Proc. 90 (SM1): 29-61.

50. Mitchell, J. K. 1976. Fundamentals of soil behavior. John Wiley and Sons, New York, 442 pp.

51. Mitchell, J. K. and W. N. Houston. 1969. Causes of clay sensitivity. ASCE, Journal of Soil Mech. Found. Eng. Div., Proc. 95(SM3): 845-871.

52. Mitchell, J. K., R. G. Campanella and A. Singh. 1968. Soil creep as a rate process. ASCE, Journal of Soil Mech. Found. Eng. Div., Proc. 94(SM1): 231-253.

53. Mitchell, J. K., A. Singh and R. G. Campanella. 1969. Bonding, effective stresses and strength of soils. ASCE, Journal of Soil Mech. Found. Engr. Div., Proc. 95(SM5): 1219-1246.

54. Moore, W. J. 1972. Physical chemistry, 4th ed. Prentice-Hall Inc., Englewood Cliffs, New Jersey, 844 pp.

55. Morgenstern, N. R. and J. S. Tchalenko. 1967. Microscopic structures in kaolin subjected to direct shear. Geotechnique 17(4): 309-328.

56. Murayama, S. and T. Shibata. 1961. Rheological properties of clays. Proc. 5th Int. Conf. Soil Mech. 1: 269-273.

57. Nelson, J. D. 1973. Influence of clay fabric on bonds and dilatation. Proc. Int. Symp. on Soil Structure, pp. 155-160.

58. Noble, J. J. 1968. Effect of temperature on strength of soils. Ph.D. thesis, Iowa State University, Ames, Iowa.

59. Noble, J. J. and T. Demirel. 1969. Effect of temperature on strength behavior of cohesive soils. Highway Research Board, Spec. Report No. 103, pp. 204-219.

60. O'Brien, N. R. 1971. Fabric of kaolinite and illite floccules. Clays and Clay Mins. 19(6): 353-360.

61. Ohta, H. and T. Shibata. 1973. An idealized model for soil structure. Proc. Int. Symp. on Soil Structure, pp. 123-131.

62. Peacock, W. H. and H. B. Seed. 1968. Sand liquefaction under cyclic loading simple shear conditions. Journal of Soil Mech. Found. Eng. Div., Proc. 94(SM3): 689-708.

63. Rehbinder, P. 1970. On the rheologicy of thixotropically structurized disperse systems. Proc. 5th Int. Cong. on Rheology 2: 375-385.

64. Ripple, C. D. and P. R. Day. 1966. Suction responses due to homogeneous shear of dilute montmorillonite water pastes. Proc. 14th Nat. Conf. Clay and Clay Mins. 15: 307-316.

65. Roscoe, K. H. 1953. An apparatus for the application of simple shear to soil samples. Proc. 3rd Int. Conf. Soil Mech. Found. Eng. 1: 186-191.

66. Roscoe, K. H. 1961. Contribution to the discussion of soil properties and their measurement. Proc. 5th Int. Conf. Soil Mech. Found. Eng. 5: 105-107.

67. Roscoe, K. H., R. H. Bassett and E. R. L. Cole. 1967. Principal axes observed during simple shear of a sand. Proc. Geotech. Conf., Oslo 1: 231-237.

68. Ruenkrairergsa, T. 1973. Swelling pressure of sodium montmoril-
    lonite in relation to interlayer spacing. Ph.D. thesis, Iowa State
    University, Ames, Iowa.

69. Sankaran, K. S. and D. Venkateshwar. 1974. Mechanistic response of
    expansive clays. Soil Science 118: 289-298.

70. Schmid, W. E. 1960. A rheological failure for clay soils. In
    Progress Report on ONR, Project No. NR-981-177, Contract No. 1858
    (54).

71. Schmid, W. E. 1962. New concepts of shearing strength for saturated
    clay soils - Part 1. Soils 1: 31-42.

72. Schmid, W. E. 1962. New concepts of shearing strength for saturated
    clay soils - Part 2. Soils 2: 19-26.

73. Sergeyev, Y. M., D. Y. Budin, V. I. Osipov and V. S. Shibakova.
    1973. The importance of the fabric of clays in estimating their
    engineering-geological properties. Proc. Int. Symp. Soil Structure,
    pp. 243-248.

74. Shibata, T. and D. Karube. 1969. Creep rate and creep strength of
    clays. Proc. 7th Int. Conf. Soil Mech., pp. 361-367.

75. Shockley, G. W. and R. G. Ahlvin. 1960. Non-uniform in triaxial
    test specimens. Int. Res. Conf. on Shear Strength of Cohesive Soils,
    ASCE, pp. 341-357.

76. Sides, G. R. 1971. Soil microstructure and sample disturbance
    observations in the stereoscan electron microscope. Proc. Roscoe
    Symp., Cambridge University, pp. 89-98.

77. Sides, G. and L. Barden. 1971. The microstructure of dispersed and
    flocculated samples of kaolinite, illite and montmorillonite.
    Canadian Geotech. Journal 8: 391-399.

78. Singh, A. and J. K. Mitchell. 1968. General stress-strain time
    function for soils. ASCE, Journal of Soil Mech. Found. Eng. Div.,
    Proc. 94(SM1): 21-46.

79. Singh, A. and J. K. Mitchell. 1969. Creep potential and creep
    rupture of soils. Proc. 7th Int. Conf. Soil Mech., pp. 379-384.

80. Sloane, R. L. and T. F. Kell. 1966. The fabric of mechanically
    compacted kaolin. Proc. 14th Nat. Conf. Clays and Clay Mins., pp.
    289-296.

81. Smalley, I. J. and J. G. Cabrera. 1969. Particle association in compacted kaolinite. Nature 222: 80-81.

82. Smalley, I. J., J. G. Cabrera and C. Hammond. 1973. Particle nature in sensitive soils and its relation to soil structure and geotechnical properties. Proc. Int. Symp. on Soil Structure, pp. 184-189.

83. Sowers, G. F. 1963. Strength testing of soils. American Society of Testing and Materials, STP, No. 361, pp. 3-31.

84. Tan, T. K. 1958. Discussion of soil properties and their measurements. Proc. 4th Int. Conf. Soil Mech. 3: 87-89.

85. Ter-Stepanian, G. 1975. Creep of a clay during shear and its rheological model. Geotechnique 25(2): 299-320.

86. Terzaghi, C. 1931. The static regidity of plastic clays. Journal of Rheology 2(3): 253-262.

87. Tovey, N. K. 1971. A selection of scanning electron micrographs of clays. CUED/C, Soils/TR.5a, University of Cambridge.

88. Tovey, N. K. 1973. Techniques in scanning electron microscopy. A series of lectures given at instrumentation course held at University of Cambridge, Dept. of Engineering, Cambridge, England.

89. Tovey, N. K. and K. Y. Wong. 1973. The preparation of soils and other geological materials for the SEM. Proc. Int. Symp. on Soil Structure, pp. 59-67.

90. van Olphen, H. 1963. Introduction to clay colloid chemistry. Interscience, New York, 301 pp.

91. Vyalov, S. S., N. K. Pekarskaya and R. V. Maksimyak. 1970. Physical essence of processes of deformation and failure of clayey soils. Soil Mech. and Found. Eng. (Trans. from Russian) 1: 12-16.

92. Whited, D. 1975. Chemical additives as compaction aids for fine grained soils. M.S. thesis, Iowa State University, Ames, Iowa.

93. Wu, T. H., D. Resendiz and R. J. Neukirchner. 1966. Analysis of consolidation by rate process theory. ASCE, Journal of Soil Mech. Found. Eng. Div., Proc. 92(SM6): 229-247.

94. Yong, R. N. and B. P. Warkentin. 1975. Soil properties and behavior. Elsevier, Amsterdam, 444 pp.

95. Zaretskii, Y. K. and S. S. Vyalov. 1971. Structural mechanics of clay soils. Soil Mech. and Found. Eng. (Trans. from Russian) 3: 153-155.

ACKNOWLEDGMENTS

The author gratefully acknowledges the support of this study which was provided by the National Science Foundation and the Engineering Research Institute of Iowa State University.

To Dr. T. Demirel, the author's major professor, the author owes a debt of gratitude for his invaluable guidance, encouragement, assistance and true friendship in all phases of this study, without which this work would not have been possible.

The wise guidance, encouragement, assistance and friendship extended by Dr. R. A. Lohnes throughout the investigation is acknowledged with sincere appreciation.

The author is grateful to the other members of his graduate committee, namely, Dr. J. L. Mickle, Dr. W. H. Scholtes and Dr. W. F. Klaiber.

The author also wishes to express his appreciation to all members of the Civil Engineering Department, especially to graduate and undergraduate assistance of the Soil Engineering Division for their help and friendship during the last three years.

APPENDIX A: CREEP TEST RESULTS OF

BENTONITE CLAY (B SERIES)

In B series tests, difficulties were met in determining the strain rate-shear stress and strain-rate-temperature relationships for the bentonite clay. The scatter which occurred in the experimental data are seen in plots of $\dot{\gamma}_f$ versus τ and $\frac{1}{T}$ as shown in Figures A1 and A2, respectively. This scatter from the linear relationship predicted by the theory can be attributed to the following factors: general experimental errors including the variations in the moisture contents of the specimens and differences in the initial structure of the specimens due to thixotropic hardening. In B series, separate test specimens were prepared and cured for a fixed time period of 7 days to allow enough time for same thixotropic effect in each specimen prior to testing. The preparation of separate specimens occasionally caused moisture variations over 1-2 percent of the dry weight of the clay. However data points in Figures A1 and A2 did not follow a systematic scatter which would be explained in terms of moisture content variations of the specimens only. The behavior of the specimens was considered to be affected by thixotropic hardening.

The phenomenon of thixotropy is known to be due to structural effects (48,32,24). Thixotropically hardened state corresponds to the most stable arrangement of particles. Shearing and remolding induce a displacement or change in the configuration of the particles. As a result, the structural bonds are ruptured leading to destruction of the structure and loss in strength. As soon as the shearing ceases the system tends to return to its original state by reforming the structural bonds. The structural changes necessary to return the system to hardened state is a spontaneous process, but it cannot take place instantaneously due to limited mobility of particles in water. This limitation arises from
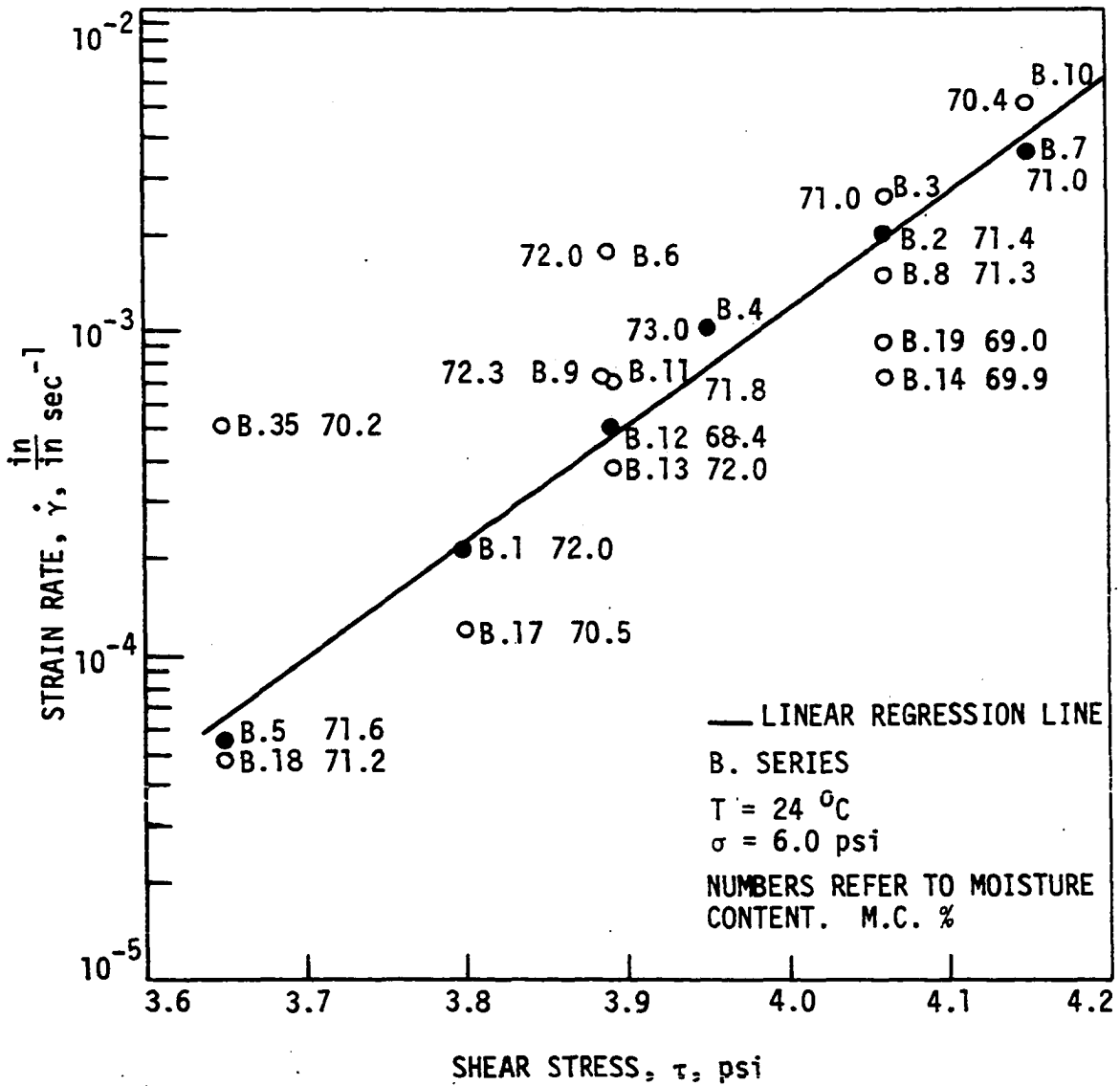
Figure A1. Plots of shear stress τ versus strain rate γ̇ at inflection points (mobilization ratio of 1.0) of creep curves for B series
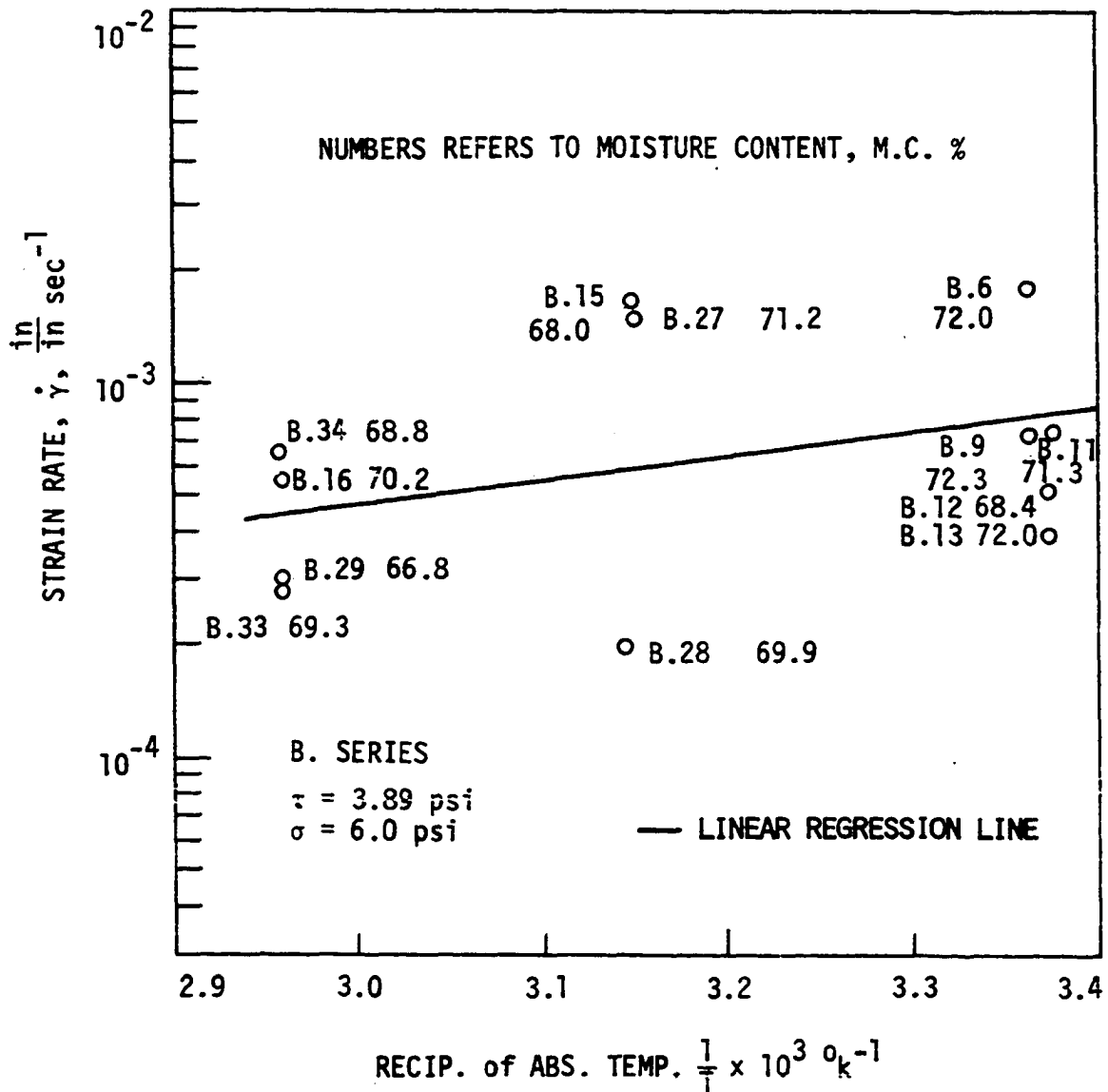
Figure A2. Plots of reciprocal of absolute temperature $\frac{1}{T}$ versus strain rate $\dot{\gamma}$ at inflection points (mobilization ratio of 1.0) of creep curves for B series

viscose resistar.ce :* -:.-:- to particle movement (48). Since the viscosity of water is temperature dependent, being lower at higher temperatures, an increase in the rate and magnitude of the hardening is expected with increasing temperatures. The hardening and thickening of drilling muds when heated (15) and reported higher viscosities (18) are in agreement with these considerations. The real mechanism of structural changes giving rise to thixotropic behavior has not yet been clear. According to Mitchell (48,50) hardened and remolded states of the structure can be visualized as flocculated and dispersed particle arrangements, respectively. Leonard and Low (38) suggest that the loss in strength is due to a change in the structure of the adsorbed water on clay surfaces. According to Borst et al. (15), bentonite muds thicken at high temperatures because the interlayer distances in montmorillonite films decrease. Their suggestion was supported by scanning electron microscopy studies on thixotropically hardened gels (15). Although direct evidences cannot be given the first two of the mechanisms can reasonably be considered as the major source of thixotropic behavior in clay soils.

It should be observed at this point, however, the data scatter is much more pronounced when temperature is varied. This is due to strong dependence of thixotropic hardening rates on temperature. Therefore at constant temperature $\log \dot{\gamma}$ versus τ relationships could be used with a reasonable degree of confidence whereas $\log \dot{\gamma}$ versus $\frac{1}{T}$ relationships could not. The scatter of experimental points in Figure A1 can still be attributed to the thixotropy effects as follows. The behavior of the specimens were possibly affected by residual thixotropic hardenings which

cannot be totally eliminated in ordinary remolding procedures. The relationship between τ and log $\dot{\gamma}_f$ was found by repeating the experiments at different stress levels as shown in Figure A1. The mobilization and rupture ratios were evaluated for the tests having $\dot{\gamma}_f$ values closest to the linear regression line only (shown by solid circles on Figure A1) due to considerable time involved in determining these ratios for all the points. Hence a statistical analysis of the results was not made. However the regression line in Figure A1 furnishes the statistical evaluation. The log $\dot{\gamma}$ versus τ plots for each mobilization and rupture ratios are given in Figures A3 and A4. The results of regression analysis and calculated creep parameters are summarized in Table A1. The relationship between β' and M and R ratios are shown in Figure A5. It is interesting to note that the variation of β' shows the same trend observed in Grundite clay.

The temperature dependence of hardening appeared to control the behavior of the bentonite clay. Higher testing temperatures resulted in slower creep rates indicating an opposite sign for activation enthalpy as shown in Figure A2. To eliminate different magnitudes of hardenings occurring at different temperatures, all specimens were heated to maximum testing temperature of 65°C for 20 hours, then they were cooled down to actual testing temperatures. However prolonged heating caused uncontrollable moisture variations among the specimens. An attempt was made to modify the shear box so that the specimens would be kept in mineral oil while heating to control moisture losses. This attempt failed due to the mechanical difficulties met in building a reservoir for mineral oil around
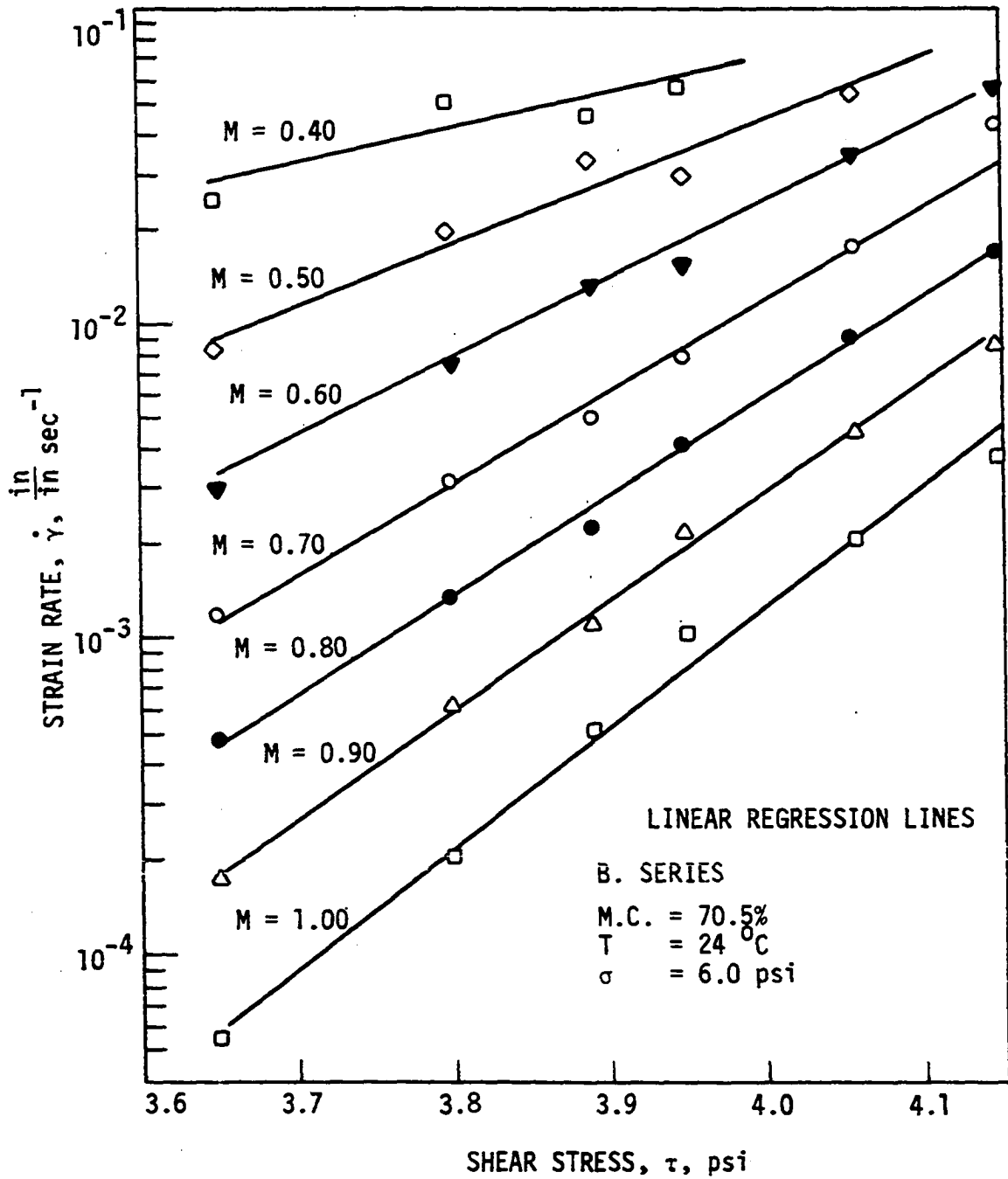
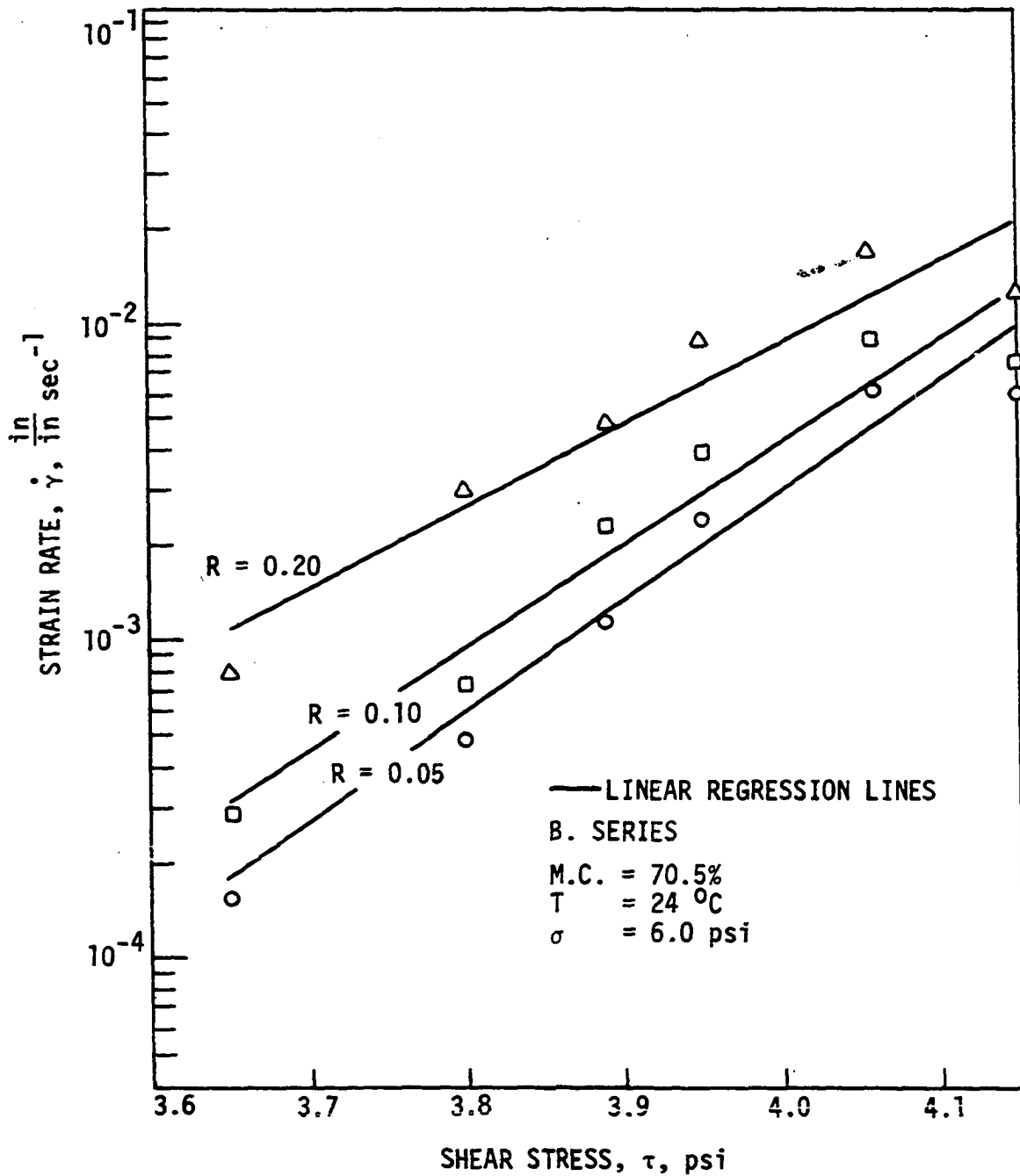Figure A3.   Plots of shear stress τ versus strain rate γ̇ at various
mobilization ratios M for B series

Figure A4. Plots of shear stress τ versus strain rate γ̇ at various rupture ratios R for B series

the shear box. This problem did not allow a correct determination of
temperature-creep rate relationships for bentonite clay at the time this
research was undertaken.

Table A1. B series creep parameters

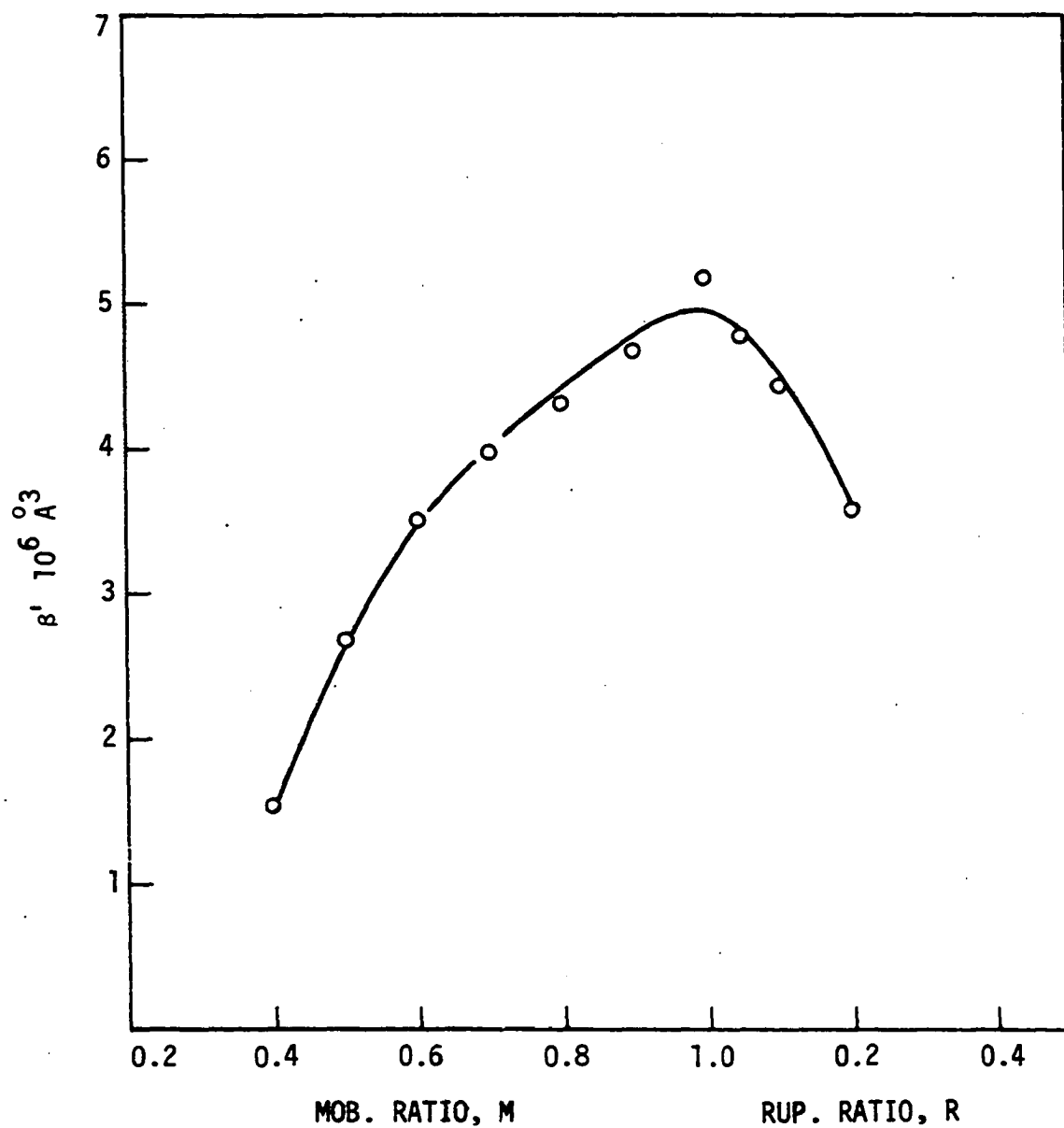| M or R | Linear regression analysis $\log \dot{\gamma}$ vs. τ | | | β' 10^6 $\overset{\circ}{A}^3$ | $(\beta')^{1/3}$ $\overset{\circ}{A}$ |
	Slope β	Intercept C_1	Corr. Coeff. r		
M=0.40	1.095	-3.542	0.908	1.52	115
0.50	1.924	-7.062	0.976	2.69	139
0.60	2.529	-9.756	0.998	3.50	152
0.70	2.874	-11.435	0.998	3.98	158
0.80	3.115	-12.734	0.998	4.31	163
0.90	3.384	-14.088	0.997	4.68	167
1.00	3.738	-15.862	0.995	5.17	173
R=0.05	3.455	-14.357	0.981	4.78	168
0.10	3.188	-13.132	0.966	4.41	164
0.20	2.573	-10.353	0.949	3.56	153

Figure A5. Plot of mobilization ratio M and rupture ratio R versus flow
volume β' for B series (M.C.=70.5%, normal stress=6.0 psi)

APPENDIX B: MOBILIZATION TIME t_M VERSUS SHEAR STRESS PLOTS FOR C.2, C.3 AND C.4 SERIES TESTS RESULTS OF COMBINED ANALYSIS
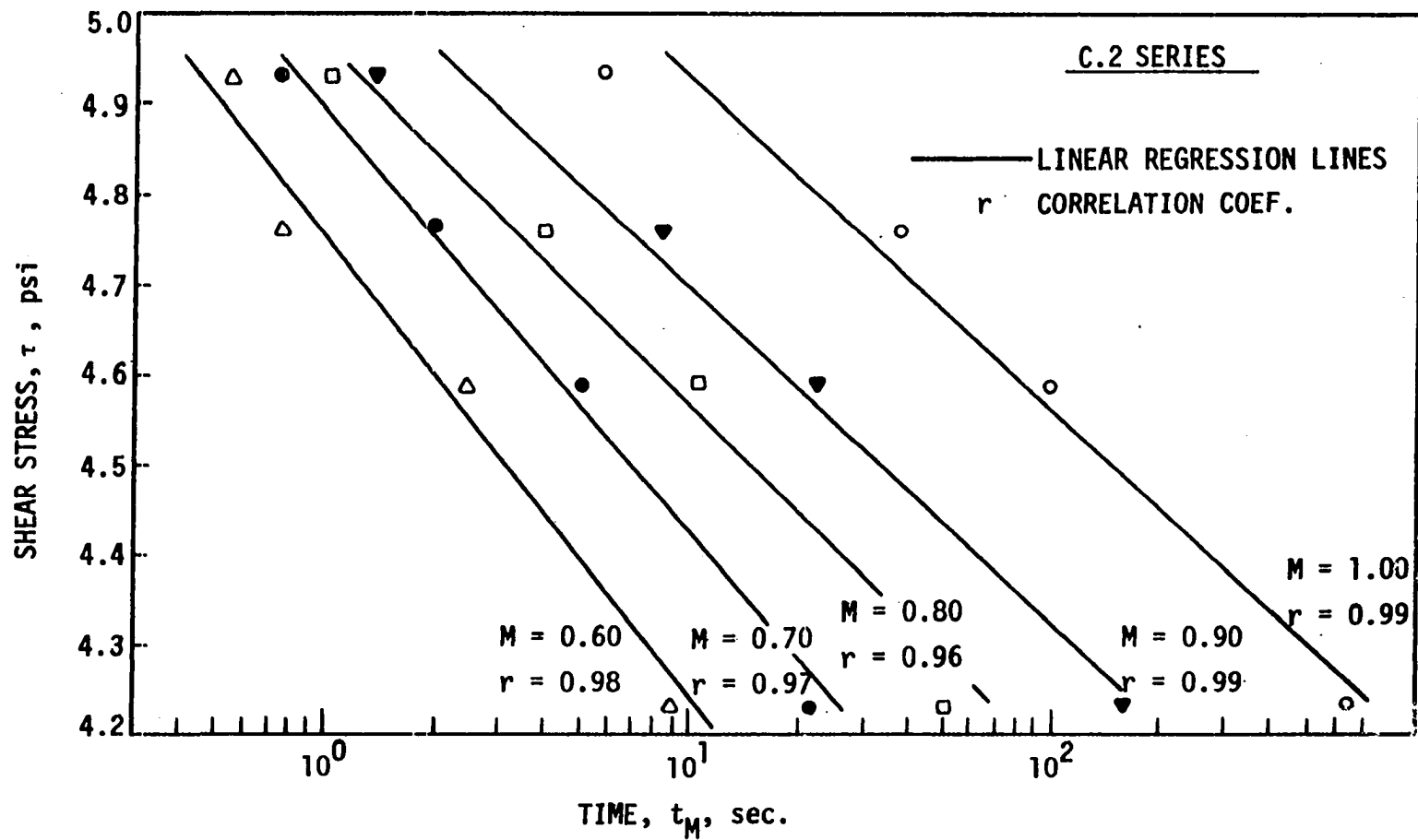
Figure B1. Plots of mobilization time t_M versus shear stress τ plots at various mobilization ratios M for C.2 series (M.C.=35.6%, normal stress=6.0 psi)
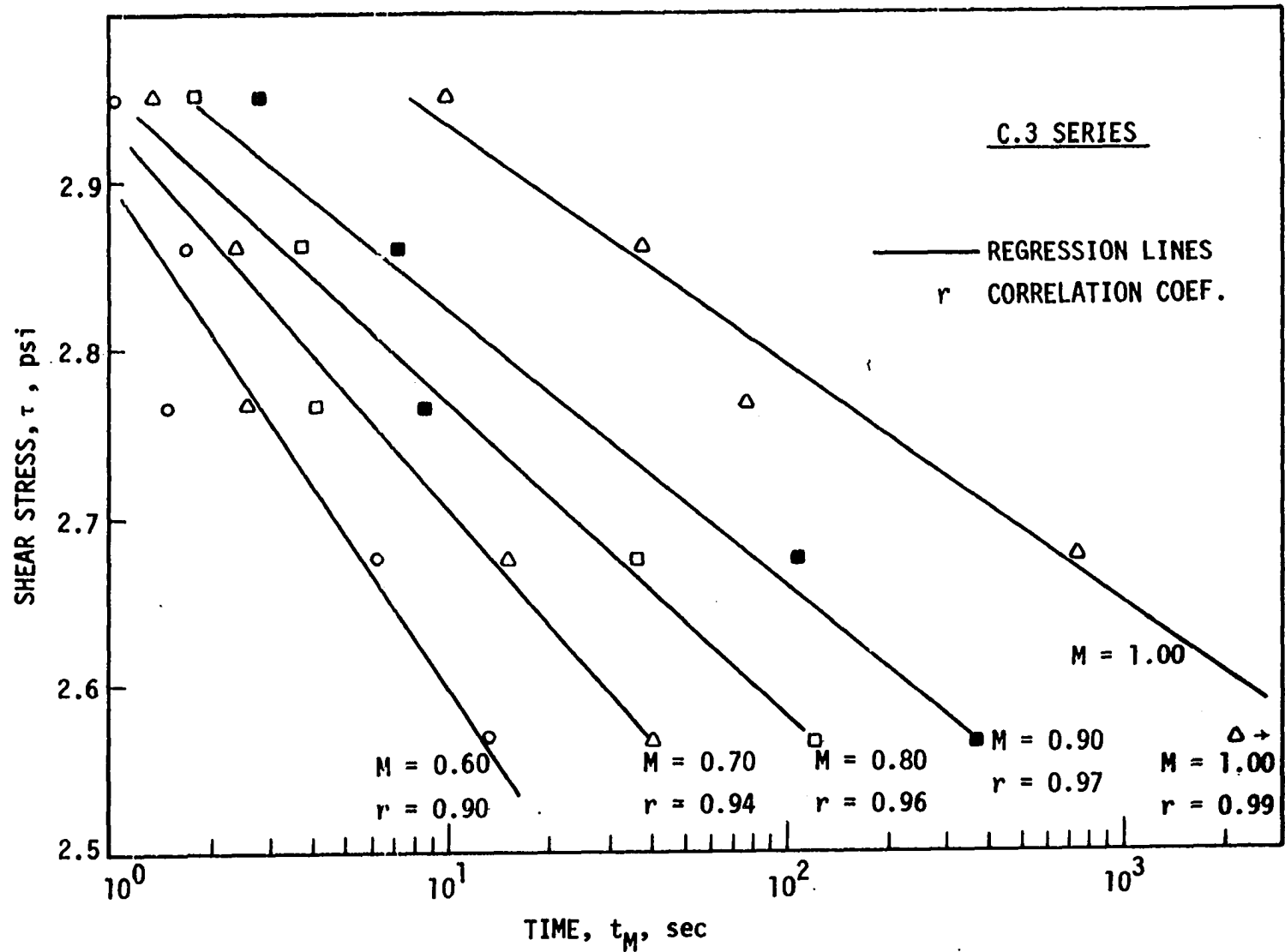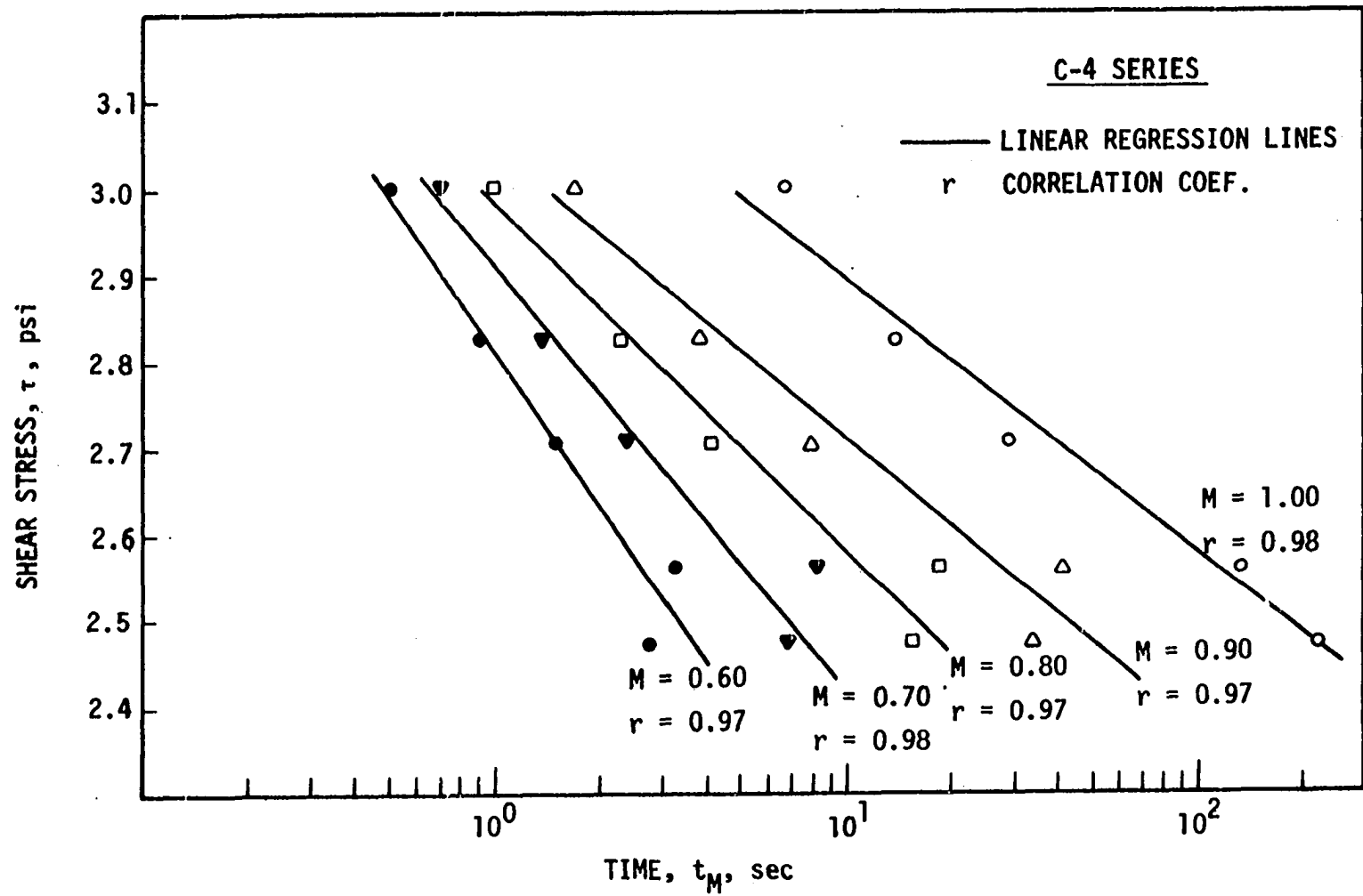
SHEAR STRESS, τ , psi

2.9

2.8

2.7

2.6

2.5

C.3 SERIES

——— REGRESSION LINES

r   CORRELATION COEF.

M = 1.00

M = 0.60
r = 0.90

M = 0.70
r = 0.94

M = 0.80
r = 0.96

M = 0.90
r = 0.97

M = 1.00
r = 0.99

10^0 10^1 10^2 10^3

TIME, t_M, sec

115

Figure B2.   Plots of mobilization time t_M versus shear stress τ at various mobilization ratios M for C.3 series (M.C.=41.1%, normal stress=6.0 psi)

Figure B3. Plots of mobilization time t_M versus shear stress τ at various mobilization ratios M (C.4 series, M.C.=46.0%, normal stress=6.0 psi)
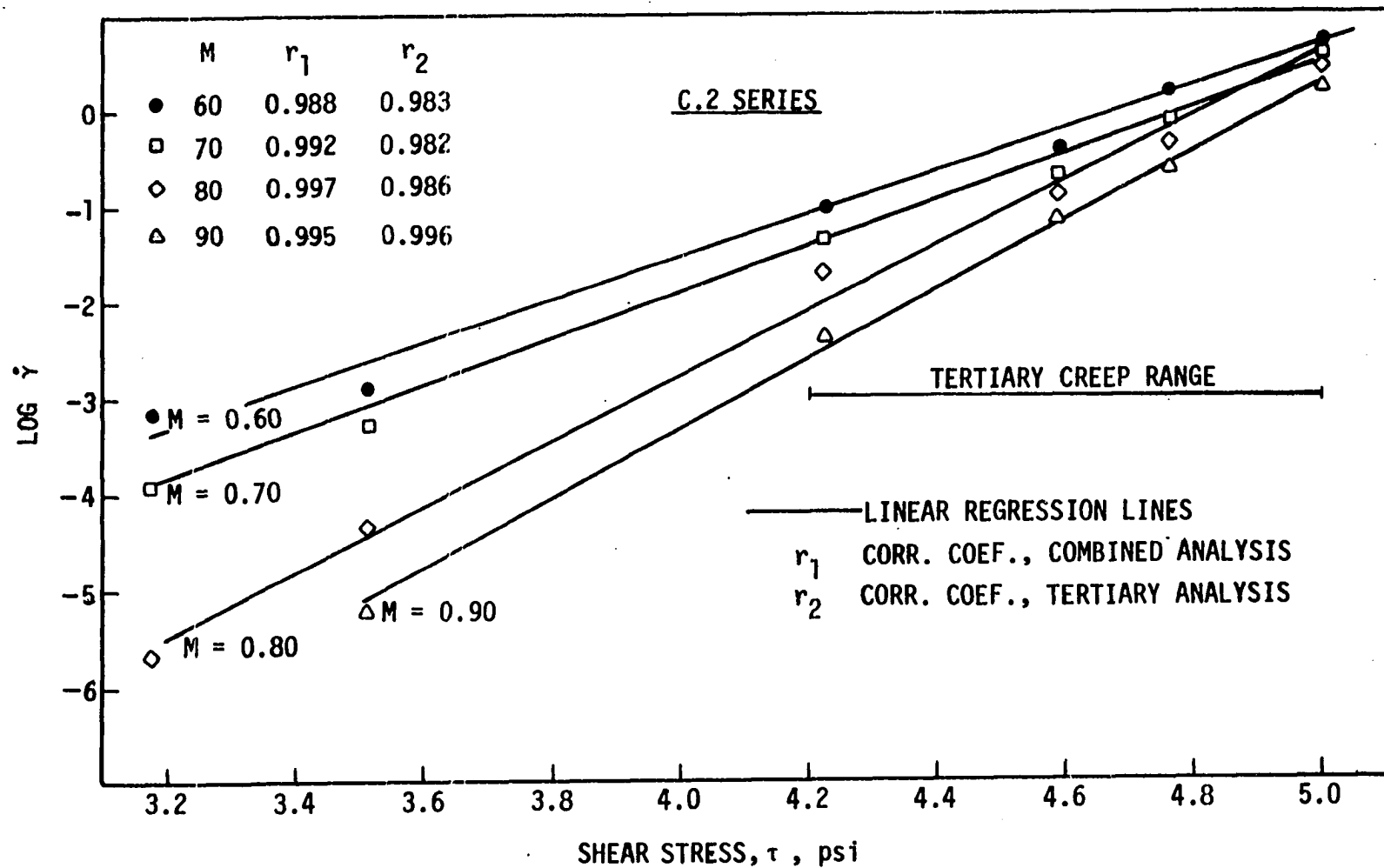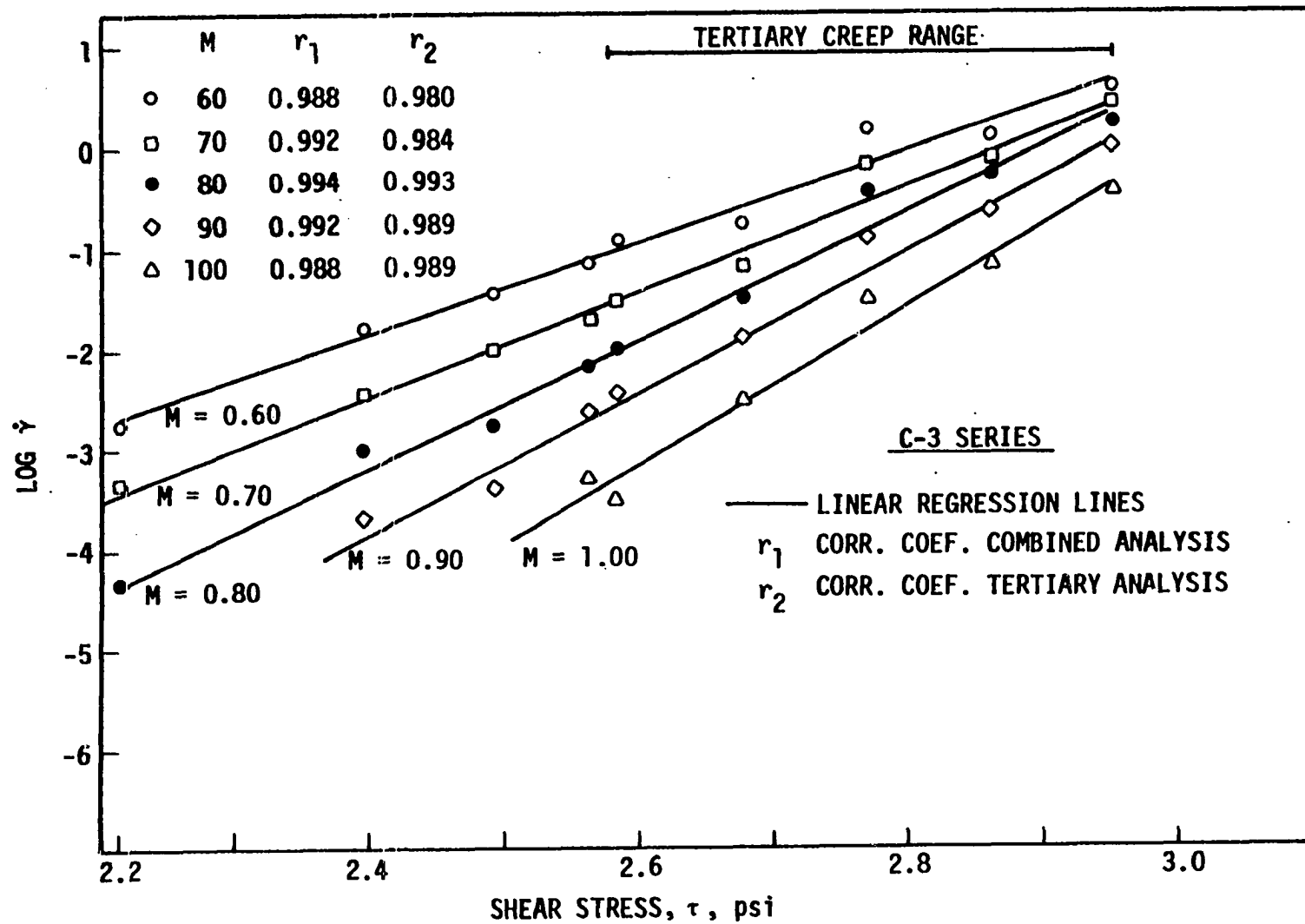
Figure B4.   Plots of log strain rate $\dot{\gamma}$ versus shear stress τ combining tertiary and terminal stress levels at various mobilization ratios M (C.2 series, M.C.=35.6%, normal stress=6.0 psi)

Figure B5. Plots of log strain rate $\dot{\gamma}$ versus shear stress τ combining tertiary and terminal stress levels at various mobilization ratios M (C.3 series, M.C.=35.6%, normal stress=6.0 psi)